SHM-BASED CONDITION ASSESSMENT OF BRIDGES USING GAUSSIAN PROCESS REGRESSION

LI MING

M.Phil

The Hong Kong Polytechnic University

2017

The Hong Kong Polytechnic University

Department of Civil and Environmental Engineering

SHM-BASED CONDITION ASSESSMENT OF BRIDGES USING GAUSSIAN PROCESS REGRESSION

LI Ming

A thesis submitted in partial fulfilment of the requirements for the degree of Master of Philosophy

August 2017

CERTIFICATE OF ORIGINALITY

I hereby declare that this thesis is my own work and that, to the best of my knowledge and belief, it reproduces no material previously published or written, nor material that has been accepted for the award of any other degree or diploma, except where due acknowledgement has been made in the text.

_____ (Signed)

__LI Ming_____ (Name of student)

To my parents

ABSTRACT

The structural health monitoring (SHM) technology enables to gain information about the in-service performance of bridges. By integrating the monitoring data from online SHM systems, the structural condition of the monitored structure can be evaluated and the health status can be evolutionarily traced. The advancement in SHM technology has been evolving from the monitoring-based diagnosis to the monitoring-based prognosis. Conventional analytical methods process the monitoring data with deterministic parameters and coefficients and have difficulties in determining the uncertainties stemming from the measurement noises, modeling errors, time-varying environmental effects, and etc. In recent years, the Bayesian modeling approach with Gaussian process (GP) has earned attention because of its characteristic which allows for the probabilistic processing and has great capability of flexibility in modeling different kinds of relationships as well. The covariance function in GP can determine the distribution of target function, and should be carefully chosen in order to fit the real covariance distribution of the data regression relationship. Usually the squared exponential (SE) covariance is chosen in GP because it corresponds to a linear combination of infinite number of basis functions and has the largest flexibility. But when the relationship characteristic is known a priori, the explicitly defined covariance function may perform better than the general-purposed SE one. The work described in this thesis is devoted to exploring the flexibility of GP in modeling different

relationships by explicitly modifying the model, for the purpose of structural health condition assessment using the monitoring data.

A Gaussian process regression (GPR) model is first formulated to establish the relationship between the temperature and expansion joint displacement for the Ting Kau Bridge (TKB). Apart from a general-purposed GPR model defined with SE covariance function (SE-GPR), the explicit covariance function is derived for a linear GPR (L-GPR) model based on the observed linear relationship. The log marginal likelihood maximization method is used to optimize the hyperparameters in GPR models. The performance of the optimized L-GPR model and SE-GPR model are evaluated and compared using the same sample data set. The results show that the L-GPR model with explicit linear covariance function which fits the linear relationship performs better in linear regression and prediction. The outperformed L-GPR model is further used to predict the expansion joint displacement under extreme design temperature. By comparing with the designed allowable maximum and minimum values, the structural health condition of the TKB is examined.

In practice, a simple linear relationship may not be adequate, therefore a generalized model is needed. The L-GPR model is further extended to generalized linear model. Before applying simple linear model on the inputs, the inputs are first projected into some high dimensional space using a set of basis functions. The covariance function for a generalized linear relationship is then derived and applied to a polynomial

relationship. An explicit polynomial GPR model (P-GPR) is formulated to establish the relationship between the lateral displacement and wind data for the Tsing Ma Bridge. Among the first three order polynomial relationships considered in this study, the P-GPR with second order polynomial (P-GPR2) is selected as the optimal GPR model with the largest log marginal likelihood and smallest root mean square error. The outperformed P-GPR2 model is further used to predict the lateral displacement under extreme design wind speed at 53.3 m/s. The wind direction for maximum displacement prediction is considered in two cases: most probable direction and most unfavorable direction. The predicted total displacement is compared with the designed allowable value to check the structural health condition.

LIST OF PUBLICATIONS

Journal papers:

Li, M., & Ni, Y. Q. (2016). Modal identifiability of a cable-stayed bridge using proper orthogonal decomposition. *Smart Structures and Systems*, 17(3), 413-429. (SCI)

Ni, Y. Q., & Li, M. (2016). Wind pressure data reconstruction using neural network techniques: A comparison between BPNN and GRNN. *Measurement*, 88, 468-476. (SCI)

Conference papers:

Ni, Y. Q., & Li, M. (2015). Reconstructing Wind Pressure Measurement Data by Neural Network Technique. *Proceeding of the 7th International Conference on Structural Health Monitoring of Intelligent Infrastructure*, 1-3 July 2015, Torino, Italy.

Li, M., & Ni, Y. Q. (2016). Bayesian blind source separation and structure change detection using monitoring strain data. *Proceeding of the 7th Cross-Strait Summer School Workshop on Structural Monitoring and Vibration Control in Civil Engineering*, 5-7 July 2016, Taipei, Taiwan.

ACKNOWLEDGEMENTS

First of all, I would like to take this opportunity to express my heartfelt gratitude to my chief supervisor, Prof. Y. Q. Ni, for his enlightening guidance, constructive suggestions, detailed comments and insight, and strong sense of responsibility throughout my research study and preparation of this thesis. I appreciate all his consistent and illuminating instruction to make this thesis completed. I benefit greatly from his enthusiasm in scientific research, his punctilious working attitude, and his rigorous scholarship. I would also like to thank my co-supervisor, Dr. Sriram Narasimhan, from Department of Civil and Environmental Engineering, University of Waterloo, Canada, for his generous support and inspiring advices in the course of my study.

I would like to express my sincere thanks to my colleagues Mr. Y. W. Wang, Dr. Y. X. Xia, Mr. C. Xu, Dr. H. P. Wan, and Mr. R. Chen, for their very precious discussions and valuable suggestions during the research study and completion of this thesis.

I would like to acknowledge the financial support provided by The Hong Kong Polytechnic University, including the studentship, the payment for attendance of international conferences and research-associated equipment. I am also grateful for the kind help from the staff members at the university.

Finally, I would like to express my thanks to my parents, other family members, and friends, for their everlasting love, encouragement, comfort, and support during the past years.

TABLE OF CONTENTS

LIST OF FIGURES

LIST OF TABLES

LIST OF ABBREVIATIONS

Abbreviation	Description
AASHTO	American Association of State Highway and Transportation Officials
ASCE	American Society of Civil Engineers
BMS	Bridge management system
CDM	Continuum damage mechanics
FHWA	Federal Highway Administration
FOSM	First-order second-moment
GP	Gaussian process
GPR	Gaussian process regression
GPS	Global positioning system
HKO	Hong Kong Observatory
L-GPR	Linear Gaussian process regression
MC	Monte Carlo
MLP	Multi-layer perceptron
NDE	Non-destructive evaluation
PDF	Probability distribution function
P-GPR	Polynomial Gaussian process
PSD	Power spectral density
RBF	Radial basis function

RMSE	Root mean square error
RUL	Residual useful life
SE	Squared exponential
SE-GPR	GPR model with squared exponential covariance function
SHM	Structural health monitoring
SVM	Support vector machine
TKB	Ting Kau Bridge
TMB	Tsing Ma Bridge
WASHMS	Wind and Structural Health Monitoring System
WIM	Weigh-in-motion

LIST OF SYMBOLS

Symbol	Description
Chapter 2	
R	Reliability
P_f	Probability of failure
N	Total number of random sampling simulations
$n(g(\mathbf{x}_i) \leq 0)$	The number of sets when $g(\mathbf{x}_i) \leq 0$
$M(t)$	Safety margin of a specified failure mode
$R(t)$	Time-dependent resistance
$S(t)$	Time-dependent load effect
T	A given time period
Chapter 3	
$D = \{(\mathbf{x}_i, y_i) \mid i = 1, \ldots, n\}$	Training set of n observations
$\mathbf{x}_i$	Input vector of dimension d
y_i	Scalar output
$m(\mathbf{x})$	Mean function
$k(\mathbf{x}, \mathbf{x}'), K(X, X)$	Covariance function
ε	Gaussian noise
$GP(\cdot, \cdot)$	Gaussian process
X	Given inputs

X_*	Testing inputs
$f(X_*)$, $\mathbf{f}_*$	Predictive outputs
$\boldsymbol{\mu}_*$	Predicted output
Σ_*	Covariance of $\mathbf{f}_*$
σ_f^2	Signal variance
l	Isotropic length-scale
σ_n^2	Noise variance
$\boldsymbol{\theta}$	Hyperparameter vector
A_i	The *i*th subarea
A	Gross area of cross section
T_i	Measured temperature of the *i*th subarea
T_e	Effective temperature
α, β	Parameters in the simple linear regression model
$\sigma_\alpha^2, \sigma_\beta^2$	Variance of α, β
J	Matrix of ones

Chapter 4

$\phi(\mathbf{x})$	Basis function which maps a *d*-dimensional input vector into an *N* dimensional feature space
$\mathbf{w}$	Vector of weights (parameters)
Σ_p	Covariance matrix of $\mathbf{w}$

$\hat{D}$	Wind-induced total displacement of bridge
$\bar{D}$	Mean displacement
σ_D	Standard deviation of displacement
m_p	Statistical peak factor
σ_f^2	Signal variance
σ_0^2	Variance of constant term parameter
l	Characteristic length-scale
σ_n^2	Noise variance
y_i	The *i*th measured displacement response
y_i^{pred}	The *i*th predicted displacement response

CHAPTER 1

INTRODUCTION

1.1 Research Background

Civil structures serve as essential components in a society and therefore their safety and serviceability are of great importance to maintain a civilized society and a productive economy. The smooth operation of civil structures is the ultimate goal of engineering, academic, and management industries. As essential public infrastructure, bridges serve as an important part of civil infrastructure. As expected, bridges are built for enhancing the quality of life of the society. Bridges can be categorized based on different criteria. According to their structural configuration, bridges can be mainly categorized as beam bridges, cantilever bridges, arch bridges, truss bridges, and cable-supported bridges. Cable-supported bridges are usually suitable and competitive for long spans. The suspension bridges enable to extend the span length to even longer distance than the cable-stayed bridges. According to the specific landform of their location, bridges can be over water sources, hilly areas, transport hub with roads and railways passing underneath, or long-span bridges even across ocean or linking a group of islands. According to the played role in their lifetime, bridges can carry transportation services for persons, cattle, vehicles, water or other resources carried across in pipes or conveyors. Some major bridges can benefit the people of an entire

nation such as the bridges across Yangtse River or Yellow River in China (Feng, 2008), the bridges across Ganga River in India (Ponnuswamy, 2008), and the Honshu-Shikoku Connection across many islands in Japan (Wu *et al.*, 2003). They can even benefit more than one country as in the case of the Oresund Link Crossing over the Baltic ocean (Mathiessen, 2000). Ponnuswamy (2008) addressed that no other creation of a civil engineer has such a general appeal and fascination to the people. Bridges deserve special concerns not only because of their vast investment, but also because of the cost of the traffic disruptions and even the catastrophic casualties to the society if structural damage or failure occurs. However, by their very nature, in-service bridges are consistently subjected to traffic volumes, heavy truck loads, as well as environmental factors such as temperature, humidity, scour and chemical attack. In addition, they may suffer extreme events such as typhoon, earthquake or ship-collision occasionally. Therefore, they are deteriorating under the combined actions of the above factors as well as the material aging. Recent bridge failures such as the Laval Overpass in Canada (2005), the I-35W Bridge in Minneapolis, USA (2007), the I-5 Skagit River Bridge in Washington (2013), and the Belo Horizonte overpass in Brazil (2014), remind us that it is not only a problem of the past but also a problem of today. There has been a rising awareness of the existing bridge structural condition.

Civil structures are defective due to many aspects, for example, improper design or construction, deterioration due to environments, and long-term fatigue along service life time. According to the American Society of Civil Engineers (ASCE), up to half of

the infrastructures are potentially structurally deficient, and the investment of these structures may cost about US$1.6 trillion in a five-year period (ASCE, 2005). During the past few decades, a large number of large-scale and complex civil structures such as long-span bridges, high-rise buildings, and large-space structures, have been constructed in China because of the rapid economy development. In addition, extensive infrastructure development programs have been deployed in Hong Kong, and there are several major infrastructure projects under way. The increasing number of large-scale and complex civil structures cost huge investment during their construction and require much more maintenance efforts to ensure their stable functioning in the society. Technology innovations are therefore required in structural design, construction, maintenance, and management fields. According to other countries' experiences, maintenance of these structures from damage will cost enormous cost and efforts for the next few decades (Chang *et al.*, 2009).

The integrity of structures has been achieved by means of manual operations of inspection. The traditional inspection methods include non-destructive evaluation (NDE) and interpretation of data based on conventional technologies and expertise experiences. At that time, assessment criteria according to the codes of practice are the principal assessment methods, which are usually conservative and costly. These methods cannot provide effective monitoring of the aged structures. When emergent events occur such as earthquakes, the conventional manual investigation methods cannot provide immediate assessment since the extensive safety checks need time and

cost. In addition, the human investigations of some structures such as nuclear power plants are not accessible.

Practical and effective ways for monitoring the civil structures in service, evaluation their safety conditions, and arrangement of their maintenance decisions have long been of great interest. Recently the long-term structural health monitoring (SHM) technology is developed in the engineering field to achieve the objectives mentioned above. Based on a comprehensive sensory system and a sophisticated data processing system, the SHM technology enables to monitor the in-service performance of structures and subsequently make decision on their maintenance, so that the structural safety and serviceability can be maintained. An integral SHM system includes a sensory system, a data acquisition system, a data processing and archiving system, a communication system, and a damage detection and prediction system. With the advanced information technology and structural analysis algorithms, the integrity of in-service structures can be monitored in real time. As data collection systems, the first two systems are embedded on the structures. While the other three are usually located in the control office of administrative departments, serving as analysis systems. An integral SHM system can accomplish assignments including monitoring the operational loadings of the structure, structural performance assessment under in-service conditions, damage and deterioration detection, and inspection and maintenance decision making (Aktan *et al.*, 2000; Ko & Ni, 2005; Brownjohn, 2007; Frangopol *et al.*, 2008; Zhu & Frangopol, 2013).

With technology development, SHM systems have been implemented in a number of long-span bridges around the world for long-term monitoring since 1990. After that, researchers and practitioners have made efforts on how to utilize these advanced systems and the monitoring data to realize structural condition evaluation. Algorithms from many fields have been integrated in civil engineering field to provide better solutions. Using long-term monitoring data from SHM systems, the present study aims to develop a structural condition evaluation approach based on Gaussian process (GP) techniques. This study starts with the development of a linear GP model to establish the relationship between the temperature and expansion joint displacement using the monitoring data from the Ting Kau Bridge (TKB). Since a linear relationship is usually inadequate in many practical cases, the GP model is then extended to model a generalized linear relationship, using the lateral displacement and wind monitoring data from the Tsing Ma Bridge (TMB). With the formulated GP models, the structural condition evaluation and prediction are realized.

1.2 Research Objectives

The aim of this MPhil study is to develop a structural condition evaluation and prediction method based on Gaussian process regression (GPR) models. The long-term monitoring data from cable-supported bridges in Hong Kong are used for formulation and evaluation of the GPR models in this study. The specific objectives of this study are:

(i) Development of a linear GP regression (L-GPR) model based on the explicit definition of model functions using the monitoring data of temperature and expansion joint displacement from the TKB. The GPR model with general-purposed model functions have been commonly used in most of the studies. But GPR models with explicit key functions definition are seldom used. Therefore, it is needed to formulate an explicit GPR model and evaluate the performance by comparison with the general-purposed GPR model. Using the monitoring temperature and expansion joint displacement data from the TKB, an L-GPR will be formulated to establish the relationship between variables and predict the expansion joint displacements under designed extreme temperatures.

(ii) Development of a generalized linear GPR model based on the explicit definition of model functions using the lateral displacement and wind data from the TMB. A simple linear relationship may not be adequate in practice, therefore a generalized model is needed. Based on the simple linear model, a generalized linear model is extended by a projection of variables before the linear combination. The projection is flexible to any functions thus the generality still holds. Using the lateral displacement and wind data from the TMB, a generalized linear GPR model is formulated to model the polynomial relationship (P-GPR) between the variables and the performance comparison between the explicit P-GPR and the general-purposed GPR is evaluated.

Finally, the structural health evaluation and prediction will be realized using the generalized linear GPR model.

1.3 Thesis Organization

This thesis comprises five chapters. A brief description of each chapter is provided in the following.

Chapter 1 gives an introduction to the research background and the research objectives of this MPhil study. The outline of the thesis is provided.

Chapter 2 reviews the important literature relevant to this MPhil study. The SHM techniques and structural response measurements including temperature monitoring, wind monitoring, and displacement monitoring are introduced. To evaluate the structural health condition, reliability theory as a probabilistic performance measurement is introduced. Condition assessment methods including traditional inspection-based and SHM-based are reviewed. Compared with traditional subjective inspection methods, SHM techniques provide more accurate and objective condition assessments. In the last part, supervised learning methods are introduced. Supervised learning algorithms especially GP contribute to different SHM-based condition assessment and damage detection approaches.

Chapter 3 focuses on the development of a linear GPR (L-GPR) model, to characterize the linear relationship between the temperature and expansion joint displacement

using the monitoring data from the TKB. Apart from a general-purposed GPR model with squared exponential (SE) covariance function (SE-GPR), the explicit covariance function is derived for the L-GPR model. The hyperparameters in two GPR models are optimized using the log marginal likelihood maximization method. The performance of the optimized L-GPR and SE-GPR models are evaluated using the same sample data set. The outperformed GPR model is selected to further predict the expansion joint displacement under extreme design temperature. And the structural health condition is examined by comparison with the designed allowable maximum and minimum values.

Chapter 4 further extends the L-GPR model proposed in Chapter 3 to a generalized linear GPR model. Before applying simple linear model, the inputs are first projected into some high dimensional space based on a set of basis functions. The covariance function for a generalized linear relationship is then derived and applied to a polynomial relationship. A polynomial GPR (P-GPR) model is formulated to establish the relationship between the lateral displacement and wind load using monitoring data from the TMB. Polynomial relationship with first three orders are considered and the most suitable model is selected based on the criteria including log marginal likelihood and root mean square error. The outperformed GPR model is further used to predict the lateral displacement under extreme design wind speed and wind direction. The predicted total displacement is compared with the designed allowable value to examine the structural health condition.

Chapter 5 summarizes all the contributions, findings and conclusions achieved from theoretical researches and corresponding applications in this MPhil study, with regard to the research objectives. Recommendations for future works are also provided.

CHAPTER 2

LITERATURE REVIEW

2.1 Structural Health Monitoring

Civil infrastructure plays an important role in the society. To enhance the quality of life and protect the vast investment, safety and serviceability of the infrastructure deserve special concerns. Under in-service circumstances, infrastructures are subjected to material deterioration, structural damage, and adverse environmental impacts from time to time. All those factors which have influences on the nature and degradation degree of the in-service infrastructures may finally lead to the unserviceability of the structure. On purpose of ensuring the safety of these public assets and providing efficient maintenance, it is of great importance to conduct structural condition assessment of in-service civil structures during their operation (Aktan *et al.*, 1996; Yanev, 2003; Ratay, 2005; Brownjohn, 2007). Traditional visual inspection can detect damage when it becomes visible. It also requires the inspectors to assess the structural elements based on experience, which makes the inspection limited and subjective (Aktan *et al.*, 1997; FHWA, 2001).

Concerning objective measuring of structural conditions, there has been growing awareness of integrating structural health monitoring (SHM) with condition assessment (Aktan *et al.*, 2000; Wong & Ni, 2009). With the development of sensor

technologies such as fiber optical sensors (Ansari, 2009; Villalba & Casas, 2013), piezoelectric sensors (Santoni *et al.*, 2007; Laflamme *et al.*, 2012), wireless sensors (Cho *et al.*, 2010; Chae *et al.*, 2012), vision-based sensors (Park *et al.*, 2010; Jahanshahi & Masri, 2012), and so on, field monitoring data including load effects and structural responses of instrumented structures can be continuously provided. By integrating advanced technologies in sensing, data acquisition, data processing and analysis, communication, and information management, SHM provides structural behavior information and allows to assess the in-service structure performance in real time (Mufti, 2002; Pines & Aktan, 2002; Chang *et al.*, 2003; Sohn *et al.*, 2003; Worden & Dulieu-Barton, 2004; Ko & Ni, 2005; Wu & Fujino, 2005; Brownjohn and Koo 2010; Ou & Li, 2010; Ni *et al.*, 2011; Yun *et al.*, 2011). In such way, the loading conditions and resistance of the structure are successively updated and the health status of the structure can be traced in a real-time way. Structural condition assessment with field monitoring takes the inherent uncertainties into consideration. By using the site-specific monitoring data, uncertainties and inaccuracies in modeling the operational live loads can be reduced, and therefore a more accurate and objective structural condition assessment can be achieved. With an instrumentation system, appropriate maintenance actions can be executed with regard to the in-service conditions of the structure throughout its life cycle (Frangopol *et al.*, 2008; Zhu & Frangopol, 2013).

2.1.1 Temperature monitoring

Bridges are subject to varying environmental temperature. Due to the solar radiation and ambient air temperature, temperature of bridge components varies daily and seasonally. The temperature change in bridge components will induce the overall deflection and deformation of bridges significantly. If the bridge deformation is restrained, the thermal stress is induced by the structure indeterminacy and non-uniform temperature distribution. Extremely large thermal stresses can even damage the bridge. Due to the heat transfer, temperature is usually nonuniformly distributed at different locations over the entire structure and is different from the ambient temperature. Therefore, in many monitoring systems, temperature is frequently measured including both structural temperature and air temperature. With accurate temperature distribution over the structure, the thermal effect on the structural responses can be evaluated quantitatively.

Structural responses induced by temperature variation have been studied for a long time, including thermal behaviors such as longitudinal movements, thermal stresses based on numerical and experimental studies (Zuk, 1965; Capps, 1968; Priestley, 1978; Elbadry & Ghali, 1983). Bridge design code AASHTO (1989) has included provisions regarding bridge longitudinal movements due to thermal effects. With the development of SHM technology, bridge performance has been widely monitored with regard to the temperature-induced effects. Apart from the thermal effects on

longitudinal movements (Cheung *et al.*, 1997; Li *et al.*, 2008; Deng *et al.*, 2010), the structural vibration property variation due to temperature effects has also been studied for decades. Both laboratory experiments and field monitoring exercises have been reported concluding that the changing temperature condition has a significant influence on structural vibration properties. The relationship between temperature variation and the structural vibration properties was first studied by Adams *et al.* (1978) as a pioneer study, focusing on the axial resonant frequency change of a bar related to temperature variation. After continuously monitored for nearly a year (Peeters & De Roeck, 2001), the first four vibration frequencies of the Z24 Bridge in Switzerland were found varing about 14~18% during the one-year monitoring period. A study on the Confederation Bridge showed that during a six-month period, the girders temperature varied from -20 °C to +25 °C, while the frequencies varied about 5% (Desjardins *et al.*, 2006). Xia *et al.* (2006) studied the effects of temperature variation on vibration properties including frequency, mode shape, and damping ratio using a continuous concrete slab. The significant variation caused by temperature effect may even mask the damage incurred on the bridge if the damage only caused insignificant frequency changes (Farrar *et al.*, 1994; Xia *et al.*, 2006).

In SHM systems, the temperature monitoring sensors are usually deployed at a few limited locations. In order to obtain the temperature distribution across the entire bridge, heat transfer analysis is of great importance. With the development of analysis methods and aid of computer technology, 1D to 2D finite element models have been

developed for the temperature distribution of structure components (Elbadry & Ghali, 1983; Wang, 1994). The finite difference heat flow models have also been studied for the temperature distribution on bridge members (Riding *et al.*, 2007). With temperature distribution over the entire structure, the thermal effects on the structural responses can be evaluated quantitatively and accurately.

2.1.2 Wind monitoring

For structures built in a wind-prone region, wind environment around the structure is particularly crucial for the structure safety and should be monitored. Due to global climatic change, typhoons become stronger and more frequent than ever before. Large civil structures built in strong wind regions are vulnerable to wind-induced damage. Strong wind may induce unexpected loadings, cause bridge instability and excessive vibrations, and subsequently threaten the bridge functionality and safety. Because of the location attitude of bridge structures, the wind characteristics at boundary layer are usually used to represent the wind environment around the bridges. The wind loads acting on a large structure can be categorized as static forces due to mean winds, and dynamic loadings including buffeting excitations which are caused by fluctuating forces from turbulence, flutter instabilities which occur at very high wind speeds due to the self-excited aerodynamic forces, and vortex shedding excitations which usually occur in low wind speed and low turbulence conditions. All these loadings will either come alone or as a combination (Cai and Montens, 2000; Holmes, 2015).

For large-scale bridge structures, especially cable-supported bridges which are more flexible, appropriate wind tunnel tests are usually required during the design stage, in order to simulate the wind environment, determine the wind characteristics, examine the bridge responses under various winds, and ensure an appropriate design of the entire structure. With the development of SHM technology, the field wind monitoring can provide accurate information on real wind environment and therefore contribute to the bridge vibration behavior analysis. Anemometers are widely used as traditional sensors for wind monitoring, which usually includes wind speed and wind direction. Researches have been reported on extracting the wind components using the measured wind data obtained from propeller anemometers and ultrasonic anemometers (Xu & Zhan, 2001; Xu & Chen, 2004). Sometimes wind pressure transducers are deployed to study the wind load and its distribution on a particular part of the bridge structure. The locations of the pressure transducers should be appropriately selected to eliminate possible disturbances from ambient structure components.

Usually the wind loads within boundary layer are assumed to be ergodic or stationary random process. Under typhoon conditions, however, this assumption may fail, especially at the regions with complex terrain (Kareem, 2008). The longitudinal turbulence components induced by the longitudinal wind speed may not agree with Gaussian distribution. With the measured wind data during typhoons, the existing stationary wind model was verified. According to Schroeder *et al.* (1998), traditional methods may overestimate the turbulence intensity from the wind loads. To overcome

this problem, Xu & Chen (2004) proposed a non-stationary wind model to obtain proper wind characteristics from the monitoring wind data.

Moreover, the wind induced vibration responses also contribute to the structure fatigue. Fatigue assessment and bridge integrity assessment have been studied with the measured wind environment taken into account. Fatigue analysis due to buffeting effect has been conducted for the Normandy Cable-Stayed Bridge in France, but the background of buffeting responses and wind direction were not considered (Virlogeux, 1992). Later a wind-induced fatigue damage study has been carried out on Yangpu Cable-Stayed Bridge in Shanghai, China, considering both the background component and wind direction effects. It was found that the wind direction has a significant influence on the bridge fatigue damage, but the predicted life based on wind-induced effect is much longer than the designed bridge life cycle (Gu *et al.*, 1999). The typhoon-induced fatigue was evaluated by Li *et al.* (2002), using the monitoring data from the Tsing Ma Bridge (TMB) under one typhoon event. With long-term SHM monitoring, Xu *et al.* (2009) extended the continuum damage mechanics method to evaluate the long-term fatigue damage of the TMB.

2.1.3 Displacement monitoring

As a geometry configuration, bridge displacement reflects the bridge structure performance condition effectively. Any structural response, no matter dynamic or static, leads to displacement. Large displacement or deformation caused by any reason

may threaten the normal operation of the bridge. Excessive displacement can even damage the bridge. Therefore, the displacement monitoring is needed in SHM. Traditional displacement transducers are often used to measure the movement of the key components of a bridge, for example the relative displacements between the towers and bridge deck. With technology development, the global positioning system (GPS) technique has become a common way to measure the displacement responses. With the assistance of real time kinematic technique, the nominal accuracy of GPS can achieve 1 cm $\pm$ 2 parts-per-million (ppm) in horizontal direction and 2 cm $\pm$ 2 ppm in vertical direction. To assess the measurement accuracy of static and dynamic displacement using GPS technique, motion simulation tables have been developed in three orthogonal directions for civil engineering application (Chan *et al.*, 2006).

Among other types of sensory systems, GPS is a powerful tool to measure both static and dynamic displacement responses of civil structures and has been widely applied to long-span bridges (Ashkenazi & Roberts, 1997; Fujino *et al.*, 2000; Miyata *et al.*, 2002; Ni *et al.*, 2004; Guo *et al.*, 2005). As a supplement to the Wind and Structural Health Monitoring System (WASHMS) instrumented on three cable-supported bridges in Hong Kong, a GPS system has been deployed to monitor the displacement response of the bridge towers, cables and deck (Wong *et al.*, 2001; Wong, 2004).

The bridge displacement response reflects the structural performance and bridge integrity condition. Static displacement induced by thermal effects is an important

indicator which needs to be monitored. With the development of SHM techniques, the temperature effect on bridge displacement has been monitored in-situ on concrete bridges (Cheung *et al.*, 1997; Li *et al.*, 2008; Deng *et al.*, 2010). An integrated approach combining the temperature distribution with the structural model was applied to the TMB field monitoring data to quantitatively monitor and assess the thermal effects on the displacement and other properties of the bridge (Xu & Xia, 2011).

The dynamic displacement contributes to the railway traffic load monitoring and vehicle traffic load monitoring, with different patterns. For bridge systems coupled with railway vehicle suspension, dynamic displacement analysis together with acceleration, and stress response analysis are important to evaluate bridge safety and vehicle comfortability (Frýba, 1996). A mathematical model was formulated by Diana and Cheli (1989) to accurately describe the bridge and train dynamic behaviors, considering the nonlinearity of the system including geometrical nonlinearity in the contact between wheel and track. The bridge vibration due to trains moving at high speeds was studied by modeling the bridge as a simple beam (Yang *et al.*, 1997). A computer-aided mode superposition method was applied to monitor the dynamic interaction of long-span suspension bridges with running trains (Xia *et al.*, 2000). The mode superposition method was then developed for a coupled railway vehicle long suspension bridge systems, considering the displacement, acceleration, and stress responses (Li *et al.*, 2010; Xu *et al.*, 2010). With GPS techniques, the deflections and

the resonant frequency of the Humber Bridge in UK were measured under known loading conditions applied by vehicles groups. The GPS measured results had close agreement with measurements from conventional methods and prediction results from a finite element model (Brown *et al.*, 1999).

The displacement induced by wind is usually a combination of static displacement and dynamic displacement. Displacement transducers are widely used as traditional sensors for displacement monitoring. The displacement transducer is capable of measuring the wind-induced dynamic displacement responses. But it may have difficulties in measuring the displacement varying at a very long period, for example the absolute static or quasi-static displacement responses of the bridge deck and towers. Therefore, the GPS technique is preferred for monitoring wind-induced displacement. The GPS technique was proven to have capability to monitor both dynamic and static displacement responses by its application to a long-span suspension bridge (Fujino *et al.*, 2000). The displacement of Humber Bridge in UK was monitored using GPS technique, and remarkable accuracies of the order of a few millimeters in all three directions were achieved, under both weak wind and strong wind conditions (Ashkenazi & Roberts, 1997). The GPS measured displacement under a couple of strong typhoons was analyzed focusing on a power spectral density (PSD) and spatial correlation of wind-speed fluctuation, and response of the deck (Miyata *et al.*, 2002). The total displacement response monitoring is essential for monitoring the structural

performance condition and evaluating the bridge structural integrity, and is of great importance for the disaster prevention assessment.

2.2 Structural Reliability and Condition Assessment

2.2.1 Structural reliability

Uncertainty is inevitable in bridge design and evaluation, and may exist in factors such as the operational loadings, geometries, material resistances, structural models, and deterioration mechanisms. The uncertainty is usually characterized by the probability distributions. The significance of uncertainty affects the determination of structural safety level. Safety factor was used to quantify the uncertainties based on past experiences and expert opinions. However, it cannot provide consistent safety evaluation on different structure types and may result in inadequacy in structural design. To provide a rational approach accounting for the uncertainties, the structural reliability theory was developed in engineering fields. In late 1970s, the reliability concept was introduced into civil structure design codes, such as the building design code in the USA (Ravindra & Galambos, 1978; Ellingwood, 1980; Ellingwood *et al.*, 1982), and the Ontario highway bridge design code in Canada (Nowak & Lind, 1979). After that the reliability theory has been gradually applied in the design and assessment specifications of civil structures (Ang & Tang, 1984; Madsen *et al.*, 2006; Ayyub & McCuen, 2011; Nowak & Collins, 2012; Thoft-Christensen & Baker, 2012; Thoft-

Christensen & Murotsu, 2012). These applications have improved the structural design in terms of safety, serviceability, and durability.

The reliability of a system is a probabilistic measure of the performance, which is defined as the probability that it will appropriately perform its specified function for a specified period of time under a specified set of environments and conditions (Leemis, 1995). The reliability can be expressed as

$$R = 1 - P_f \tag{2.1}$$

where R is the reliability, and P_f is the probability of failure. The reliability can be explained as the probability that unsatisfactory performance or failure will not occur.

In practice, the joint probability distribution in the probability of failure P_f is usually unavailable due to insufficient data and difficulty in numerical integration of the probability distribution function (PDF). To overcome these limitations, the reliability index is adopted to indirectly evaluate the probability (Ang & Tang, 1984). There are two methods for calculating the reliability index, including numerical approximation method and simulation method. The numerical approximation of reliability index calculation was performed by Cornell (1967), who estimated a linearized limit state function at the points corresponding to the mean values using the reduced variables, instead of the most probable failure points. Hasofer *et al.* (1973) proposed a method using the most probable failure points. Later Rackwitz and Flessler

(1978) extended the approach by transforming the uncorrelated random variables of various probability distributions into standardized normal distributions. When the random variables are correlated, a transformation procedure was used to first transform them into the uncorrelated standardized form (Hohenbichler & Rackwitz, 1988). The reliability index calculation only involves the first-order Taylor derivative and the second moment of the variables, thus it is called the first-order second-moment (FOSM) method. Extensive applications of this method have been reported in engineering fields (Tabsh & Nowak, 1991; Micic *et al.*, 1995; Enright & Frangopol, 1998; Estes & Frangopol, 1999; Akgül & Frangopol, 2004; Czarnecki & Nowak, 2008; Frangopol *et al.*, 2008; Nowak & Eamon, 2008). Advanced second moment methods were extended and achieved accurate results for nonlinear limit states (Hasofer & Lind, 1974; Ayyub & Haldar, 1984). Simulation methods are also used in calculating the reliability index, especially when it is difficult to apply the numerical approximation methods involving complex mathematical functions. The Monte Carlo (MC) simulation is one of the most popular algorithms (Melchers, 1999; Sundararajan, 2012). The MC method is realized by randomly sampling from the PDF to artificially simulate a large number of experiments and to observe the results (Melchers, 1999). When complex mathematical functions are involved in the reliability analysis, for example the inverse error function in the predictive models and conditional probabilities which contain intersection functions, it is extremely difficult to apply the numerical approximation method. In these cases, the MC method is more applicable.

When using the MC method in structural reliability analysis, samples of each variable x_i are generated first, and the performance function $g(\mathbf{x})$ is evaluated based on different sets of the generated random variables. For a simple MC method application, the failure probability can then be given by approximation as

$$P_f \approx \frac{n(g(\mathbf{x}_i) \leq 0)}{N} \tag{2.2}$$

where N is the total number of random sampling simulations, and $n(g(\mathbf{x}_i) \leq 0)$ is the number of sets when $g(\mathbf{x}_i) \leq 0$ (Melchers, 1999; Nowak & Collins, 2012).

In civil engineering, the structural performance is usually described by limit states, including ultimate limit state, serviceability limit state, and fatigue limit state. The ultimate lime state indicates the structural capacity loss, such as failure, deficiency in structural resistance, and structure collapse. The serviceability limit state refers to the unfulfilled service demand, such as excessive deformations and vibrations which cause the structure unserviceable. The fatigue limit state refers to the strength loss under repeated loadings. Structures usually suffer from different failures, including strength-based analysis, compressive or tensile, flexural, shear, and torsional failures. In the reliability analysis, all the failure modes should be considered and treated separately. Therefore, structural reliability in civil engineering refers to the probability that a structure will not violate a specified failure mode corresponding to a specified limit state during a specified period of time (Rafiq, 2005).

Due to the materials aging, operational loadings and environments, the civil structures experience deteriorations and the structural resistance decreases over time. As the loading and environmental conditions are inconstant and may change with time, the reliability of a structure over its service time is usually not constant and changes with time. The deterioration of different construction materials has been widely studied. The deterioration of concrete has been extensively studied and several mechanisms have been revealed (Brown, 1987; Basheer *et al.*, 1996). The steel corrosion progress was studied and the corrosion model predicting corrosion time and location was developed for steel girders by Albrecht and Naeemi (1984) first and later improved by Thoft-Christensen *et al.* (1996).

The structural performance function in civil engineering, also called limit state function or safety margin, is often written as

$$M(t) = R(t) - S(t) \tag{2.3}$$

where $M(t)$ is the safety margin of a specified failure mode, $R(t)$ is the time-dependent resistance, and $S(t)$ is the time-dependent load effects. All the uncertainties in resistance including the materials mechanical properties and the structure geometry are incorporated into $R(t)$. While the uncertainties in loading effects such as axial forces, bending moments, shear forces, torsion angles are incorporated into $S(t)$.

In engineering applications, the time-dependent factors sometimes are simplified to time-independent. When the resistance is treated as time-invariant for a given time period T with load effects still time-dependent, the failure probability is defined as the probability when the resistance cannot provide capacity for the maximum load effects during the time period T, which can be expressed as

$$p_f(T) = p\left[\min_{0<t<T} M(t) \le 0\right] = p\left[R \le \max_{0<t<T} S(t)\right] \tag{2.4}$$

When both the resistance and load effects are time-variant, but independent of each other, an upper bound approximation can be applied to reduce the problem to time-independent reliability analysis (Li, 2004)

$$M(T) = \min_{0<t<T} R(t) - \max_{0<t<T} S(t) \tag{2.5}$$

2.2.2 Condition assessment

2.2.2.1 Traditional inspection-based assessment

Data available for structural condition assessment are generally obtained from conventional visual inspections in conjunction with past experience and expertized opinions. Usually the inspection assessment is conducted on several key components and individual elements of the structure with standard rating systems. Traditional methods in general use condition rating index based on visual inspection results to measure the bridge resistance in regard to the remaining load-carrying capacity (Pontis, 2001). In USA, the bridge management systems (BMSs) are established to evaluate

the structural elements condition into discrete states considering the deterioration (Thompson *et al.*, 1998). The sufficient rating of the overall bridge condition combines serviceability and condition evaluation concerning the structural adequacy and safety, serviceability and functional obsolescence (FHWA, 2014). In UK, the visual inspection-based condition states are characterized for reinforced concrete elements under corrosion attack. The structure state is categorized into four discrete levels from 0 to 3, representing the corrosion levels of no chloride contamination, corrosion onset, cracking onset, and loose concrete or significant delamination, respectively (Denton, 2002). A condition state value larger than 3 represents an unacceptable condition state which needs to be repaired. Based on visual inspections and the rating index, the maintenance priority and strategy can be made by the bridge engineers and decision makers based on different components. Generally, the maintenance priority will be given to the civil infrastructure with unacceptable and poor condition rating levels which needs to be repaired immediately.

However, the traditional visual inspection can detect damages such as cracks, spalls, chemical deterioration, and corrosion only when it becomes visible. It also requires the inspectors to assess the structural elements based on experiences (Aktan *et al.*, 1997; FHWA 2001). Nevertheless, the relationship between visible damage signs and the bridge condition is often very difficult to establish and the actual infrastructure safety condition level might be determined inaccurately. For example, if corrosion occurs on the embedded reinforcement of a reinforced concrete, although it is invisible,

the structure with satisfactory visual condition states may actually be unsafe. Then safety concerns may raise to identify the embedded flaws inside the structure. Meanwhile, if a poor visual inspection condition is detected, but only on the surface, the structure may still be safe, leading to a false positive inspection result. As a limited and subjective measure, the condition index based on visual inspections on the surface may not accurately reflect the true resistance of structural members and hence decision making on management has to be carried out by heuristic and experiences (Aktan *et al.*, 1997).

Efforts have been made to make the visual inspections more accurate. Approaches such as fuzzy logic method (Liang *et al.*, 2001; Sasmal & Ramanjaneyulu, 2008) and neural network method (Cattan & Mohammadi, 1997; Kawamura *et al.*, 2003), have been attempted. Since these methods still base on the visual inspection results, the shortcomings mentioned above cannot be avoided.

2.2.2.2 SHM-based assessment

Concerning objective measuring of structural conditions, there has been growing awareness of integrating SHM with condition assessment (Aktan *et al.*, 2000; Wong & Ni, 2009).With advanced technologies in sensing, data acquisition, data processing and analyzing, communication, and information management, SHM provides rich information on bridge structural behavior conditions and allows to assess the structural performance condition in real time (Chang & Lee, 2002; Mufti, 2002; Pines & Aktan,

2002; Sohn *et al.*, 2003; Worden & Dulieu-Barton, 2004; Ko & Ni, 2005; Brownjohn, 2007;Ou & Li, 2010; Yun *et al.*, 2011). In addition, the structure can be monitored in a localized or globalized way without the limitation of traffic restriction or closure. In such way, the resistance and load effects of the in-service structure are successively updated and the health status of the structure can be traced in a real-time way. Structural condition assessment with field monitoring takes the inherent uncertainties into account. By using the site-specific monitoring data, modeling inaccuracy in live load characterization can be reduced, leading to a more accurate and objective structural condition assessment. With an instrumented system, appropriate maintenance actions and strategies can be arranged according to the bridge in-service conditions during the entire life cycle (Frangopol *et al.*, 2008; Zhu & Frangopol, 2013).

In the past decades, vibration-based damage detection methods have been developed usually based on physical properties changes, mainly in two categories: parameter identification (Carden & Fanning, 2004; Friswell, 2007; Catbas, 2009) and pattern recognition (Worden & Manson, 2007; Sohn & Oh, 2009; Gul & Catbas, 2010). Theoretical and experimental researches provided foundations of the underlying philosophy with regard to the vibration-based damage detection, but the assessment of structural damage in large-scale bridges is still challenging in practice. Success has been shown in simulations, experimental studies and field applications under controlled conditions such as the Z24 Bridge (Maeck *et al.*, 2001). The effectiveness of damage detection methods still needs to be examined for practical in-service civil

structures (Brownjohn, 2007). In practice, due to the interference of environment and operational loadings and large scale of long-span bridges, it is significantly challenging to detect damage through the SHM data. An experimental verification of vibration-based damage detection method on a large-scale structure showed that modal characteristics are insensitive to localized structural damage (Friswell & Penny, 1997).

In addition to the valuable vibration responses in condition assessment, in-service monitoring data of strain response is also one of the most important measurements in structural condition assessment, inspection, and decision making on maintenance of structures (Ni *et al.*, 2011; Xia *et al.*, 2012). Strain data can directly indicate the performance and safety reserve of a bridge component (Bergmeister & Santa, 2001; Koshiba *et al.*, 2001), and provide information on the resistance capacity of the entire bridge. In addition, strain measurements would be better suitable for local damage assessment on the bridge structures than vibration data. In practice strain sensors are intentionally placed at critical locations on a bridge where large strains are expected to be observed and may exceed the material resistance (Chakraborty & DeWolf, 2006). Strain response can provide operational stress information at the monitored structure location, and is able to characterize local damage when strain gauges are appropriately deployed.

For newly-built structures where the term “damage” is inappropriate, a number of condition assessment methods have been developed by incorporating SHM data into reliability theories in recent years (Peil, 2005; Catbas *et al.*, 2008; Frangopol *et al.*, 2008; Hosser *et al.*, 2008). The reliability-based condition assessment has the capability to accommodate the uncertainties in both structure parameters and long-term monitoring data (Lark & Flaig, 2005; Nowak & Czarnecki, 2005; Wisniewski *et al.*, 2009). With long-term SHM data, the structural reliability can be updated continuously by the Bayesian statistical inference. This concept has been applied in NDE-based fatigue reliability updating (Zheng & Ellingwood, 1998; Zhang & Mahadevan, 2000). A methodology for effectively incorporating the data collected through in-service health monitoring to update the performance prediction was developed by Rafiq (2005).

2.3 Supervised Learning

2.3.1 General approaches

Condition assessment and damage detection are generally conducted based on two approaches: model-driven methods and data-driven methods. Model-driven methods are based on the physical model establishment for the target structure with high accuracy, usually involving finite element modeling. The abnormality detection can be achieved by comparison between the model and the measured data from the real structure. For a model corresponding to a structure under normal condition, any

abnormal responses deviated from the normal condition model can be inferred as damage. Data-driven approaches are based on statistical models representing the system using the monitoring data from the target structure. For example, a probability density function can be established for a system under the normal condition. Deviations from the normal condition model are detected when the measured data have different probability distribution from the normal condition. Data-driven approaches have been studied for years, mainly drawn from pattern recognition discipline, or more broadly, the machine learning discipline (Worden & Manson, 2007).

The machine learning problems attempt to establish the computational relationships between monitoring variables. Classic computation performs the variables calculation based on the mathematic algorithms with pre-defined instructions. On the contrary, in machine learning problems the computational rules are inferred or learned from the observed evidence. Machine learning theory has drawn attentions focusing on problems including classification, regression, and density estimation (Cherkassky & Mulier, 2007). The classification problems aim to assign a set or vector of inputs with a class or a label. The observations may be sparse for a classification problem. The regression problems aim to construct a mapping relationship between a group input variables and an output variable using the observation samples. Density estimations aim to estimate the probability density function for the variables from observation samples. These problems have increasing difficulty from classification to density estimation (Vapnik, 1998).

Based on the algorithm learning outcomes, machine learning problems can be classified into unsupervised learning and supervised learning. The unsupervised learning aims to characterize the measurement variables and study on the structure behind the measurements. The supervised learning focuses on the establishment of relationships between the input and output data. The unsupervised learning framework is suitable for density estimation problems, while the supervised learning framework is usually for regression problems with continuous outputs, or classification problems with discrete outputs.

Manson *et al.* (2003a, 2003b) and Worden *et al.* (2003) developed robust SHM-based novelty detection methods, and validated using experiments on real aircraft structures. The features for novelty detection were first extracted from the raw data signals. Then a novelty detector was constructed by learning the particular characteristics of the given dataset in an unsupervised manner. When new data samples are acquired, the characteristics can be tested and compared with the given dataset. Only samples from the normal condition were used for characterization, while no samples of data from the damaged structure were used in the unsupervised learning. An outlier analysis was proposed and the training data were assumed to be multivariate Gaussian distributed (Worden & Manson, 2007). The calculations of threshold levels were provided by Worden *et al.* (2000). When the assumption is not the case, complicated probability density functions were introduced, for example the Kernel Density Estimation (Silverman, 1986). Other possible unsupervised learning techniques applied to novelty

detection includes artificial neural networks (Nairac *et al.*, 1997), support vector machines (SVMs) (Manevitz & Yousef, 2001), etc.

When the damage existence is known, the research focuses move on to the damage localization problem. With damage occurrence detected, machine learning has also been applied to address the damage localization problem, which is the Level II in Rytter's damage hierarchy (Rytter, 1993). The damage localization problem can be achieved by the regression framework, where the output is set as the coordinate of the damaged structures. Owing to the restrictions upon actually damaging the structure, the damage localization problem can also be cast as classification problems (Worden & Manson, 2007). Worden and Staszewski (2000) proposed a classification framework for impact detection on a composite panel based on neural networks and genetic algorithms. The neural network used in their study was formulated based on the standard multi-layer perceptron (MLP) (Bishop, 1995), using nine novelty indices as inputs and the predicted damage class as output. The MLP networks successfully acted as a statistical classifier for damage class identification and also provided the estimated Bayesian posterior probabilities at the same time. Their results further proved that if the formulated network is trained to mapping each pattern vector to a class associated with the highest output, the network is equivalent to a Bayesian decision rule (Bishop, 1995).

The supervised learning also contributes to the next phase of damage assessment involving severity investigation (Manson *et al.*, 2002). Manson *et al.* (2002) casted the problem in a regression framework as a continuation of previous study, where the output damage class results from the MLP neural network were trained to establish the connection with the severity of the damage. After the novelty detection and damage localization study, the analysis moved to the damage severity assessment, still using the MLP neural networks as analysis tools. The regression framework was constructed to map the novelty indices to the damage severity. The neural network was formulated using the values of novelty indices as inputs and the predicted damage severity as output. The neural networks were trained and validated using training data and validation data respectively, and the performance of neural networks wasevaluated using testing data.

Doebling *et al.* (1996) summarized the initial efforts on damage identification problems before the year 1996. Later Sohn *et al.* (2003) expanded the survey and showed more research efforts between 1996 and 2001. Apart from the neural networks, SVMs become promising in the statistical learning theory fields. SVM-based models have been shown to have outperformance with higher accuracy than the neural networks in supervised learning problems in many cases (Cristianini & Scholkopf, 2002). Motivated by statistical learning theory, SVMs generalized the basic foundations of machine learning problems (Vapnik, 1998; Vapnik, 2013). The algorithm is defined to learn the relationship between two sets of data: *d*-dimensional

input data denoting as $\mathbf{x}$, and one-dimensional output denoting as y. Based on the two sets of training data $(\mathbf{x}_k, y_k); k = 1, \ldots, N$, the relationship is inferred. Without loss of generality, the algorithm is able to represent either regression problem or classification problem. If the output variable y is continuous, the SVM problem becomes one of the regression problems. If the output variable y is a class label, the problem becomes one of the classification problems. Worden and Manson (2007) has applied SVM as a classifier to the same damage identification problem reviewed above. The SVM outperformed the MLP neural network and got higher percentage of correct classifications than the MLP neural network. As a universal algorithm, the SVM approach has ability to easily fit the polynomial or neural network discriminants. This feature allows SVM approach to be optimized easily based on its model basis. In addition, the SVM approach has a convex quadratic characteristic and therefore it always has only one global minimum point.

2.3.2 Gaussian process

In recent years, Gaussian process (GP) has received increasing attention to solve difficult machine learning problems in the community. GP serves as a promising Bayesian machine learning approach by defining a prior distribution over the function spaces. The GP models are effective because of their flexible non-parametric modeling features, which need no information on the physical structure of the system. Instead of defining parameter values in model formulation, a prior GP is directly defined over

function spaces with Mercer kernel functions and the Bayesian framework for probabilistic inference. GP is an effective approach to model function distributions with given mean and covariance functions. Given a set of observation samples, GP enables to learn the posterior distribution of the target function and estimate the values of the function at other unobserved points. Based on its characteristics, GP provides simple and effective solutions for regression and classification problems in probabilistic manners. Besides the estimated means of the function values, GP also provides the optimized model parameters based on the log marginal likelihood maximization methods. Casted in a Bayesian framework, GP probabilistic model enables to estimate the uncertainty during the prediction procedures. In addition, the data-driven feature of GP makes it unrestricted and suitable for any algebraic structure and thus ensures a high modeling flexibility and great expressive power. For these reasons, GP models become very popular in machine learning and regression problems. Studies of GP have been reported on establishment of spatial or temporal relationships between multivariate random variables.

The idea of using GP as prior distribution defined directly over functions was motivated by Neal (2012), who introduced the priors over weights into artificial neural networks. The kriging model, which is similar to GP, has been used for spatial data characterization since a long time (Cressie, 2015). In GP, the function output $f(x_i)$ is defined as a collection of random variables corresponding to the input x_i in a more formal way. Any infinite subset of the function outputs is assumed to have a joint

multivariate Gaussian distribution (Rasmussen, 1997). Recently a thorough overview of GP methods and relevant modifications has been provided by Rasmussen and Williams (2006). After the GP was expressed as a general-purpose framework, research interests have been focused on GP models for supervised learning problems including regression and classification. The connection between GP method and other machine learning methods such as multilayer perceptron, spline interpolation, or SVMs have been interpreted. The equivalence between GP models and neural networks has been proven by Neal (2012), on condition that the neural network is formulated with one hidden layer with infinite number of hidden neurons. After that, Rasmussen (1997) first introduced the empirical formulation of GP in a probabilistic form within Bayesian framework. A noise model has been developed and the prior probability distributions of input variables were defined using matrix operations. Later the connections between GP and other machine learning methods such as generalized Radial Basis Functions (RBF), spline smoothing techniques and SVMs were interpreted by MacKay (1997) and Seeger (2004).

In spite of all the advantages and interesting features of GP, shortcoming exists making the application of GP limited. The problem is that practical applications of GP from the massive measured data are inevitably hindered by the prohibitive cost of the required computations. The naive implementation of GP requires computational cost of $O(n^3)$, where n is the number of training cases (Rasmussen & Williams, 2006). Given a large number of sample observations, exact inferences in normal GP will

become intractable. Therefore, the effective computation simplification methods of the GP framework have gain attention to make GP framework more suitable for practical use.

Approximation algorithms are good choices for computation simplification. Over these years, various approximation methods based on sparsity have been proposed to reduce the computational costs of GP regression (Quiñonero-Candela & Rasmussen, 2005; Keerthi & Chu, 2006; Snelson & Ghahramani, 2006, 2007; Melkumyan & Ramos, 2009; Vanhatalo & Vehtari, 2012). Instead of using the entire training data set, most of the approximation algorithms estimate the posterior distribution based on a subset of training points. The key point of the sparse approximation algorithms is that only one subset of the latent variables is employed exactly, while the others are treated as approximation, thus the computational cost can be reduced. The subset used for training can be selected based on either the heuristics methods (Herbrich *et al.*, 2003; Seeger *et al.*, 2003), or the pseudo datasets obtained during the optimization of the hyperparameters using the log marginal likelihood maximization methods (Snelson & Ghahramani, 2006). In summary, the approximation techniques can be categorized into two cases: either based on sparse method approximating the full posterior with lower rank matrices, or based on the methods approximating the matrix–vector multiplication conjugate gradient. Other methods such as moving window strategy proposed by Wan and Ni (2017) treat the training data in piecewise, thus leading to a

considerable relief in the computational burden associated with the reconstruction of GP model.

As a very popular machine learning and regression model, GP has been increasingly used to for solving a wide range of engineering problems, such as model updating (Khodaparast *et al.*, 2011; Erdogan *et al.*, 2014; Wan & Ren, 2015), uncertainty quantification (Fricke *et al.*, 2011; Wan *et al.*, 2017a), and sensitivity analysis (Rohmer & Foerster, 2011; Wan & Ren, 2014; Wan *et al.*, 2017b).

Not many applications of GP exist in the SHM scientific literature. Hensman *et al.* (2010) proposed the use of single target GP in complex structures for locating stress waves using thermoelastic expansion with a high-power laser, to effectively detect damage without incurring the additional complexity of basis function placement. The GP model with RBF kernels was formulated for relationship regression and the data for all possible combinations of sensors were trained in the GP model as different subsets. In the GP regression model, the time differences of laser flight between sensors were treated as input data, and the ultrasonic stimulation locations were treated as target outputs. The performance of GP to determine the testing locations was evaluated using testing data. It was found that the GP successfully learned the mapping structure and could be generalized for prediction effectively. Torres-Arredondo and Fritzen (2012) reported an impact stress waves monitoring and studied an automatic approach for impact magnitude estimation and localization in isotropic structures

based on Bayesian analysis with single target GP. Anderson *et al.* (2014) integrated GP into a structural dynamic analysis framework using spatial maps of frequency-domain features.

Studies have been reported on GP serving as a structural health prognosis approach. As a data-driven method, GP is capable of predicting the system status under the unobserved conditions or in the future, using information from the monitoring data. Therefore, it has advantages when the system is complex and no simple physical model is available. Mohanty *et al.* (2009) proposed a life prognosis method for metallic structure based on a nonlinear GP model to study the relationship between fatigue affecting variables and crack growth of the metallic structure. Liu *et al.* (2010) proposed a prognosis approach to estimate the residual useful life (RUL) of a composite specimens in real time. The prognosis approach was based on an off-line GP model to estimate the cumulative fatigue damage under test fatigue loading. The damage states of future stage were then updated using GP model and thus the condition based prognosis was achieved. More recently, Gaussian process regression (GPR) has been used for damage progress prediction using cracks in aluminum specimens (Mohanty *et al.*, 2011). Comparative studies have been reported on the data-driven techniques for prognostics including SVM, GPR, and neural network-based approaches (Goebel *et al.*, 2008; Srivastava & Das, 2009).

2.4 Summary

This chapter reviews important literature relevant to this thesis. The SHM techniques and structural response measurements including temperature monitoring, wind monitoring, and displacement monitoring are introduced. To evaluate structural health condition, reliability theory as a probabilistic measure of the performance is introduced. Condition assessment methods including traditional inspection-based and SHM-based are reviewed. In comparison with traditional subjective inspection methods, SHM techniques provide more accurate and objective condition assessments. SHM captures the structural responses of bridges continuously, and is expected to make contributions to structural condition assessment for the safe operation of the structure.

In the last part, supervised learning methods are introduced. Supervised learning algorithms especially GP in particular contribute to different SHM-based condition assessment and damage detection approaches. The conventional methods such as artificial neural network and support vector machine are capable of modelling different kinds of relationships. However, these methods process data with deterministic parameters, and have difficulties in determining the uncertainties. In contrast, the Bayesian approach provides a probabilistic treatment where the uncertainties can be estimated during the prediction process, and maintains high flexibility at the same time.

Therefore in this study, the GP is focused on as a promising Bayesian machine learning tool.

As a promising supervised learning approach, there is growing interest in integrating GP with SHM data for structural health evaluation. Due to the flexibility of GP models, the general-purposed model formulation may not be adequate enough for SHM problems with known priors. Therefore, explicit model formulations need to be established. This MPhil study aims to develop a structural health evaluation and prediction method based on GP models together with the monitoring data from cable-supported bridges in Hong Kong. As a result of the literature review, critical issues in this MPhil study are listed below.

(i) Development of a linear GPR (L-GPR) model based on the explicit definition of model functions. The GPR model with general-purposed model functions have been used in most of the studies. But GPR models with explicit key function definitions are seldom studied. Therefore, it is needed to formulate an explicit GPR model and evaluate the performance in comparison with the general-purposed GPR model. Using the monitoring data of temperature and expansion joint displacement from the TKB, an L-GPR will be formulated to establish the relationship between variables and predict the expansion joint displacements under designed extreme temperatures.

(ii) Development of a generalized linear GPR model based on the extension of L-GPR and explicit definition of model functions. A simple linear relationship may not be adequate in practice, therefore a generalized model is needed. Based on the simple linear model, a generalized linear model can be extended by a projection of variables before the linear combination. The projection is flexible to any functions and thus the generality still holds. Using the lateral displacement and wind data from the TMB, a generalized linear GPR model will be formulated to characterize the polynomial relationship (P-GPR) between the data and the performance comparison between the explicit P-GPR and the general-purposed GPR will be evaluated. The structural health evaluation and prediction will be realized using the generalized linear GPR model.

CHAPTER 3

SHM-BASED CONDITION ASSESSMENT OF BRIDGES USING L-GPR MODEL

3.1 Introduction

Civil structures suffer from severe operational loads and complex environmental influences which make them deteriorate once they are built. The deterioration over time leads to the concern regarding the safety and serviceability of in-service infrastructure. The structural condition evolution deserves continuous monitoring, in order to make effective maintenance and management arrangements of the infrastructure assets (Yanev, 2003; Ebeling, 2004; Ko & Ni, 2005; Ratay, 2005; Brownjohn, 2007; Xia *et al.*, 2012). The continuous evolution monitoring is of great value for the well-being of people, protecting significant capital investments, and promoting the regional and national prosperity. With various types of sensors, structural monitoring becomes popular and can provide engineers with rich information on structural condition for health assessment (Catbas & Aktan, 2002; Chang *et al.*, 2003; Sohn *et al.*, 2003; Ni *et al.*, 2011). By integrating the monitoring data from an online structural health monitoring (SHM) system, the structural condition of the monitored structure can be assessed and the health status can be evolutionarily traced (Wong, 2004; Lin *et al.*, 2005; Mohamad *et al.*, 2011; Zhou *et al.*, 2014).

Bridges are subject to varying environmental temperature. Due to the solar radiation and ambient air temperature, temperature of bridge components varies daily and seasonally. The temperature changes in bridge components will induce the overall deflection and deformation significantly, especially for long-span bridges. Expansion joints, which are designed to accommodate the relative movements between bridge decks and their abutments, are important components in bridge structures. The movement at expansion joint for a 500 m long concrete bridge was measured about 226 mm during a three-year period (Cheung *et al.*, 1997; Li *et al.*, 2008). For long-span Runyang Suspension Bridge with a 1490 m main span, the measured seasonal longitudinal displacement was reported to be about 500 mm (Deng *et al.*, 2010).

The expansion joint becomes a vulnerable part of bridges due to its structural characteristics and the passing-by traffic loads impacts, especially in long-span bridges, resulting considerable repair and maintenance costs (Roeder, 1998; Chang & Lee, 2002; Lima & de Brito, 2009; Guo *et al.*, 2014). According to the records, repair actions of the expansion joints at Runyang Suspension Bridge ware taken two years after the bridge was open to traffic. The expansion joints at Jiangyin Suspension Bridge were reported to have excessive wear and transversal shear failure of bearings several years after it opened to service. The expansion joints were maintained and repaired several times and finally got replaced in August 2007 (Guo *et al.*, 2014). These maintenance and failures show the importance of health status of the expansion joints.

The development of SHM enables to gain insight into the in-service performance of bridges. Based on the long-term monitoring data from SHM systems, research efforts have been made to condition assessment of bridge expansion joints. Ni *et al.* (2007) proposed a procedure for the condition assessment of the expansion joints under extreme conditions, using the monitored displacement and temperature data from the Ting Kau Bridge (TKB). A linear relationship was shown in their study between the expansion joints displacement and the temperature. The maximum expansion joints displacements under extreme conditions were predicted using the fitted relationship. Similar linear relationship has also been observed in Runyang Suspension Bridge (Deng *et al.*, 2009). In the above studies, extreme displacements were emphasized for severe temperature conditions. However, in these studies, the relationships between the expansion joints displacement and the bridge temperature were established in parametric regression models with deterministic coefficients. In real practice, uncertainties existing in the expansion joints movement should be considered in an optimal model. Therefore, the Gaussian process (GP) as a probabilistic approach taking into account uncertainties, would be a better choice for regression modeling, namely Gaussian process regression (GPR).

GP is formulated as non-parametric models. Instead of defining parameter values in model structures, a prior GP distribution is directly defined over function values. GP implements kernel machine learning in a Bayesian framework with several key advantages. First, GP provides probabilistic distributions and enables to estimate the

uncertainties during the prediction procedure. Meanwhile, GP performs the learning and optimization of parameters in the kernel functions. Within the Bayesian framework, GP enables to integrate statistical methods, provide valid estimations of uncertainties during the prediction, and also the generic optimized model selection at the same time (Wu *et al.*, 2012). The data-driven feature of GP makes it unrestricted to any algebraic structure and thus ensures a high modeling flexibility and great expressive power (Wan & Ni, 2017). In GP, the probability distribution over functions is defined by the specification of covariance functions. As the most commonly used covariance function in GP, the squared exponential (SE) covariance function corresponds to a linear combination of an infinite number of basis functions (Rasmussen & Williams, 2006). On one hand, this characteristic makes the SE covariance function an advantage with the high flexibility for estimating any form of basis functions. On the other hand, due to its general-purpose characteristic, the SE covariance function may not perform satisfactorily when the target function's overall trend is known a priori. Therefore, the performance of SE covariance may not always be satisfactory and needs to be verified.

With the prior knowledge on target function, an explicit linear covariance function for GPR (L-GPR) is adapted in this chapter. The formulation and optimization of GPR model is first conducted in the context of Bayesian inference. Then the performance of GPR based on explicit linear covariance function is evaluated and compared with GPR based on SE covariance function. By comsidering regression and prediction

performance, the outperformed GPR model is selected and used for further extreme expansion joint displacement prediction and condition assessment using the monitoring data from the TKB.

3.2 Gaussian Process Regression

3.2.1 Basic GPR model

GP solves regression problems based on a non-parametric model. Unlike the Bayesian linear model of which the inference is based on the distribution over parameters, GP defines the probability distribution over functions, and the subsequent Bayesian inference is directly implemented in function spaces. GP is defined as a collection of random variables corresponding to the input $\mathbf{x}_i$. Any infinite subset of the function outputs is assumed to have a joint multivariate Gaussian distribution. The specification of a GP distribution is fully dependent on its mean function and covariance function.

Consider the training set $D=\{(\mathbf{x}_i, y_i) \mid i=1,\ldots,n\}$ of n observations, where $\mathbf{x}_i$ is the input vector of dimension d, and y_i is the scalar output. The observation is assumed to be drawn from the following process model with Gaussian noise $\varepsilon \sim N(0,\sigma_n^2)$:

$$y_i = f(\mathbf{x}_i) + \varepsilon \tag{3.1}$$

Thus, the mean function $m(\mathbf{x})$ and covariance function $k(\mathbf{x},\mathbf{x}')$ of the process $f(\mathbf{x})$ are defined as

$$m(\mathbf{x}) = E[f(\mathbf{x})]$$
$$k(\mathbf{x}, \mathbf{x}') = E[(f(\mathbf{x}) - m(\mathbf{x}))(f(\mathbf{x}') - m(\mathbf{x}'))] \tag{3.2}$$

and the GP can be denoted as (Rasmussen & Williams, 2006)

$$f(\mathbf{x}) \sim GP(m(\mathbf{x}), k(\mathbf{x}, \mathbf{x}')) \tag{3.3}$$

Usually for simplicity, the mean function is taken as zero, i.e. $f(\mathbf{x}) \sim GP(0, k(\mathbf{x}, \mathbf{x}'))$.

Thus, the joint distribution over noisy observations given input X is also Gaussian with zero mean, as denoted below:

$$\mathbf{y} \mid X \sim N(0, K(X, X) + \sigma_n I) \tag{3.4}$$

Given the training samples $(X, \mathbf{y})$ and testing points X_*, the objective of GPR is to find the predicted outputs $f(X_*)$ with probabilistic confidence levels. According to the Bayesian theorem, the joint posterior distribution of the training outputs $\mathbf{f}$ and predicted outputs $\mathbf{f}_*$ is

$$p(\mathbf{f}, \mathbf{f}_* \mid \mathbf{y}) = \frac{p(\mathbf{y} \mid \mathbf{f}) p(\mathbf{f}, \mathbf{f}_*)}{p(\mathbf{y})} \tag{3.5}$$

The posterior distribution of predicted outputs $\mathbf{f}_*$ can be obtained by marginalizing the training output $\mathbf{f}$ using integration:

$$p(\mathbf{f}_* \mid \mathbf{y}) = \int p(\mathbf{f}, \mathbf{f}_* \mid \mathbf{y}) d\mathbf{f} = \int \frac{p(\mathbf{y} \mid \mathbf{f}) p(\mathbf{f}, \mathbf{f}_*)}{p(\mathbf{y})} d\mathbf{f} \tag{3.6}$$

Given the joint prior distribution of the training outputs $\mathbf{f}$ and predicted outputs $\mathbf{f}_*$, the likelihood of *n* observations $\mathbf{y}$ can be expressed as:

$$p(\mathbf{f}, \mathbf{f}_*) = N\left(\mathbf{0}, \begin{bmatrix} K(X,X) & K(X,X_*) \\ K(X_*,X) & K(X_*,X_*) \end{bmatrix}\right) \tag{3.7}$$

$$p(\mathbf{y} \mid \mathbf{f}) = N(\mathbf{f}, \sigma_n{}^2 I) \tag{3.8}$$

Since all terms in Equation (3.6) are Gaussian, the posterior distribution over predicted outputs after integration is also Gaussian and can be express as

$$p(\mathbf{f}_* \mid \mathbf{y}) = N(\boldsymbol{\mu}_*, \Sigma_*) \tag{3.9}$$

where $\boldsymbol{\mu}_*$ is the predicted output, Σ_* is the covariance of $\mathbf{f}_*$, which can be used to estimate the confidence levels (Rasmussen & Williams, 2006):

$$\mu_* = K(X_*, X)(K(X,X) + \sigma_n{}^2 I)^{-1}\mathbf{y} \tag{3.10}$$

$$\Sigma_* = K(X_*, X_*) - K(X_*, X)(K(X,X) + \sigma_n{}^2 I)^{-1}K(X, X_*) \tag{3.11}$$

By now the prediction is achieved using a GPR model.

3.2.2 Covariance function selection and hyperparameter optimization

It is important to select proper mean function and covariance function to achieve a valid GP. In general, any real-valued mean function $m(\mathbf{x})$ is acceptable. Given a mean function $m(\mathbf{x})$, the zero mean GP can be adopted to characterize the difference between the observations and the mean function. Generally, the mean function is set to be zero. However, the covariance function $k(\mathbf{x}, \mathbf{x}')$ is a crucial ingredient in a GP. The covariance function specifies the probability distribution over functions. Given a number of input points, the corresponding covariance matrix can be written out

element-wise. With the covariance matrix, a random Gaussian vector can be generated and the generated values can be seen as a function of the inputs. The covariance function measures the distance between input vectors and specifies the target function needed to be trained by defining the similarity between two function values corresponding to two input indices. It should fulfil the requirement that for any set of elements $x_1,\ldots,x_m \in X$, the resulting matrix

$$K = \begin{bmatrix} k(x_1,x_1) & \cdots & k(x_1,x_m) \\ \vdots & \ddots & \vdots \\ k(x_m,x_1) & \cdots & k(x_m,x_m) \end{bmatrix} \tag{3.12}$$

is a valid covariance matrix corresponding to some multivariate Gaussian distribution. For a smooth function, it is basic to assume that if the input vectors $\mathbf{x}$ have close values, the corresponding target values y are likely to have similar values too. Therefore, the training points which are close to a test point should provide more information about the prediction at that testing point than other training points far from the testing point. In other words, the covariance function in GP defines the nearness or similarity.

The SE covariance function is most commonly used as a general-purpose covariance function (Mohanty *et al.*, 2009; Rohmer & Foerster, 2011; Anderson *et al.*, 2014; Wan & Ren, 2015), which is defined as

$$k(\mathbf{x},\mathbf{x}') = \sigma_f{}^2 \exp\left(-\frac{1}{2l^2}\left\|\mathbf{x}-\mathbf{x}'\right\|^2\right) \tag{3.13}$$

where $\sigma_f{}^2$ is the signal variance which controls the variance of process, and l is the characteristic length-scale which controls the distance of uncorrelation. According to

the mathematical expression, the SE covariance function provides information about target functions: the covariance is almost 1 between nearby variables, and decreases as their distance in the input space increases. The characteristic length-scale l defines the distance needed in the input space for the function values to become uncorrelated. As the characteristic length-scale increases, the points which are far away will have higher correlations than before, and the sampled functions tend to be smoother overall. This covariance function is infinitely differentiable, implying that a GP with SE covariance function has mean square derivatives of all orders. Functions defined by a GP prior with a SE covariance function tend to be locally smooth with high probability. The SE covariance function is the most widely used one in the GP learning field.

Free parameters in the covariance function, for example σ_f, l, and σ_n, can be varied, and are noted as hyperparameters. The values of these hyperparameters are unknown and need to be determined. This can be achieved by maximizing the log marginal likelihood of the training outputs given the inputs. Due to the Gaussian characteristic in GPR, its Bayesian inference is special because the integrals over the parameters is analytically traceable. The maximization of marginal likelihood can be achieved through the partial derivatives. The computational overhead of computing derivatives is small, and a gradient based optimizer is advantageous. In GP problem, the local maximum in gradient based optimization corresponds to a particular interpretation of the data. Since the relationship characteristic is explicitly defined and the size of dataset is clustered, the data in this study should be sufficient to get global

optima.

Denoting the hyperparameters as $\boldsymbol{\theta} = [\sigma_f, l, \sigma_n]$, the optimization can be expressed as

$$\boldsymbol{\theta}_{\max} = \arg\max\{\log p(\mathbf{y} \mid X, \boldsymbol{\theta})\} \tag{3.14}$$

where

$$\log p(\mathbf{y} \mid X, \boldsymbol{\theta}) = -\frac{1}{2}\mathbf{y}^T K_y^{-1}\mathbf{y} - \frac{1}{2}\log\left|K_y\right| - \frac{n}{2}\log 2\pi \tag{3.15}$$

$$K_y = K(X, X) + \sigma_n I \tag{3.16}$$

The partial derivatives of the marginal likelihood can be expressed as (Rasmussen & Williams, 2006)

$$\begin{aligned} \frac{\partial}{\partial \theta_j}\log p(\mathbf{y} \mid X, \boldsymbol{\theta}) &= \frac{1}{2}\mathbf{y}^T K_y^{-1}\frac{\partial K_y}{\partial \theta_j}K_y^{-1}\mathbf{y} - \frac{1}{2}\mathrm{tr}\left(K_y^{-1}\frac{\partial K_y}{\partial \theta_j}\right) \\ &= \frac{1}{2}\mathrm{tr}\left(\left(\boldsymbol{\alpha}\boldsymbol{\alpha}^T - K_y^{-1}\right)\frac{\partial K_y}{\partial \theta_j}\right) \quad \text{where } \boldsymbol{\alpha} = K_y^{-1}\mathbf{y} \end{aligned} \tag{3.17}$$

The completive steps of a GP model for regression and prediction are summarized below:

(1) Define the GP as $GP(m(\mathbf{x}), k(\mathbf{x}, \mathbf{x}'))$ with initial prior mean function $m(\mathbf{x})$ and covariance function $k(\mathbf{x}, \mathbf{x}')$ with hyperparameters $\boldsymbol{\theta}$.

(2) Compute the log marginal likelihood and its partial derivatives, as expressed in Equations (3.15)-(3.17).

(3) Set initial values of hyperparameters $\boldsymbol{\theta}$ and optimize them by optimization strategy defined in Equation (3.14) using the conjugate gradient method.

(4) Evaluate the predicted mean and covariance using Equations (3.10) and (3.11).

3.3 Case Study: Temperature-Induced Expansion of a Cable-Stayed Bridge

3.3.1 TKB and its SHM system

The TKB in Hong Kong is a cable-stayed bridge with three towers. The two main bridge spans have length of 448 m and 475 m respectively, and two side spans have length of 127 m each (Bergermann and Schlaich 1996). The bridge deck carries vehicle transportation in two directions with carriageways width of 18.8 m each. Between the two carriageways is a 5.2 m gap, linked by I-shape main crossgirders at 13.5 m intervals. Each carriageway grillage consists of two longitudinal steel girders along the deck edges with steel crossgirders at 4.5 m intervals, and a precast concrete deck panel on top. The three towers are 170 m, 194 m and 158 m high respectively and composed of concrete structure with steel boxes attached to the top section. The deck is supported by 384 stay cables in four cable planes anchored to the deck edge girders at 13.5 m intervals. There are eight longitudinal stabilizing cables, with length up to 464.6 m, diagonally connecting the top of the central tower and the bridge deck at the foot of the side towers. Because of the slenderness of the single-leg towers, the three towers are stiffened by a total of 64 transverse stabilizing cables in the lateral direction. Figure 3.1 is a photo of the TKB.

Figure 3.1 Ting Kau Bridge (TKB)

After the completion of construction, a sophisticated long-term monitoring system has been deployed on the TKB. The Wind and Structural Health Monitoring System (WASHMS) was devised by the Highways Department of the Hong Kong SAR Government to monitor the structural health and performance of the bridge under in-service conditions (Wong, 2004; Ko & Ni, 2005). The WASHMS is an integration of six systems, namely sensory system, data acquisition and transmission system, data processing and control system, structural health evaluation system, structural health data management system, and inspection and maintenance system (Wong & Ni, 2009). There are 238 sensors permanently deployed on the TKB, including 45 accelerometers (including uniaxial, biaxial, and triaxial), 7 anemometers (including ultrasonic-type and propeller-type), 2 displacement transducers, 83 temperature sensors, 88 strain gauges (including 66 linear and 22 rosette), 7 global positioning system (GPS) receivers, and a weigh-in-motion (WIM) sensing system with 6 sensors (Wong, 2007; Ni *et al.*, 2011). Two displacement transducers (DSGAW01 and DSGPW01) are

deployed at expansion joints located at two ends of the continuous bridge deck, in order to measure the longitudinal movements of the bridge deck at the expansion joints. Among a total of 83 temperature sensors deployed, 51 of them are installed on the deck cross section to monitor the structure components temperature of steel, concrete, asphalt, and also ambient atmosphere. The locations of displacement and temperature sensors on the TKB are illustrated in Figure 3.2 to Figure 3.4. The displacement is acquired at a sampling rate of 2.56 Hz and the temperature measurement data is acquired at 0.07 Hz respectively.

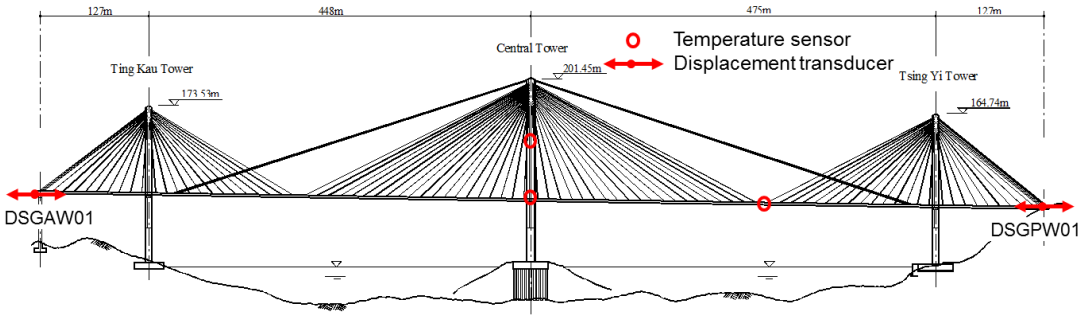

Figure 3.2 Location of displacement and temperature sensors on TKB

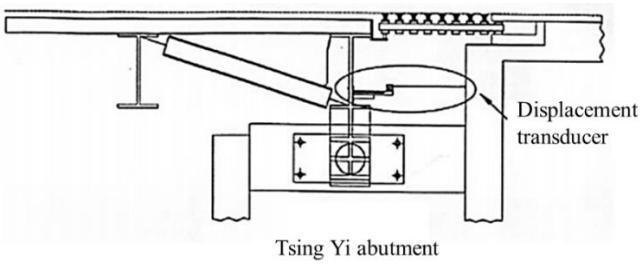

Figure 3.3 Details of displacement transducer at Tsing Yi abutment

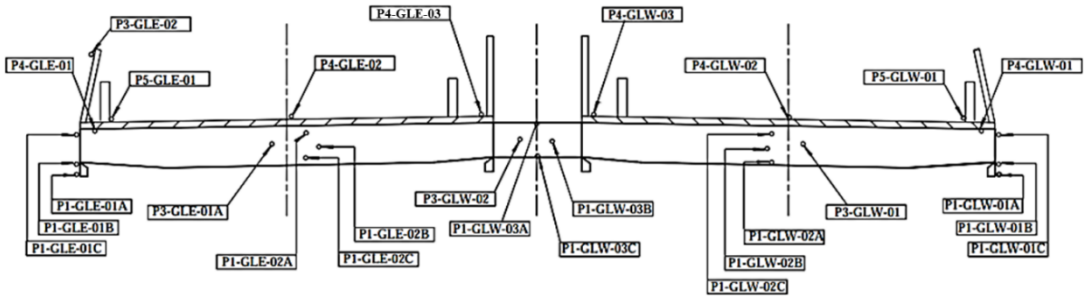

Figure 3.4 Deployment of temperature sensors on deck cross section

3.3.2 Data pre-processing

One-year monitoring data obtained from the TKB are used in this study. The measured displacement and temperature data are pre-processed to obtain the hourly-average values. For large structures like bridges, the temperature distribution is different across deck cross-section. When using all temperature data simultaneously, the redundancy existent in the dataset leads to unsatisfactory results. Therefore, the measured temperature cannot be directly used as the entire structure temperature. The effective temperature is introduced to represent the overall temperature along the deck cross section, which contributes to the thermal movements of the bridge deck. The calculation of effective temperature is based on a weighted average of different temperatures measured at different subareas across the deck section, while the weighting factor is assigned based on the percentage of each subarea in the total cross section area. The effective temperature T_e can be obtained from:

$$T_e = \sum \frac{A_i}{A} T_i \tag{3.18}$$

where A_i is the ith subarea, A is the total area of the cross section, T_i is the measured temperature of the ith subarea. In this study, the effective temperature is calculated using the measured temperatures at 39 different locations on the deck cross section, including 15 from steel components and 24 concrete components. The calculated effective temperature and the displacements at the expansion joints are plotted in Figure 3.5 and Figure 3.6.

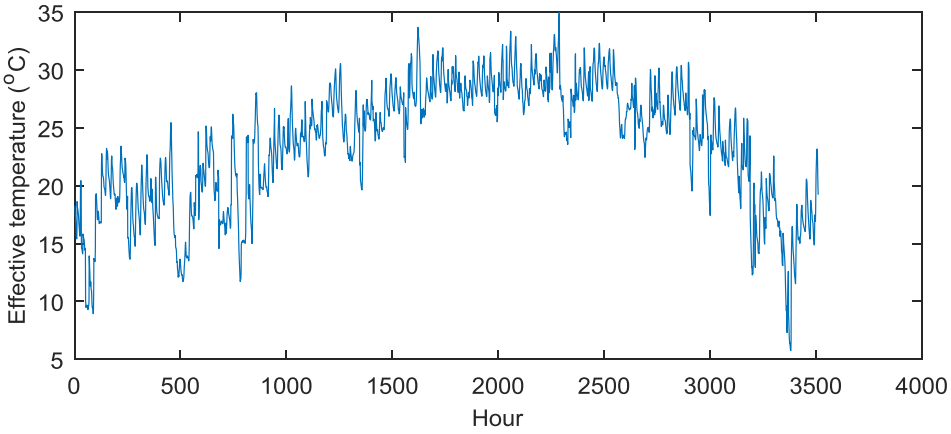

Figure 3.5 Hourly-averaged effective temperature for one year

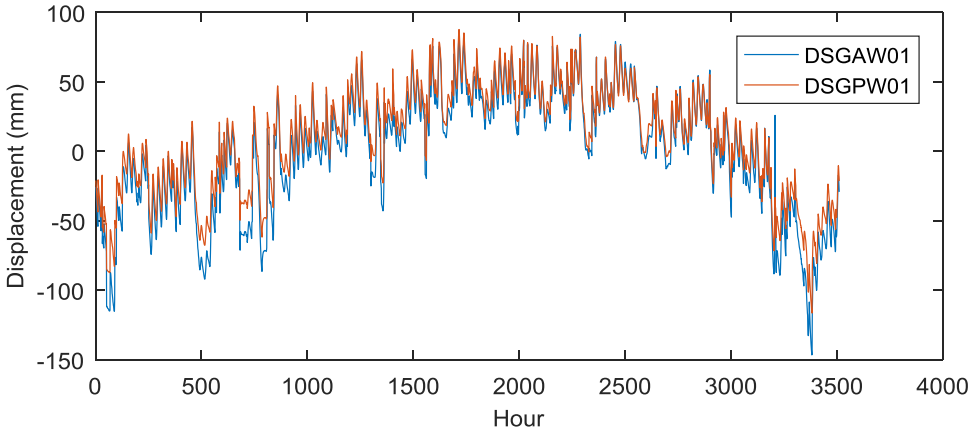

Figure 3.6 Hourly-averaged displacements at two expansion joints for one year

According to Figure 3.5 and Figure 3.6, the hourly-averaged effective temperature and expansion joint displacements show similar changing trend for one-year observation.

A detailed comparison of 48-hours observation samples is plotted in Figure 3.7. The changes of displacement coincide with the effective temperature variation very well. The delay of displacement variation than effective temperature can also be observed. As shown in Figure 3.8 and Figure 3.9, good linear relationship between expansion joints displacement and effective temperature can be observed. Therefore, the regression relationship between expansion joints displacement and effective temperature is assumed to be linear relationship for further GPR model formulation.

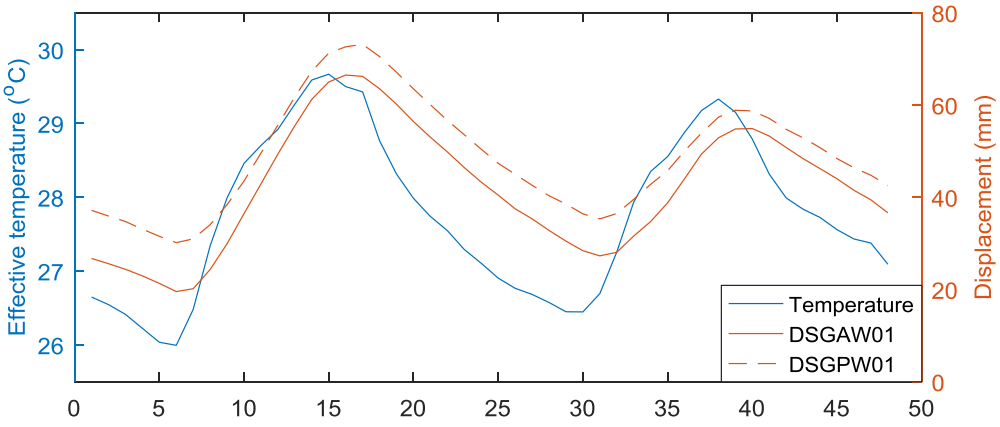

Figure 3.7 Effective temperature and expansion joints displacement variation in 48 hours

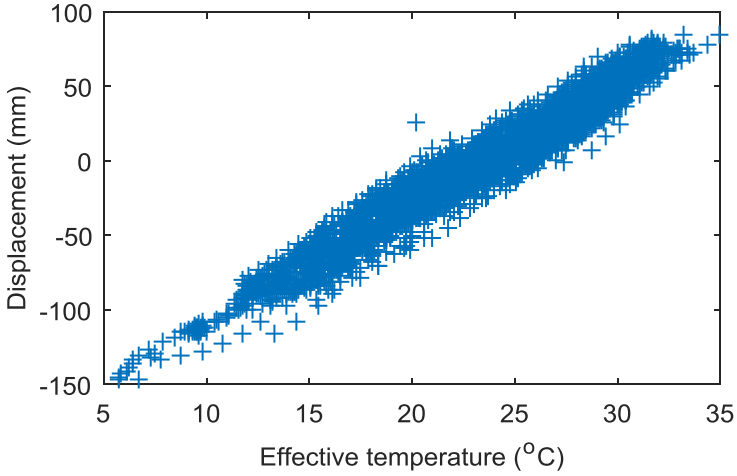

Figure 3.8 Relationship between expansion joint displacement and effective temperature at DSGAW01

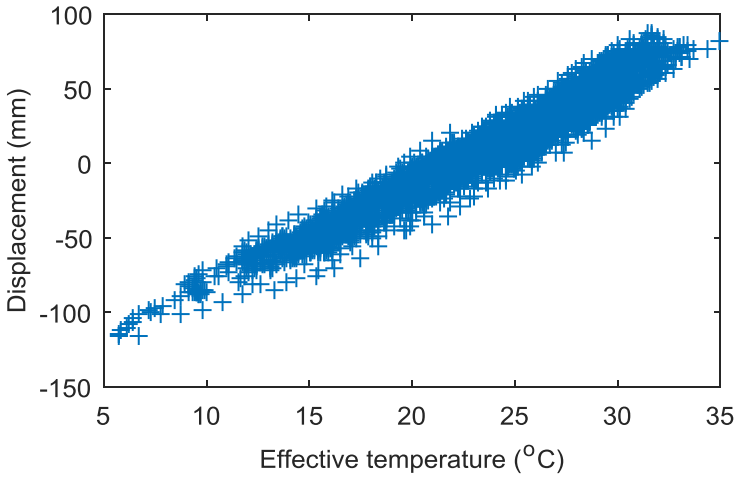

Figure 3.9 Relationship between expansion joint displacement and effective temperature at DSGPW01

3.3.3 Selection of case-specific covariance function

Although the SE covariance function is a common choice for GP, when the relationship is known, an appropriate covariance function based on the exact relationship between variables will reduce the uncertainty and lead to more accurate results. Therefore an accurate covariance function based on the exact regression relationship is derived and adapted in this section. The performance of GPR with true covariance function and SE covariance function will be compared.

A linear relationship between the expansion joint displacement and the effective temperature is observed in the previous section. Thus, a simple linear regression model might be more suitable for the assessment:

$$y_i = f(x_i) + \varepsilon_i = \alpha x_i + \beta + \varepsilon_i \tag{3.19}$$

where ε_i is the Gaussian noise with zero mean and variance σ_n^2, α and β are parameters in the simple linear regression model with independent Gaussian prior with zero mean and variance σ_α^2 and σ_β^2 respectively:

$$\begin{aligned} \alpha &\sim N(0, \sigma_\alpha) \\ \beta &\sim N(0, \sigma_\beta) \\ \varepsilon &\sim N(0, \sigma_n) \end{aligned} \tag{3.20}$$

Therefore, the prior mean and covariance are

$$m(x) = E[\alpha x_i + \beta] = 0 \tag{3.21}$$

$$\mathrm{k}(x, x') = E[(\alpha x + \beta)(\alpha x' + \beta)] = x \cdot x' \cdot \sigma_\alpha^2 + \sigma_\beta^2 \tag{3.22}$$

The prior on the noisy observations becomes

$$\mathrm{cov}(\mathbf{y}) = K(X, X) + \sigma_n^2 I \tag{3.23}$$

where $K(X, X) = \sigma_\alpha^2 J + \sigma_\beta^2 X^T X$, J is a matrix of ones.

By substituting Equations (3.22) and (3.23) into Equations (3.10) and (3.11), the prediction results for a linear relationship can be achieved.

3.3.4 Performance evaluation and comparison

3.3.4.1 Hyperparameter adaptation

Several runs have been conducted for hyperparameter optimization. It is observed that

the optimized hyperparameters have consistent values for different runs and the prediction results are consistent. For the L-GPR model, set the initial values of hyperparameters $\sigma_\alpha = \sigma_\beta = 1$, so that the parameters α and β have unit variance. The initial noise standard deviation is set as $\sigma_n = 0.1$. Although the initial values of hyperparameters have little influence on the final regression results, the initial settings are fixed so that the results are comparable for different sample sets. Given the initial hyperparameters, the log probability of the training data is -1.44×10^7. After iterations, L-GPR model hyperparameter optimization results are given in Table 3.1. The log probability increases to its maximum value of -1.27×10^4. And the optimized hyperparameters are $\sigma_\alpha = 0.1808$, $\sigma_\beta = 221.48$, and $\sigma_n = 9.05$. The variance of hyperparameters and the log marginal likelihood within the 100 iterations are plotted in Figure 3.10. It is seen that the log marginal likelihood increases rapidly in the first 20 iterations, reaches the maximum value at around 24th iteration, and then levels off after 24th iteration. The L-GPR model hyperparameters variation is presented in Figure 3.11. As shown in Figure 3.11, the noise standard deviation σ_n has similar variation trend to the log marginal likelihood. It increases in the first 20 iterations from 0.1 to 9.05 and then tends to be stable, suggesting the noise standard deviation σ_n might play an important role in the marginal likelihood. The other two hyperparameters, however, still vary after 30 iterations, but make no difference in the log marginal likelihood value. It suggests that the log marginal likelihood in L-GPR model may not be sensitive to the value of the linear weight parameter standard

deviation and the intercept parameter standard deviation. The optimized hyperparameters indicates the L-GPR model achieves the maximum log marginal likelihood when the linear weight parameter standard deviation is taken as 0.1808, the intercept parameter standard deviation taken as 221.48, and the noise standard deviation taken as 9.05.

As discussed in Section 3.2.2, the GPR model with SE covariance function (SE-GPR) is also adopted, in order to compare the performances of GPR models with different covariance functions. The hyperparameters in SE-GPR are $\boldsymbol{\theta} = [l, \sigma_f, \sigma_n]$. The initial values are set as $\boldsymbol{\theta} = [1, 1, 0.1]$, corresponding to unit characteristic length-scale, unit signal standard deviation, and 0.1 noise standard deviation. After 100 iterations, SE-GPR model hyperparameter optimization results are given in Table 3.2. The hyperparameter are optimized as $l = 6.73$, $\sigma_f = 60.72$, and $\sigma_n = 8.85$. The optimized hyperparameters indicate that the L-GPR model achieves the maximum log marginal likelihood when the characteristic length-scale is taken as 6.73, the signal standard deviation taken as 60.72, and the noise standard deviation taken as 8.85. Although the two sets of the hyperparameters from different covariance functions have different physical meanings and are not comparable, the optimized noise standard deviations are similar for two GPR models. The log probability of the training data before and after the hyperparameter optimization are -1.36×10^{7} and -1.27×10^{4} respectively, which has a comparable performance with the L-GPR. The variance of hyperparameters and the log marginal likelihood of SE-GPR model within the 100

iterations are plotted in Figure 3.12 and Figure 3.13. Similar variation pattern can be observed in Figure 3.10 and Figure 3.12. The log marginal likelihood increases rapidly in the first 20 iterations, reaches the maximum value at around 26th iteration, and then levels off after 26th iteration. The SE-GPR model hyperparameters variation is presented in Figure 3.13. As shown in Figure 3.13, all three hyperparameters tend to be stable before 30th iterations, coinciding well with the variation of the log marginal likelihood. By comparing the optimized parameters, both GPR models have consistent log marginal likelihood, suggesting the two models may have similar performance in regression and prediction.

Table 3.1 L-GPR model hyperparameter optimization

	Hyperparameter			**Log marginal**
	σ_α	σ_β	σ_n	**likelihood**
Initial value	1	1	0.1	-1.44×10^{7}
Optimized value	0.1808	221.48	9.05	-1.27×10^{4}

Table 3.2 SE-GPR model hyperparameter optimization

	Hyperparameter			**Log marginal**
	l	σ_f	σ_n	**likelihood**
Initial value	1	1	0.1	-1.36×10^{7}
Optimized value	6.73	60.72	8.85	-1.27×10^{4}

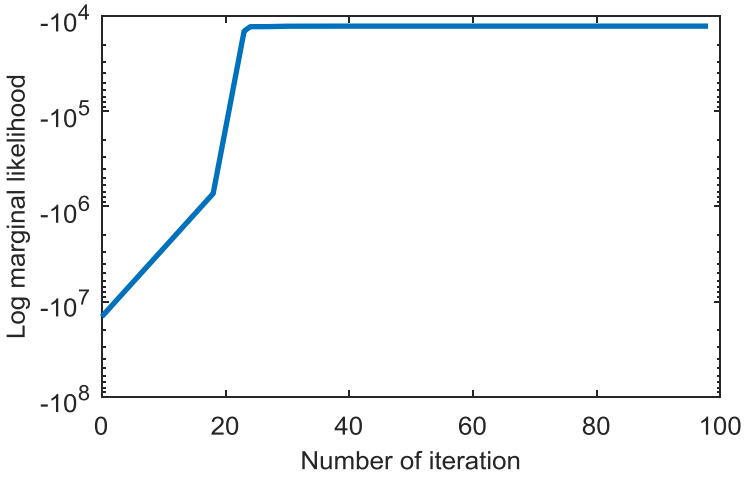

Figure 3.10 L-GPR log marginal likelihood variation

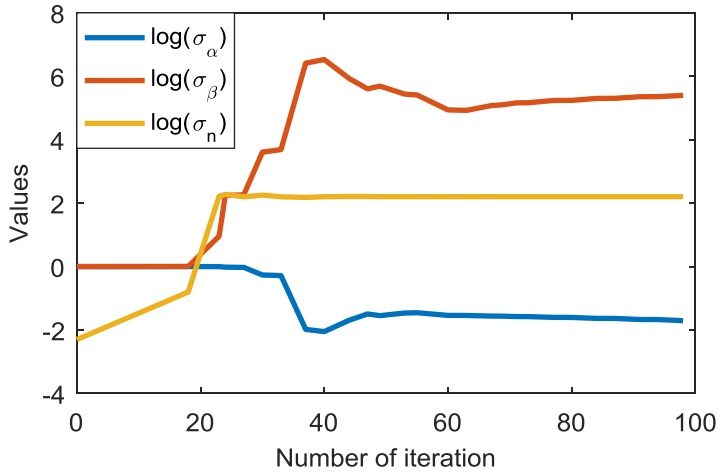

Figure 3.11 L-GPR hyperparameters variation

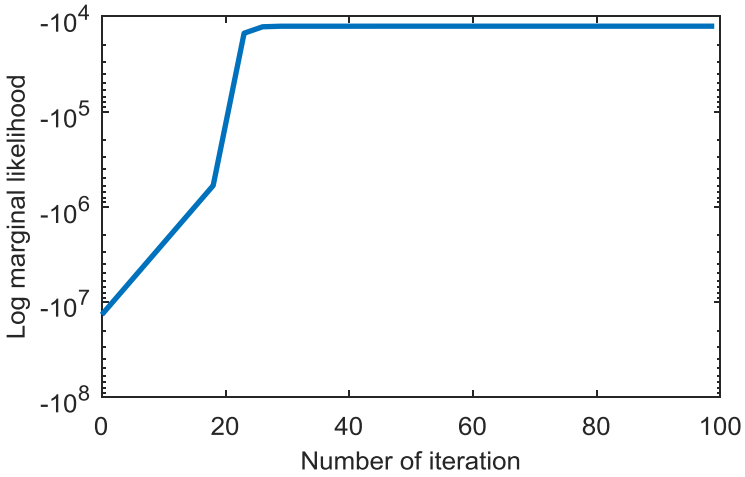

Figure 3.12 SE-GPR log marginal likelihood variation

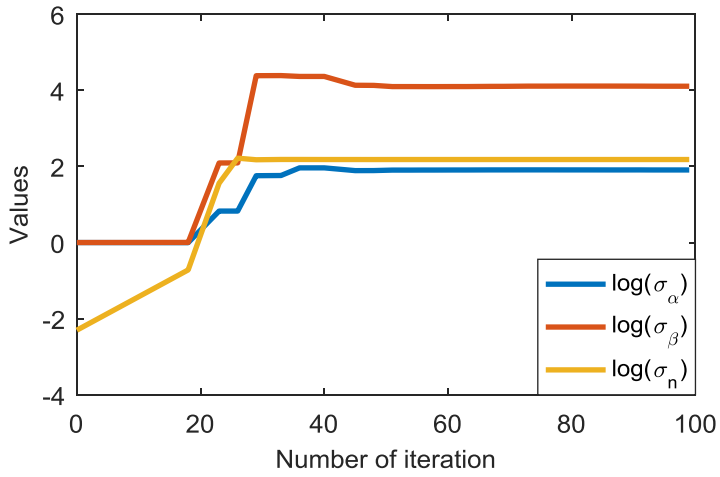

Figure 3.13 SE-GPR hyperparameters variation

3.3.4.2 Prediction performance and confidence interval

Possible temperature values between -2 °C and 40 °C at 0.05 °C interval are used as testing data for expansion joint displacement prediction using the two optimized GPR models: L-GPR and SE-GPR. Results are presented in Figure 3.14 and Figure 3.15. In Figure 3.14 and Figure 3.15, the original training measurements are plotted in blue plus symbol, and the predicted mean function are plotted in red line. To make the figures clearer for understanding, the 95% confidence interval of the predicted mean function is shaded in grey. The predicted mean displacement and the confidence interval from two GPR models for representative points are presented in Table 3.3.

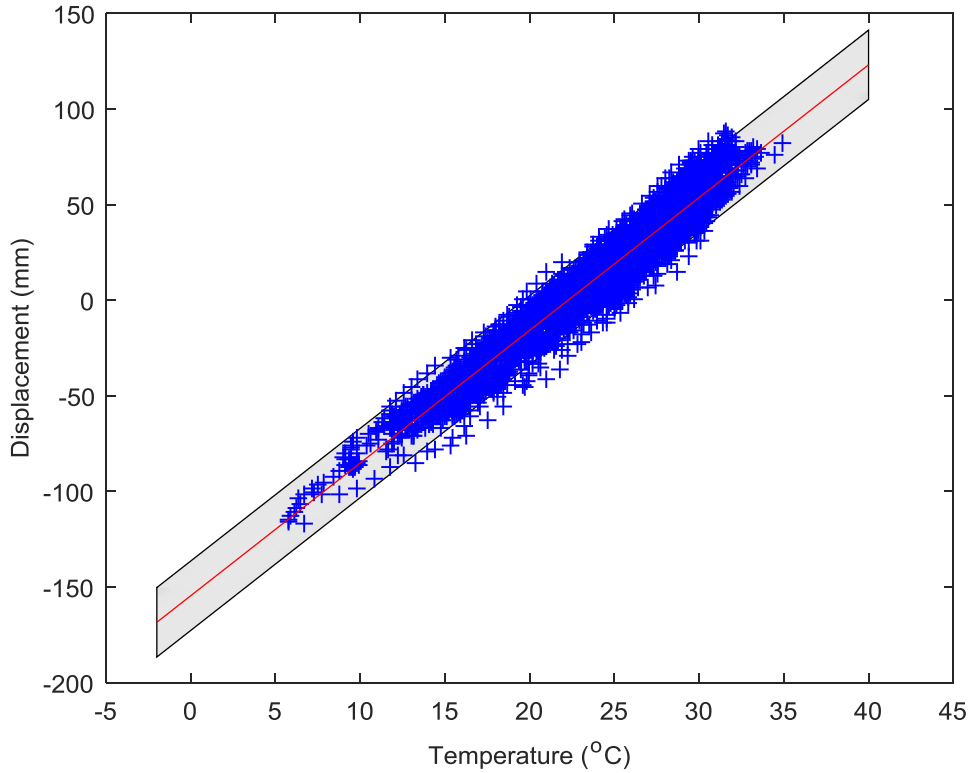

Figure 3.14 Regression and prediction based on L-GPR

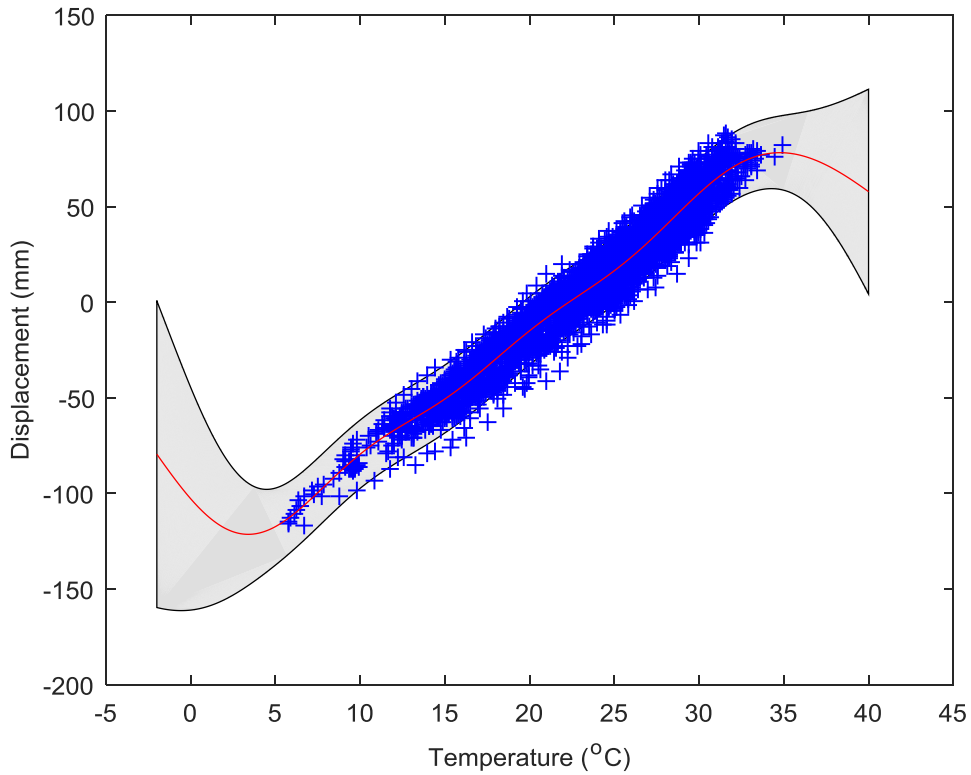

Figure 3.15 Regression and prediction based on SE-GPR

Table 3.3 Predicted displacement and confidence interval from two GPR models

	Model	Predicted displacement (mm)	Predicted variance	95% Confidence interval (mm)
-2 °C	L-GPR	-168.43	82.45	[-186.60, -150.27]
	SE-GPR	-79.52	1607.2	[-159.70, 0.66]
15 °C	L-GPR	-50.44	81.97	[-68.54, -32.33]
	SE-GPR	-50.64	78.67	[-68.38, -32.90]
20 °C	L-GPR	-15.73	81.91	[-33.83, 2.37]
	SE-GPR	-14.96	78.58	[-32.69, 2.77]
25 °C	L-GPR	18.97	81.91	[0.87, 37.08]
	SE-GPR	16.45	78.54	[-1.28, 34.17]
40 °C	L-GPR	123.09	82.13	[104.97, 141.22]
	SE-GPR	57.77	717.15	[4.21, 111.33]

It is seen in Figure 3.14 and Figure 3.15 that the regression and prediction performs quite good at the observation clusters of the sample set for both L-GPR and SE-GPR models. As the covariance function in L-GPR is explicitly defined, the estimated mean (red line) is a straight line as expected, and the uncertainties for extrapolation are almost constant even at points with no measured samples. As shown in Table 3.3, the variances predicted by L-GPR model stay around 82. However, for the SE-GPR model, although the SE covariance function is flexible for any regression relationship, it is

not explicit for a particular linear regression case. The mean function estimation for interpolation performs still acceptably with appropriate slope, although it is not a straight line but appearing with gentle curve which can be observed by eye. However, when it comes to the prediction of expansion joint displacement outside the observation ranges, the estimated mean function goes back to the distinct curve shape, which leads to inaccuracy of the predicted mean value at extrapolated regions. In addition, the uncertainties predicted by the SE covariance function become larger when the input testing temperature values move far from the measured samples. As shown in Table 3.3, the variances predicted by SE-GPR model become very large under -2 °C and 40 °C temperature. This result is coincident with the characteristic of SE covariance function.

Based on the results discussed above, the L-GPR model has better performance in linear regression assessment, due to its explicitly defined covariance function. Thus, the L-GPR model is further used for SHM-based condition assessment of the TKB.

3.3.5 Displacement prognosis based on L-GPR

Two sample sets of temperature and displacement measurement data from two expansion joints at Ting Kau side (DSGAW01) and Tsing Yi side (DSGPW01), are utilized for displacement prognosis. The optimized L-GPR model hyperparameters for the two sample sets are listed in Table 3.4. The optimized hyperparameters of the L-GPR models derived from the two sample sets have similar values, except for the

intercept parameter standard deviation σ_β. The extremely large intercept parameter standard deviation σ_β may be caused by one abnormal outlier as shown in Figure 3.17. Since this hyperparameter has little effect on the marginal likelihood, the two optimized models still have comparable performance with similar log marginal likelihood value. The regression results including mean function and 95% confidence interval for the two sample sets are plotted in Figure 3.16 and Figure 3.17, together with the original sample measurements.

Table 3.4 Optimized hyperparameters for L-GPR model at two expansion joints

	Hyperparameter			**Log marginal**
	σ_α	σ_β	σ_n	**likelihood**
DSGPW01	0.1808	221.48	9.05	-1.27×10^4
DSGAW01	0.0697	5229	9.76	-1.30×10^4

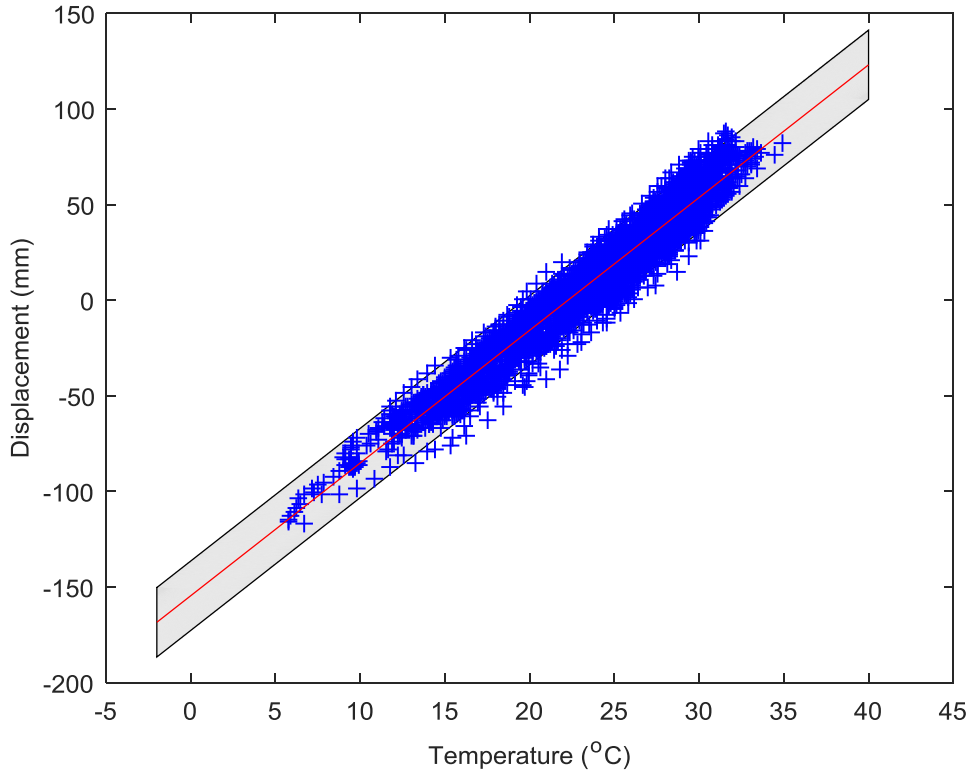

Figure 3.16 Displacement regression and prediction at DSGPW01

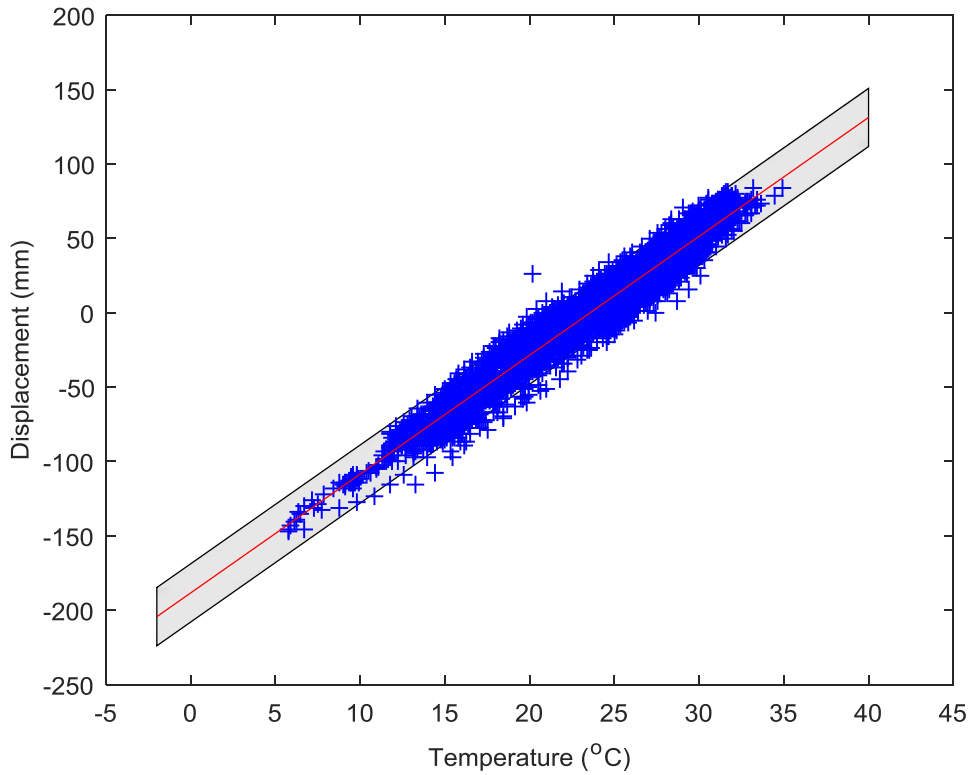

Figure 3.17 Displacement regression and prediction at DSGAW01

According to the design documents, the designed minimum and maximum effective temperatures for the TKB are -2 °C and 40 °C respectively. The two designed critical temperatures are fed into the L-GPR model as testing data, in order to predict the expansion joint displacement under designed extreme temperature, so that the bridge health condition can be assessed. The prediction results for the two expansion joints under extreme temperature values are presented in Table 3.5.

Table 3.5 Predicted displacements and confidence interval

	Temperature (°C)	**Predicted displacement (mm)**	**Predicted variance**	**95% confidence interval (mm)**
DSGPW01	-2	-168.43	82.45	[-186.60, -150.27]
	40	123.09	82.13	[104.97, 141.22]
DSGAW01	-2	-204.33	95.99	[-223.93, -184.73]
	40	131.31	95.61	[111.75, 150.87]

The predicted displacement at expansion joint DSGPW01 is -168.43 mm under -2 °C, and 123.09 mm under 40 °C. Therefore, the predicted mean displacement range of the joint DSGPW01 under designed working environment is about 291.53 mm, which is close to the designed displacement range of 297 mm. At the joint DSGAW01, the predicted displacement is -204.33 mm under -2 °C, and 131.31 mm under 40 °C. The total predicted mean displacement range at the joint DSGAW01 is 335.64 mm, close

to the designed range of 339 mm. The results show that the mean expansion displacement prediction based on L-GPR is quite credible. However, according to the 95% confidence interval estimation, the displacement range may lie in [255.24, 327.81] for DSGPW01 and [296.48, 374.79] for DSGAW01. If the 95% predicted interval is considered for the health condition assessment, risks exist that the displacement range may exceed the designed value. Therefore for the sake of safety, it is recommended to improve the temperature-induced displacement designing for similar bridges.

3.4 Summary

GPR model is formulated to establish the relationship between the temperature and expansion joint displacement using the monitoring data from the TKB. Based on the observed linear relationship, an explicit linear covariance function is derived for an explicit GPR model (L-GPR). The log marginal likelihood maximization method is used to optimize the hyperparameters in GPR models. The performance of L-GPR and SE-GPR is compared using the same sample data set. The results show that the L-GPR with an explicit linear covariance function which fits the linear relationship performs better in linear regression and prediction. The outperformed L-GPR is further used to predict the expansion joint displacements under extreme design temperatures, in order to examine the structural health condition. The predicted mean value of expansion displacement ranges are within the required design value. But the 95% confidence interval of the displacement range exceeds the design value in a certain extent. For the

sake of safety, it is recommended to improve the temperature-induced displacement designing for similar bridges.

The comparison between L-GPR and SE-GPR indicates that the covariance function is important and should be carefully chosen in order to fit the real covariance distribution of the data regression relationship. In linear regression case discussed in this chapter, the explicit linear covariance performs better than the SE.

As GPR is a non-parametric regression tool, it cannot provide the exact parametric form of regression relationship. Although GPR model is not eligible in parameter estimation points of view, it can provide the prediction in the function space directly. As a data-driven method, GP infers information from the input observation samples to predict unobserved future status of the system. This feature makes it advantageous when the system is complex and cannot be described by a simple physical model. When the regression model becomes complex with high-dimension, where the relation between variables are not clear and parameter estimation cannot be achieved, GPR will be easier for implementation and may have more appealing performance than other parametric learning methods.

CHAPTER 4

SHM-BASED CONDITION ASSESSMENT OF BRIDGES USING P-GPR MODEL

4.1 Introduction

The simple linear regression model is appropriate with virtues of simple implementation and interpretability when the output is a linear combination of the inputs. However, this also provides drawback on the model because of the limited flexibility inherent in the model. If the actual relationship between the input and output variables cannot be reasonably approximated by a linear relationship, an inaccurate simple linear model will give poor predictions with large errors. In most of the practical cases, the linear relationship may not be satisfied, therefore the simple linear model may not be suitable. To overcome this problem, a generalized linear model is extended from simple linear model. The generalization is achieved by transforming the input variables to some high dimensional space first, using a set of mapping functions and then applying the linear relationship in this mapping space. Instead of directly applying the linear relationship on the input variables, this transformation allows for any projection before linear combination without loss of generalization. For example, given a basis function as powers of x : $\phi(x) = (1, x, x^2, x^3, \ldots)^T$, a polynomial relationship can be implemented to the scalar input x .

In structural health monitoring (SHM) based condition assessment studies, a major part of regression relationships are not simple linear models. For bridges built in a wind-prone region, the wind-induce displacement response of the structure during strong winds is one of the important performance parameters to assess the bridge structural condition. The lateral displacement response of the Sutong Cable-Stayed Bridge has been reported to about 1.2 m under strong wind condition with wind speed at 40 m/s and wind direction at 0◦ (Xu *et al.*, 2013). The excessive large lateral displacement would threaten the safety of the whole bridge (Wang & Ding, 2014). For example, the Tacoma Suspension Bridge in Washington State collapsed due to severe wind vibration under the wind speed of 19 m/s (Green & Unruh, 2006).

Although the displacement response is correlated to wind loads, defining the unknown relationship to be linear may not be appropriate. The lateral displacement response induced by wind has been studied through theoretical and experimental investigations. The aerostatic stability calculation method was improved by Cheng and Xiao (2006) and the instable lateral displacement under critical static wind was calculated as 4.24 m for a long-span suspension bridge. The maximum lateral displacement response of Sidu Suspension Bridge was estimated as 32.26 cm at 1/2 main span through ANSYS finite element simulation (Long *et al.*, 2010). Wind tunnel tests have been conducted for Xihoumen Suspension Bridge, and the lateral displacement was found maximum at wind direction of 10◦ (Yu *et al.*, 2013). However, in practice, restraints exist such as the mechanism complexity and the structural uncertainties. Therefore, the lateral

displacement responses induced by wind cannot be accurately estimated based on the traditional methods. With the development of SHM technology, authentic bridge behaviors under actual operational environment can be monitored. In recent years, the ambient wind environment of long-span bridges has been widely studied (Lombardo *et al.*, 2009; Wang *et al.*, 2010; Wang *et al.*, 2013), and researches on the relationship between wind speed and wind-induced displacement have been reported (Nakamura, 2000; Xu & Chan, 2009; Wang & Ding, 2014). However, these investigations only concerned the wind speed as the influencing factor of the displacement response but the influence of wind direction was not considered. Therefore, the relationship between wind-induced lateral displacement response and wind loads including wind speed and wind direction still needs to be investigated.

In contrast with the parametric regression models estimated with deterministic coefficients, Gaussian process regression (GPR) is able to estimate the relationship with uncertainties. Its high flexibility also allows to apply the most suitable basis function $\phi(\mathbf{x})$ to the GPR model. Besides squared exponential (SE) covariance function which corresponds to a linear combination of infinite number of basis functions, explicit covariance function can also be derived and applied based on prior information of the relationship between input variables and target outputs. Neal (1997) introduced the covariance function for a linear model and then moved towards a more general Gaussian processes (GP) based on a class of smooth functions using the SE covariance function (Bernardo *et al.*, 1998). Chen *et al.* (2007) applied the covariance

function as a combination of several terms including constant bias, linear correlation, exponential correlation, and a random error term. By combining different characteristic terms in the covariance function, the GP model is flexible to handle different data structures. Details of selection and definition of the covariance functions can be found in the literature (Neal, 1997; MacKay, 1998; Rasmussen & Williams, 2006).

In this chapter, an explicit polynomial covariance function for GPR (P-GPR) is adapted to estimate the relationship between the lateral displacement and wind data for the Tsing Ma Bridge (TMB). The total displacement is analyzed in two parts: mean displacement and dynamic displacement. The dynamic displacement is determined based on certain factor and the prediction results from mean displacement. While the mean displacement part is processed using the GPR model. The formulation and optimization of GPR models are first conducted within Bayesian framework using the training data set. Then the regression and prediction performance of GPR models is evaluated in terms of the log marginal likelihood and root mean square error (RMSE) to find out the outperformed GPR model. The optimal P-GPR model is used to predict the mean displacement under extreme design wind speed and at the most unfavorable wind direction. Finally, the total lateral displacement is derived and the bridge condition is assessed.

4.2 Generalized Linear Regression Model Based on Gaussian Process

In most practical cases, simple linear model suffers from limited expressiveness. To overcome this problem, a generalized linear model is extended from the simple linear model. The generalization is achieved by transforming the input variables to some high dimensional space, using a set of mapping functions and then applying the linear relationship in this mapping space.

Consider the training set $D=\{(\mathbf{x}_i, y_i) \mid i=1,\ldots,n\}$ of n observations, where $\mathbf{x}_i$ is the input vector of dimension d, y_i is the scalar output. The observations are assumed to be drawn from the following process model with Gaussian noise $\varepsilon \sim N(0,\sigma_n^2)$:

$$y_i = f(\mathbf{x}_i) + \varepsilon \tag{4.1}$$

For the generalized linear model, $f(\mathbf{x})$ here is not a simple linear function. Instead, it can be expressed as

$$f(\mathbf{x}) = \phi(\mathbf{x})^T \mathbf{w} \tag{4.2}$$

where $\phi(\mathbf{x})$ is the key mapping function which transforms the d-dimensional input vector $\mathbf{x}$ into an N dimensional feature space, and $\mathbf{w}$ is the parameter vector of the generalized linear model. With mapping function $\phi(\mathbf{x})$, the model is extended to a more generalized form. The generalized linear model is capable of characterizing complex relationships by appropriately defining mapping function $\phi(\mathbf{x})$. Meanwhile it still enable to model simple linear relationship. For example, if the mapping function

$\phi(\mathbf{x})$ is set as $\phi(\mathrm{x}) = (1, x)^T$ for projection of a scalar input $\mathbf{x}$, the $f(\mathbf{x})$ will become a simple linear regression with elements in $\mathbf{w}$ as slope and intercept.

Assuming the parameter vector $\mathbf{w}$ is Gaussian distributed with zero mean and covariance matrix Σ_p, $\mathbf{w} \sim N(\mathbf{0}, \Sigma_p)$, the mean function $m(\mathbf{x})$ and covariance function $k(\mathbf{x}, \mathbf{x}')$ of the process $f(\mathbf{x}) \sim GP(m(\mathbf{x}), k(\mathbf{x}, \mathbf{x}'))$ become:

$$\begin{aligned} m(\mathbf{x}) &= E[f(\mathbf{x})] = \phi(\mathbf{x})^T E[\mathbf{w}] = 0 \\ k(\mathbf{x}, \mathbf{x}') &= E[f(\mathbf{x}) f(\mathbf{x}')] = \phi(\mathbf{x})^T E[\mathbf{w}\mathbf{w}^T] \phi(\mathbf{x}') = \phi(\mathbf{x})^T \Sigma_p \phi(\mathbf{x}') \end{aligned} \tag{4.3}$$

Thus $f(\mathbf{x})$ and $f(\mathbf{x}')$ are jointly Gaussian distributed with zero mean and covariance given by $\phi(\mathbf{x})^T \Sigma_p \phi(\mathbf{x}')$. Recall the basic GPR discussed in Section 3.2.1, the key terms of prediction in Equations (3.10) and (3.11) are $K(X, X)$, $K(X, X_*)$, $K(X_*, X)$, and $K(X_*, X_*)$. For generalized linear model, these key terms now can be written as $\Phi^T \Sigma_p \Phi$, $\Phi^T \Sigma_p \Phi_*$, $\Phi_*{}^T \Sigma_p \Phi$, and $\Phi_*{}^T \Sigma_p \Phi_*$ respectively, where $\Phi = \Phi(X)$, and $\Phi_* = \Phi(X_*)$ are the input matrice X and X_* in the high dimensional spaces after transformation.

4.3 Case Study: Wind-Induced Displacement of a Suspension Bridge

4.3.1 TMB and its SHM system

The TMB is a suspension bridge in Hong Kong, with a main span of 1377 m and a total length of 2.2 km. The TMB is the longest suspension bridge in the world carrying

both highway and railway traffic. The two concrete bridge towers are about 206 m high from the base level to the tower saddle. Two main cables are accommodated at four tower saddles at the top of the towers at 36 m distance in the north and south. Each set of suspenders is composed of four 75 mm diameter twisted-wire strands. At the main span and the Ma Wan side span, the deck is suspended from the main cables at 18 m intervals. In the longitudinal direction, the bridge deck is continuously expanded connecting Ma Wan and Tsing Yi. The supports for the deck at the end of Ma Wan span, Ma Wan tower, Tsing Yi tower, the end of Tsing Yi span, and piers are hinged support, rocker bearings, sliding bearings, roller support basing on a highway movement joint at upper deck and a railway movement joint at lower deck, and sliding bearings, respectively. The movement joint at the end of Tsing Yi span is designed to accommodate the longitudinal movement of the deck and release the thermal stress due to temperature effect. Carrying both highway and railway traffic, the TMB serves as a key part of the most essential transportation network linking the Hong Kong International Airport to the urban areas. The deck of the TMB is designed to have two levels with truss stiffening and non-structural edge fairing. On the upper level of the bridge deck, a dual three-lane highway is designed for vehicle traffic. While on the lower level of the deck, two railways tracks and two sheltered carriageways are designed for railway traffic and vehicle traffic for emergency. A photo of the TMB is shown in Figure 4.1, and the cross-section view of bridge deck is illustrated in Figure 4.2.

Figure 4.1 Tsing Ma Bridge (TMB)

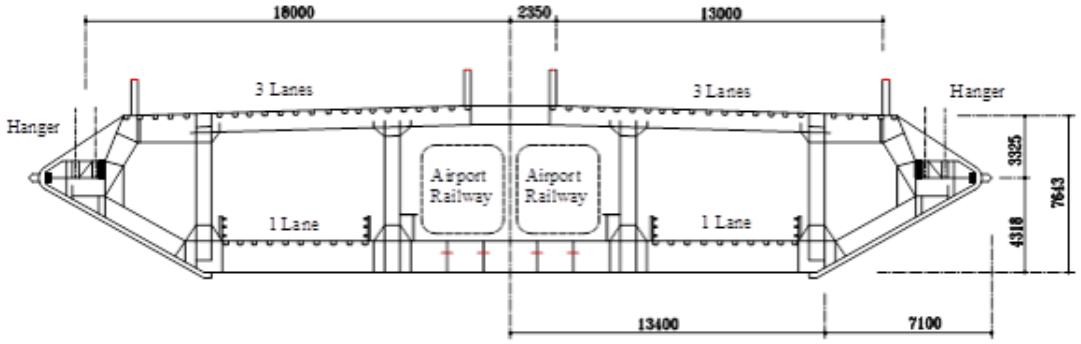

Figure 4.2 Deck cross section of TMB

The Wind and Structural Health Monitoring System (WASHMS) for the TMB consists of 283 sensors in total, including 6 anemometers, 19 servo-type accelerometers, 115 temperature sensors, 110 welded foil-type strain gauges (or dynamic strain gauges), 14 global positioning system (GPS) receivers, 2 displacement transducers, 10 level sensing stations, and 7 dynamic weigh-in motion (WIM) stations (Ni and Xia, 2016). The sensor layout and data acquisition stations on the TMB are shown in Figure 4.3.

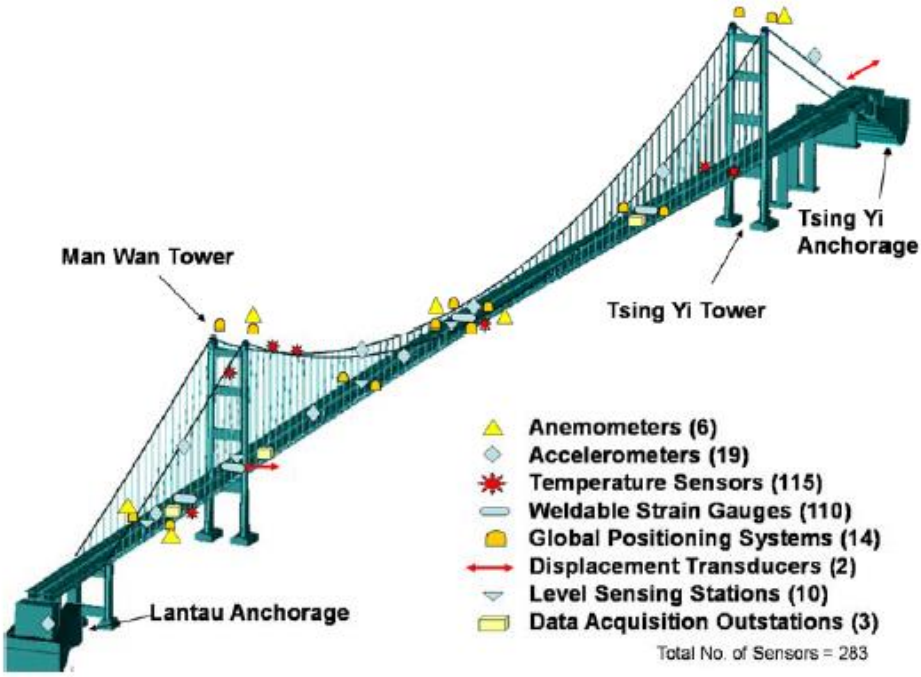

Figure 4.3 Sensor layout and data acquisition station on TMB

As part of the WASHMS, a set of GPS stations was installed on the bridge in 2000 (Wong *et al.*, 2001; Wong, 2004, 2007; Ni *et al.*, 2011). The GPS stations have a total of 14 GPS receivers deployed over several key components of the bridge, including the towers, main cables and four different sections of the bridge deck, to monitor the displacement responses of the TMB in longitudinal, lateral and vertical directions. To ensure the measurement accuracy, two base reference stations are established at the top of a storage building adjacent to the bridge monitoring room. To avoid the signal receiving obstruction caused by traffic, all the GPS receiver antennas on the bridge deck are mounted at 4 m high and with a view angle of above 15°. The sampling rate of GPS is set at 10 Hz. The deployment of GPS sensors is shown in Figure 4.4 and Figure 4.5.

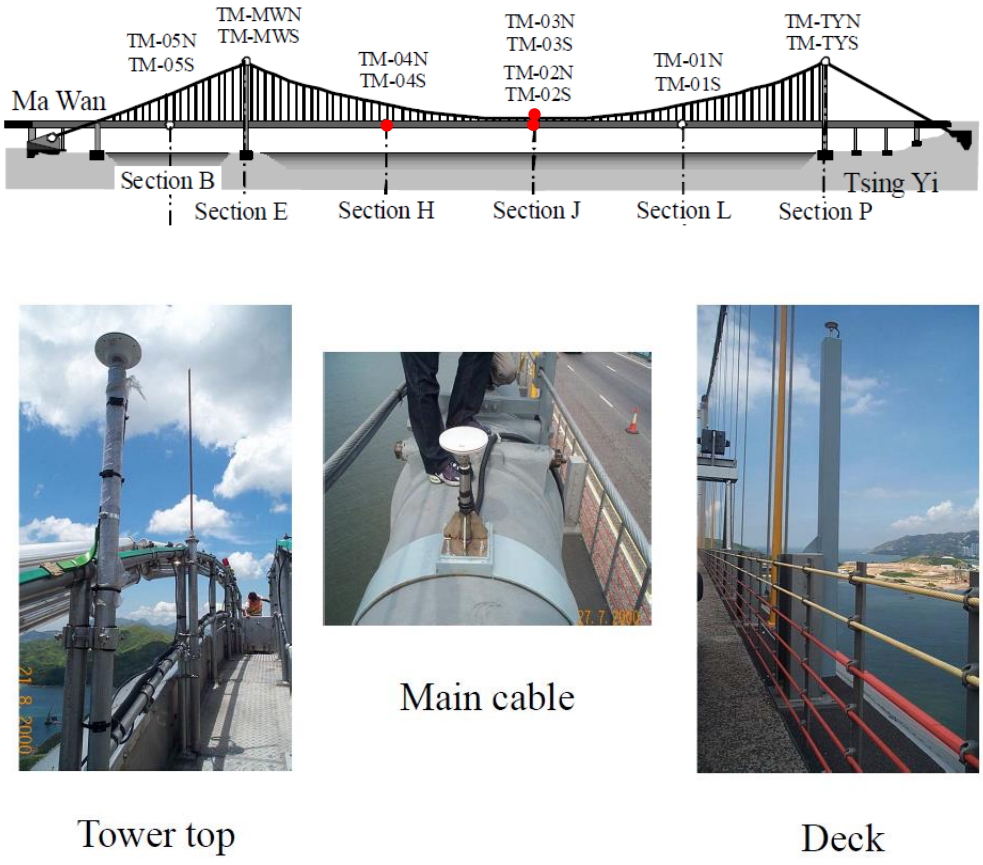

Figure 4.4 Locations of GPS stations and GPS rover stations on TMB

Figure 4.5 A GPS reference station on the roof of a storage building

There are 6 anemometers installed on the TMB, including 2 ultrasonic anemometers located at the mid-main span, 2 mechanical propeller-type anemometers at the middle of the Ma Wan side span, and 2 mechanical propeller-type anemometers on the top of the Tsing Yi tower and on the top of the Ma Wan tower, as shown Figure 4.6 (a). The anemometers at the deck level are installed on the both sides of the bridge deck and extended out for 9 m from the outmost edge of the deck, in order to eliminate the disturbance caused by the ambient structure components. The deployment of anemometers across the deck section is shown in Figure 4.6 (b). The sampling frequency of anemometers is set at 2.56 Hz.

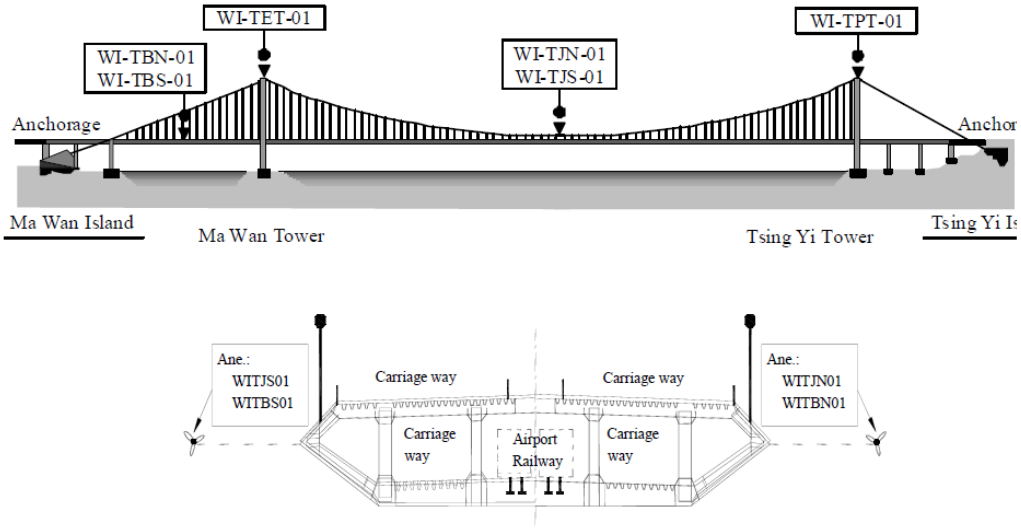

Figure 4.6 Location of anemometers along TMB and on cross section

4.3.2 Data acquisition and pre-processing

Monitoring data under 3 typhoon periods in 2011 obtained from the TMB are used in this study. According to the Hong Kong Observatory (HKO), there are 3 typhoons

hitting Hong Kong in 2011, namely Haima, Nockten, and Nesat. During the typhoon periods, strong winds were observed and Tropical Cyclone Warning Signal No. 3 or above was issued. Therefore, representative displacement responses and wind information including wind speed and wind direction during these three typhoons are used for this study. According to the HKO, the directions of the three typhoons are roughly from east direction. Based on the location and direction of the TMB, the south side of bridge is the windward side and the north side is the leeward side. Therefore, the wind data recorded from the anemometer from south side are used to represent the actual wind load acting on the bridge deck and the cables. The measured displacement and wind data are pre-processed to obtain the 10-min average values. The 10-min average wind speed and wind direction are plotted in time series in Figure 4.7 and Figure 4.8, and wind rose diagram is plotted in Figure 4.9.

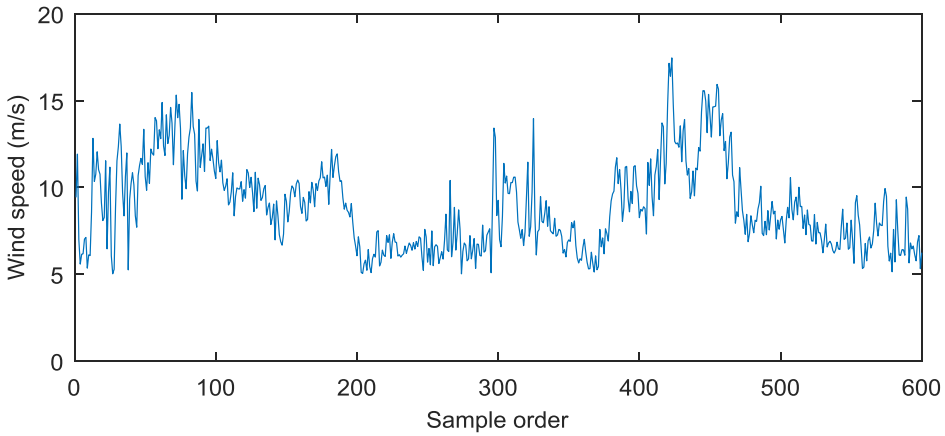

Figure 4.7 10-min average wind speed in time series

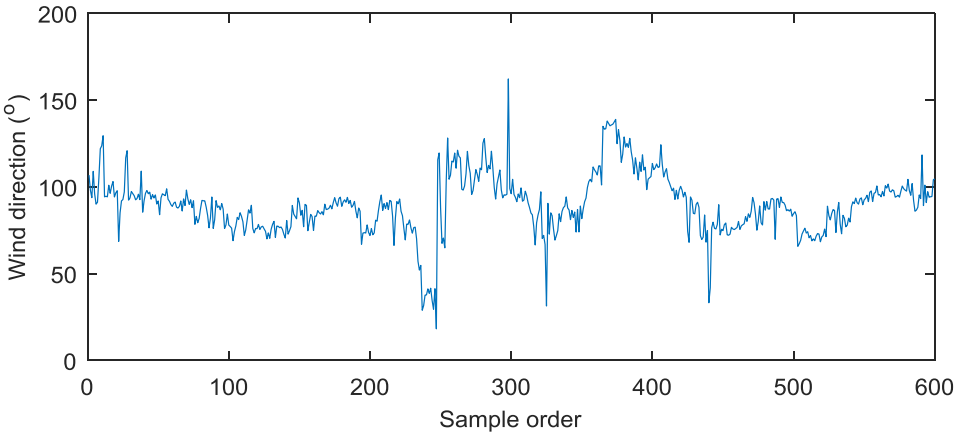

Figure 4.8 10-min average wind direction in time series

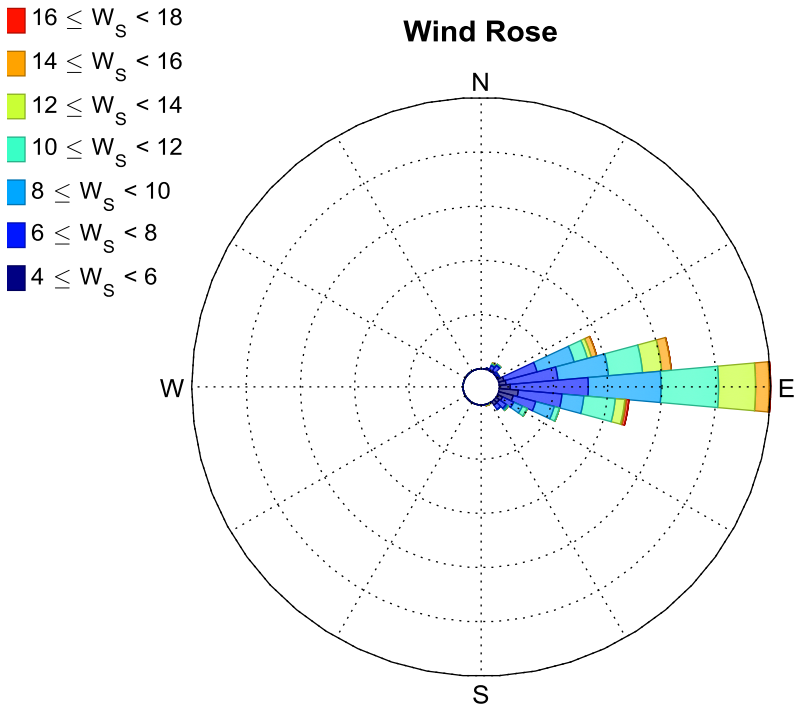

Figure 4.9 10-min average wind rose diagram

Displacement responses recorded from a GPS system usually contain displacement in three directions: longitudinal, lateral and vertical. For long-span bridges, longitudinal displacements are mainly thermal temperature-induced, while vertical displacements are mainly traffic-induced and lateral displacements are mainly wind-induced. In

addition, during a typhoon event, which lasts in general for a few hours, it is assumed that the temperature is constant and the temperature effect on lateral displacement can be ignored. Therefore, to study the relationship between wind load and wind-induced bridge displacement, the lateral displacement responses are used in this study. The wind loads acting on a large structure immersed in the wind field are composed of static wind forces due to mean winds, and dynamic wind forces due to fluctuating winds. Therefore, the displacement responses recorded by GPS containing two wind effects are first decomposed into mean displacement responses and dynamic displacement responses. The total displacement response can be expressed as

$$\hat{D} = \bar{D} \pm m_p \sigma_D \tag{4.4}$$

where $\hat{D}$ is the wind-induced total displacement of the bridge, $\bar{D}$ is the corresponding mean displacement, σ_D is the corresponding standard deviation, and m_p is the statistical peak factor (Xu & Xia, 2011). In the above equation, the dynamic displacement is expressed as $m_p \sigma_D$. The mean displacement responses of the bridge recorded by GPS is related to mean wind speed and direction, while the dynamic displacement response is related to the peak factor and standard deviation of the total displacement.

The statistical peak factor m_p is first estimated based on the relationship in Equation (4.4) using the measured data during typhoon periods. The estimation results are plotted against wind speed in Figure 4.10, Figure 4.11, and Figure 4.12 for three

locations: main cable, 1/2 main span, and 1/4 main span respectively. As shown in figures, m_p keeps almost invariant as the wind speed varies from 4 m/s to 18 m/s. It suggests that the peak factor is independent on wind speed and be a constant at particular locations. The distribution of the estimated m_p at three locations is plotted in Figure 4.13, Figure 4.14, and Figure 4.15. It seems that m_p is Gaussian distributed, and the mean values are finally used as estimated peak factor at three locations. The results are listed in Table 4.1. The estimated peak factors for dynamic displacement at main cable, 1/2 main span and 1/4 main span are all around 1.5. The estimated peak factor contributes to the prediction of the dynamic displacement component, while the mean displacement component will be studied in the following sections on its relationship with both wind speed and wind direction. Finally, the total displacement will be predicted based on both mean displacement response and dynamic displacement response.

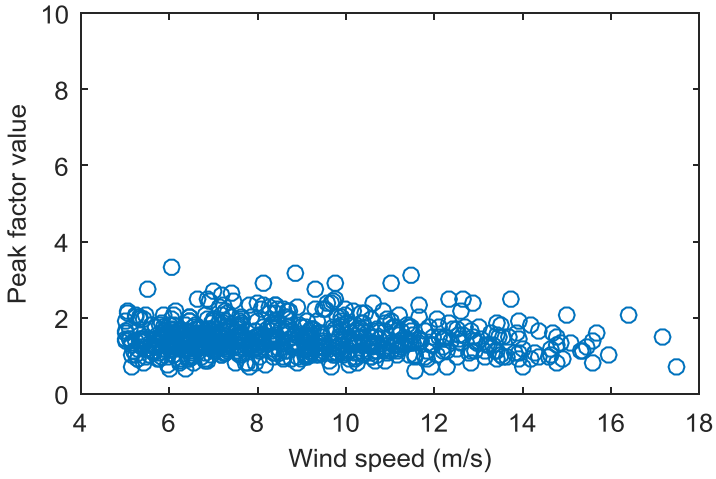

Figure 4.10 Peak factor against wind speed at main cable

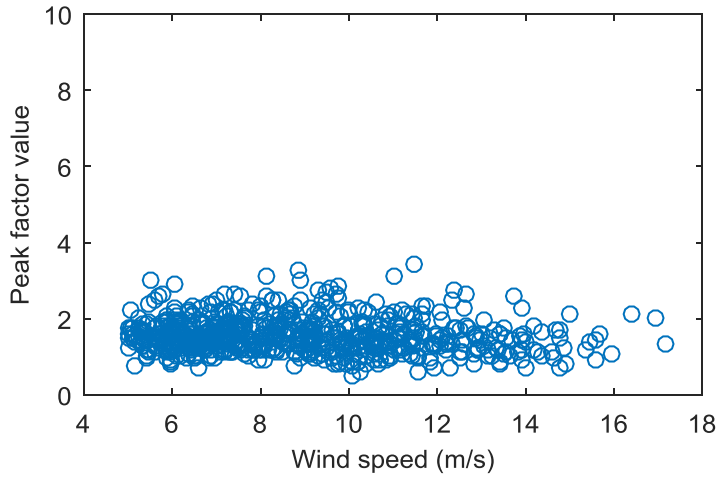

Figure 4.11 Peak factor against wind speed at 1/2 main span

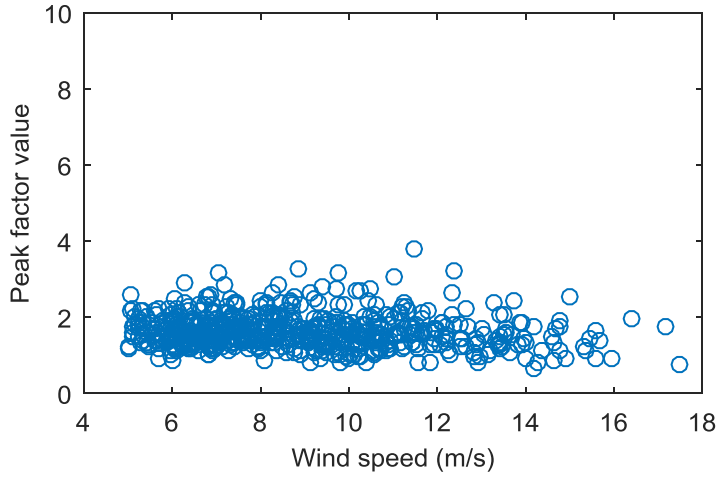

Figure 4.12 Peak factor against wind speed at 1/4 main span

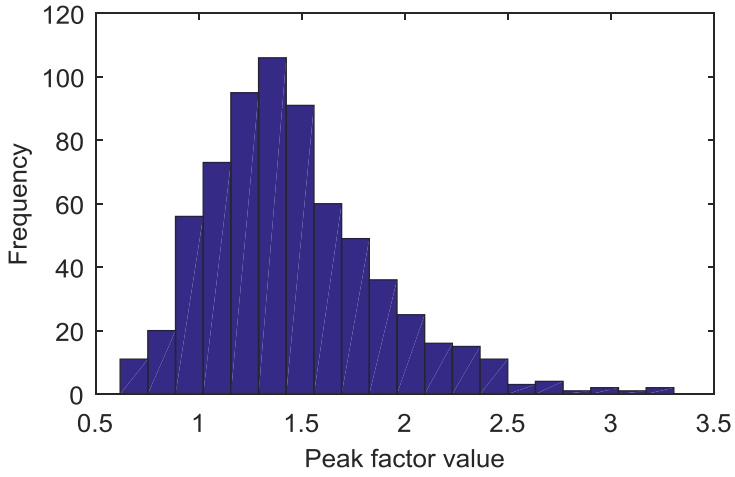

Figure 4.13 Peak factor distribution at main cable

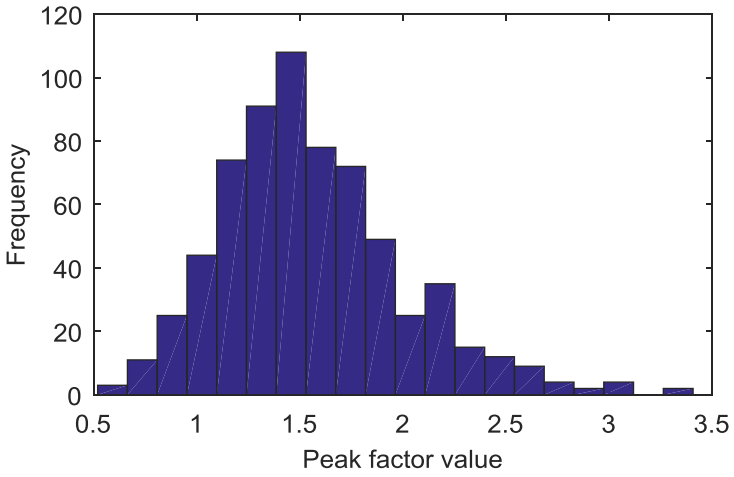

Figure 4.14 Peak factor distribution at 1/2 main span

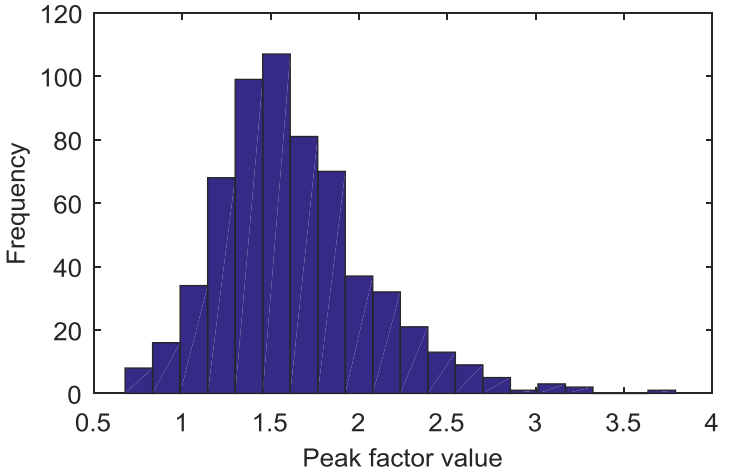

Figure 4.15 Peak factor distribution at 1/4 main span

Table 4.1 Estimated peak factor at different locations

Location	**Main cable**	**1/2 main span**	**1/4 main span**
m_p	1.46	1.56	1.63

4.3.3 Selection of case-specific covariance function

The mean displacement response y_i is assumed to be dependent on explanatory variables $\mathbf{x}_i = (x_{0i}, x_{1i}, x_{2i})^T$, where the first term x_0 always sets to be 1 to represent a constant term, x_1 denotes wind speed, and x_2 denotes wind direction. A generalized linear relationship between displacement response y_i and explanatory variables $\mathbf{x}_i$ is established through a mapping function $\phi(\mathbf{x})$. The relationship is assumed to be polynomial, which is a common choice for unknown relationship regression. By observation, the relationship does not vary a lot. Therefore, a polynomial relationship should be appropriate. For a second order polynomial, the mapping function $\phi(\mathbf{x})$ can be expressed as $\phi(\mathbf{x}) = \left(x_0^2, x_1^2, x_2^2, x_0x_1, x_0x_2, x_1x_2\right)$. Then there exists a vector $C(\mathbf{x}) = \left(x_0^2, x_1^2, x_2^2, \sqrt{2}x_0x_1, \sqrt{2}x_0x_2, \sqrt{2}x_1x_2\right)$ and the covariance of $C(\mathbf{x})$ takes the form

$$\begin{aligned}\left\langle C(\mathbf{x}), C(\mathbf{x}')\right\rangle &= \left(x_0\right)^2\left(x_0'\right)^2 + \left(x_1\right)^2\left(x_1'\right)^2 + \left(x_2\right)^2\left(x_2'\right)^2 \\ &\quad +2\left(x_0x_1\right)\left(x_0'x_1'\right) + 2\left(x_0x_2\right)\left(x_0'x_2'\right) + 2\left(x_2x_2\right)\left(x_2'x_2'\right) \\ &= \left\langle \mathbf{x}, \mathbf{x}'\right\rangle^2 = (\mathbf{x}\cdot\mathbf{x}')^2\end{aligned} \tag{4.5}$$

When the regression relationship extends from second order to a *p*th order polynomial, the mapping function $\phi(\mathbf{x})$ can be denoted as $\phi(\mathbf{x}) = \{x_0^{k_0}x_1^{k_1}x_2^{k_2} \mid \text{for all } k_0 + k_1 + k_2 = p\}$. It has been proven that there exists a mapping vector $C_p(\mathbf{x})$, whose entries are all possible *p*th order products of the entries

of $\mathbf{x} \in \mathbf{R}^N$, the corresponding covariance computing the dot product of vectors mapped by C_p can be written as

$$k(\mathbf{x}, \mathbf{x}') = \left\langle C_p(\mathbf{x}), C_p(\mathbf{x}') \right\rangle = \left\langle \mathbf{x}, \mathbf{x}' \right\rangle^p = (\mathbf{x} \cdot \mathbf{x}')^p \tag{4.6}$$

The proposition and proof can be found in detail in Schölkopf & Smola (2002). If the prior Gaussian distribution of the parameter vector $\mathbf{w}$ is considered, the covariance function is finally derived as

$$\begin{aligned} K(\mathbf{x}, \mathbf{x}') &= {\sigma_f}^2 ({\sigma_0}^2 + \mathbf{x}^T \Sigma_p \mathbf{x}')^p \\ K(X, X') &= {\sigma_f}^2 ({\sigma_0}^2 + X^T \Sigma_p X')^p \end{aligned} \tag{4.7}$$

where ${\sigma_f}^2$ is the signal variance, ${\sigma_0}^2$ is the variance of constant term parameter, and $\Sigma_p = l^2 I$ is the covariance matrix of the coefficients of $\mathbf{x}$. With the explicit covariance function form, a polynomial regression model based on GPR (P-GPR) can be achieved.

Before conducting GPR modeling, the order *p* should be determined first. Here three P-GPR models are considered, with *p* = 1, 2, 3 respectively. Based on the data pre-processing described in Section 4.3.2, it is believed that the first, second, and third order polynomial models are enough for the regression modeling. General-purposed GPR model with SE covariance function (SE-GPR) model introduced in the previous chapter is also adopted in this chapter, to evaluate the performance for regression and prediction. The GPR models used in this chapter are summarized in Table 4.2.

Table 4.2 GPR models for comparison

Model No.	Variables involved	Order of x, *p*
P-GPR1	x_1, x_2	1
P-GPR2	x_1, x_2	2
P-GPR3	x_1, x_2	3
SE-GPR	x_1, x_2	-

4.3.4 Hyperparameter adaptation

As discussed in the previous section, there exist four hyperparameters in the P-GPR model which need to be determined to obtain an optimized P-GPR model, including the signal variance σ_f^2, the variance of constant term parameter σ_0^2, the characteristic length-scale l from the explicit polynomial covariance function, and the noise variance σ_n^2 during the observation sampling. The four hyperparameters $[l, \sigma_0, \sigma_f, \sigma_n]$ are all initially set to 1, so that the P-GPR model has unit characteristic length-scale, unit signal standard deviation, unit variance of constant term parameter, and unit noise standard deviation. Similar initial values are given to the hyperparameters in SE-GPR model. The log marginal likelihood maximization is then conducted to optimize the hyperparameters.

After preliminary data processing, 600 observations including bridge mean displacement responses, mean wind speed, and mean wind direction obtained during the three typhoon events are chosen for GPR model formulation. The entire sample

set is divided into training data set, including 400 observation samples to formulate and train the GPR models, and testing data set, including 200 observation samples to test the capability of the GPR models.

After 100 iterations of log marginal likelihood maximization, the optimized hyperparameter values and maximal log marginal likelihood for the three P-GPR models with different orders and SE-GPR are obtained and listed in Table 4.3. According to Table 4.3, it seems that P-GPR1 performs worst with the smallest log marginal likelihood, suggesting the relationship between displacement and wind load is not simply linear. While the other three models, P-GPR2, P-GPR3, and SE-GPR have similar log marginal likelihood, suggesting these three models may have similar performance in regression and prediction.

Table 4.3 Optimized hyperparameters and maximal log marginal likelihood

	Hyperparameter				**Log marginal likelihood**
	l	σ_0	σ_f	σ_n	
P-GPR1	2.7967	5.0530	9.1295	11.6820	-1.56×10^3
P-GPR2	7.3021	24.1939	8.9533	9.1004	-1.48×10^3
P-GPR3	3.1510	0.9946	0.6794	9.0185	-1.48×10^3
SE-GPR	29.8211	-	148.2442	8.7511	-1.47×10^3

4.3.5 Prediction performance

In the above section, 400 training data are used to obtain the optimized GPR models. In this section, 200 testing data are fed into the optimized GPR models to evaluate their prediction capability. The RMSE is used as an indicator to evaluate the prediction results, which is

$$RMSE = \sqrt{\frac{1}{n}\sum_{i=1}^{n}(y_i - y_i^{pred})^2} \tag{4.8}$$

where y_i is the ith measured displacement response corresponding to $\mathbf{x}_i$, y_i^{pred} is the ith predicted displacement response corresponding to $\mathbf{x}_i$, and n is the total number of testing samples ($n = 200$ in this case).

Results are provided in Table 4.4 for all four models. It seems the four models have comparable performance with similar RMSE values all around 11. Among three P-GPR models, it seems the model with second order polynomial has a little better performance compared with the other two. While the SE-GPR has the smallest RMSE, suggesting it is the most flexible and has the best prediction capability for predicting the testing data obtained under similar condition to the training data. The measured and predicted testing displacement responses are plotted in Figure 4.16 and Figure 4.17 for P-GPR2 and SE-GPR respectively.

Table 4.4 Prediction RMSE of four GPR models

Model	P-GPR1	P-GPR2	P-GPR3	SE-GPR
RMSE	11.9868	11.4069	11.7566	10.5152

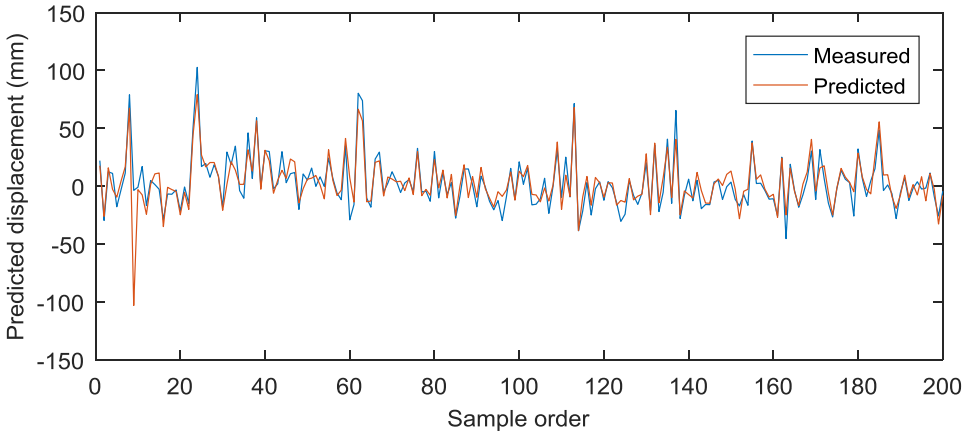

Figure 4.16 Measured and predicted testing displacement data using P-GPR2

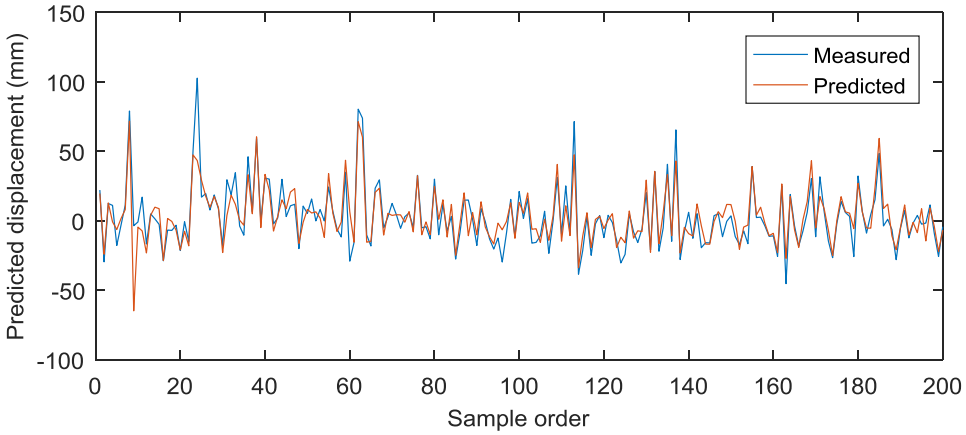

Figure 4.17 Measured and predicted testing displacement data using SE-GPR

Besides the prediction of displacement response within the observation clusters of wind speeds and directions, the displacement responses under extreme conditions are also of great interest, especially in structural condition assessment and evaluation fields. When the testing data moves from the observation cluster to outside regions,

for example under extreme conditions, the prediction capability of the four GPR models is studied in this section. Possible wind speed ranging from 0 to 54 m/s, wind direction with large probability ranges from 30° (northeast direction) to 180° (south direction) are fed into the optimized GPR models. The predicted displacement responses varying with wind speed when wind direction is fixed at 90° (east direction) are plotted in Figure 4.18 to Figure 4.21 for the four GPR models. Similarly, the predicted displacement responses varying with wind direction when wind speed when is fixed at 10m/s (mean speed) is plotted in Figure 4.22 to Figure 4.25 for four GPR models.

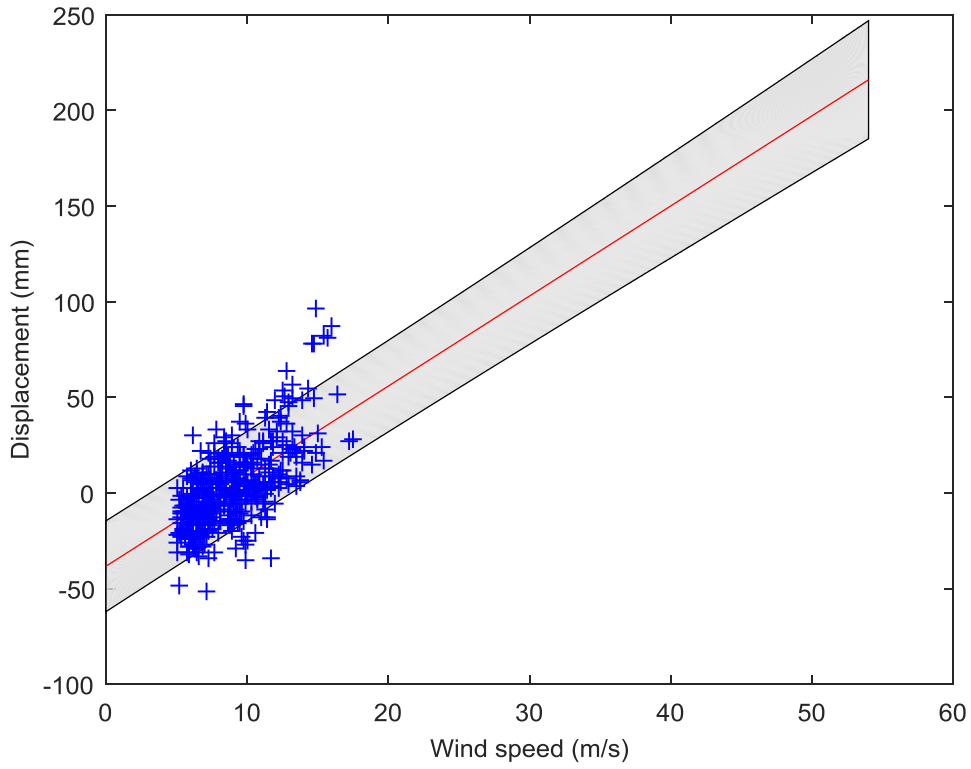

Figure 4.18 Predicted displacement under varying wind speed at 90° using P-GPR1

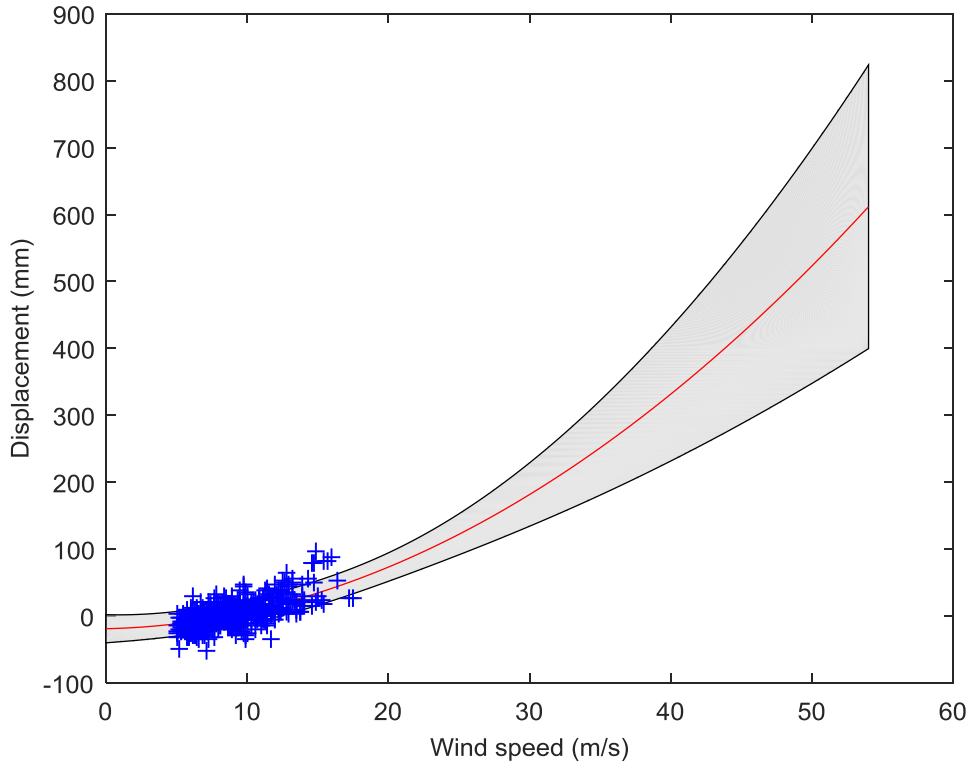

Figure 4.19 Predicted displacement under varying wind speed at 90° using P-GPR2

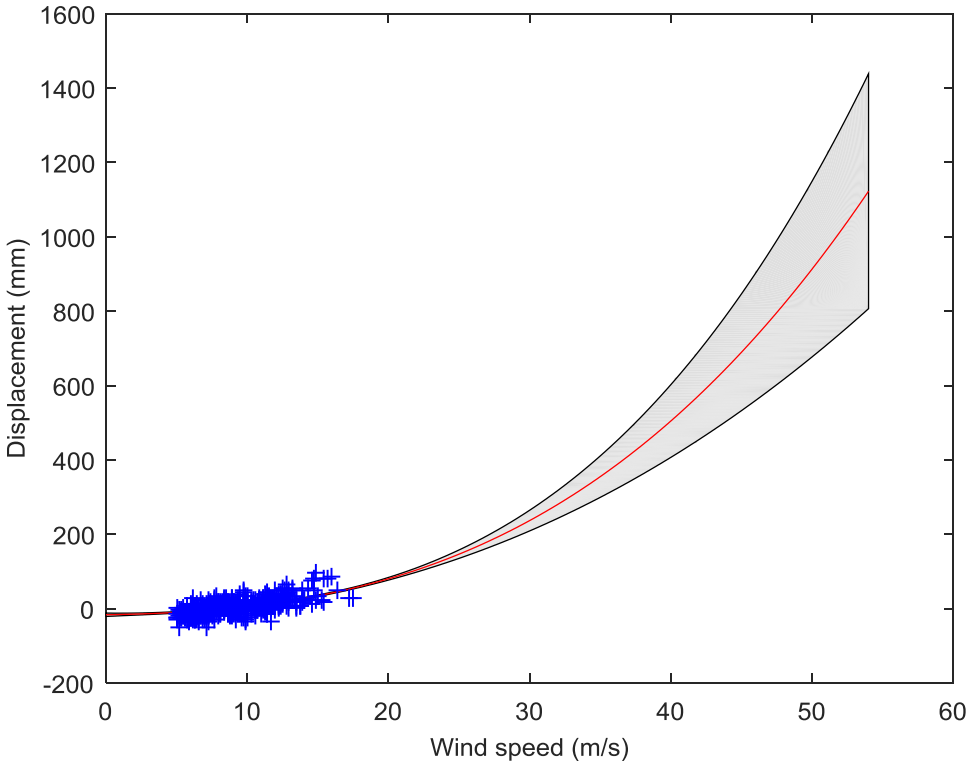

Figure 4.20 Predicted displacement under varying wind speed at 90° using P-GPR3

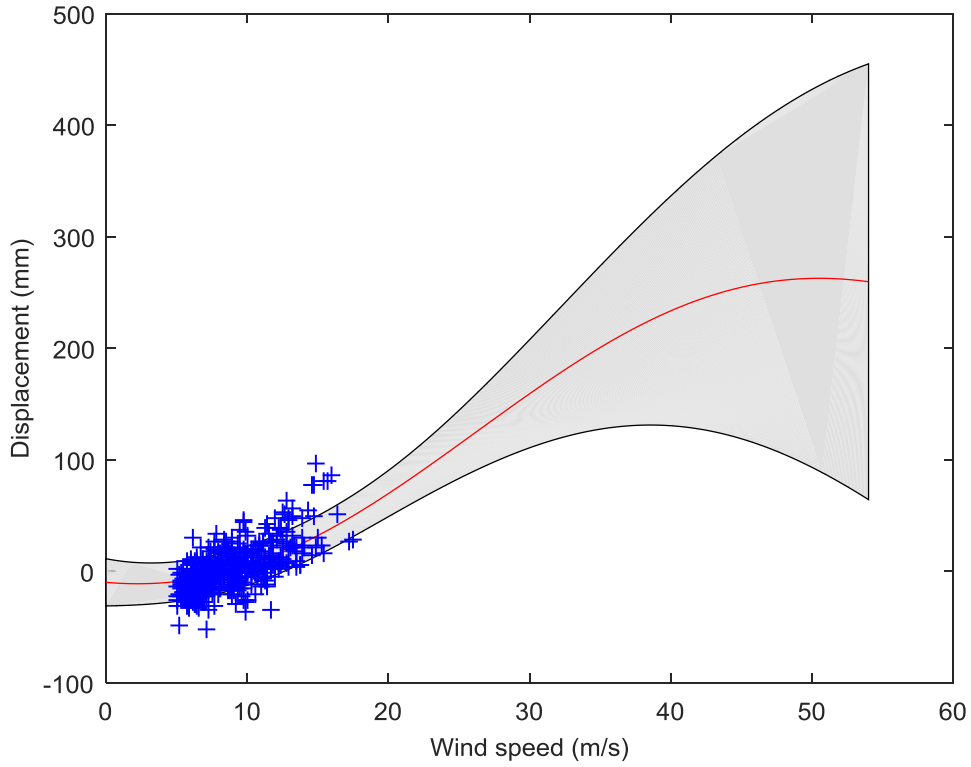

Figure 4.21 Predicted displacement under varying wind speed at 90° using SE-GPR

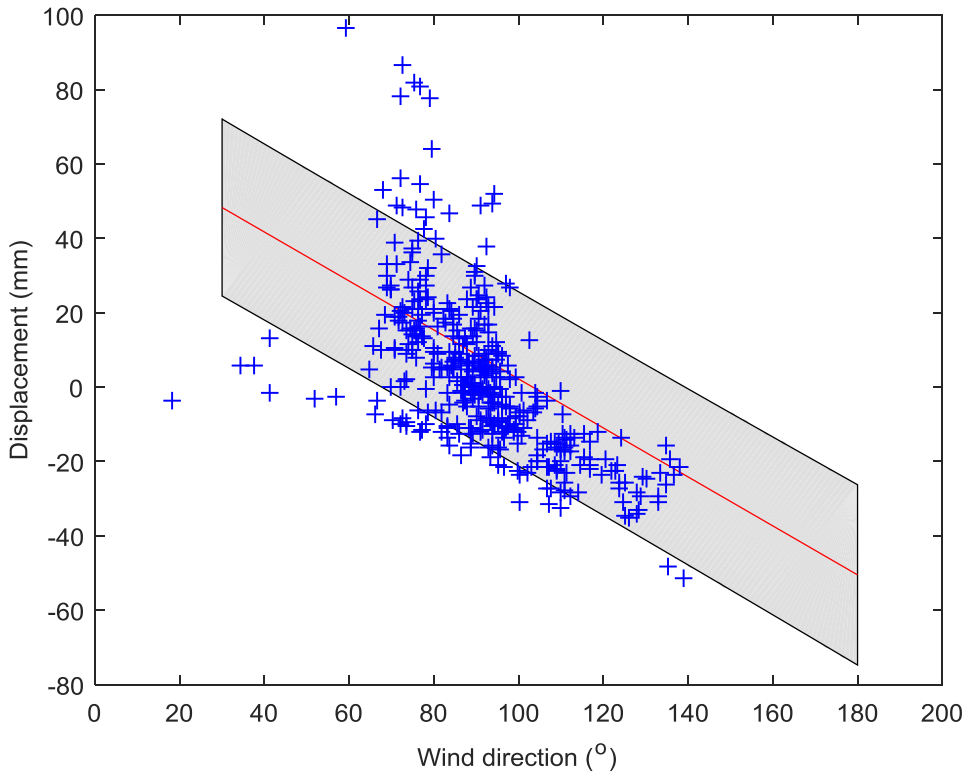

Figure 4.22 Predicted displacement under varying wind direction using P-GPR1

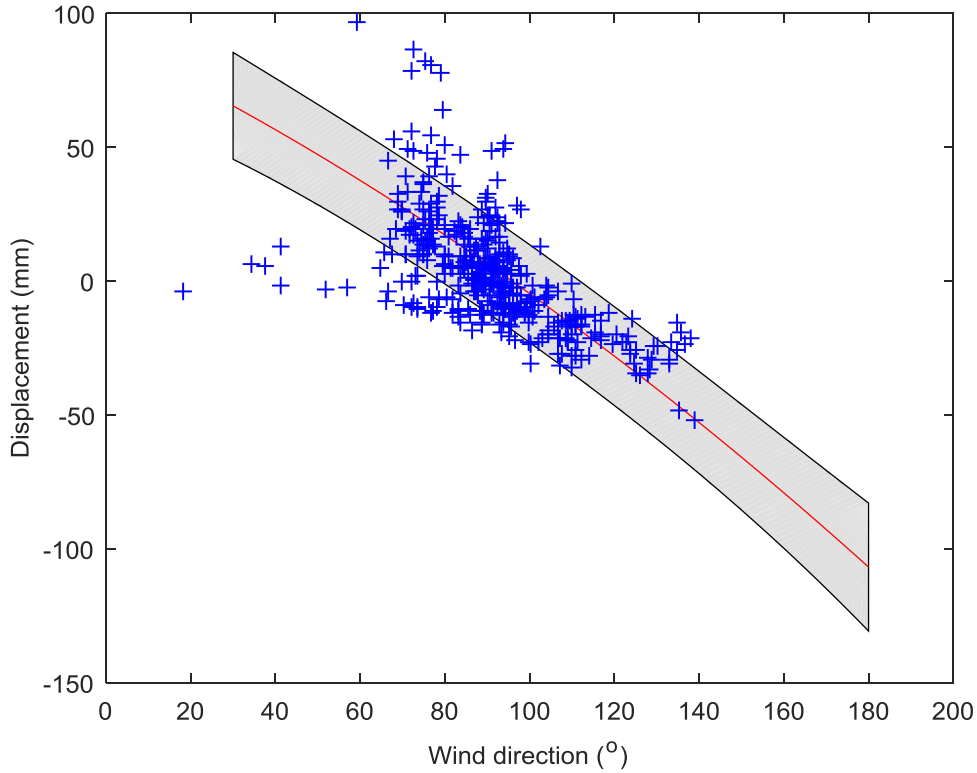

Figure 4.23 Predicted displacement under varying wind direction using P-GPR2

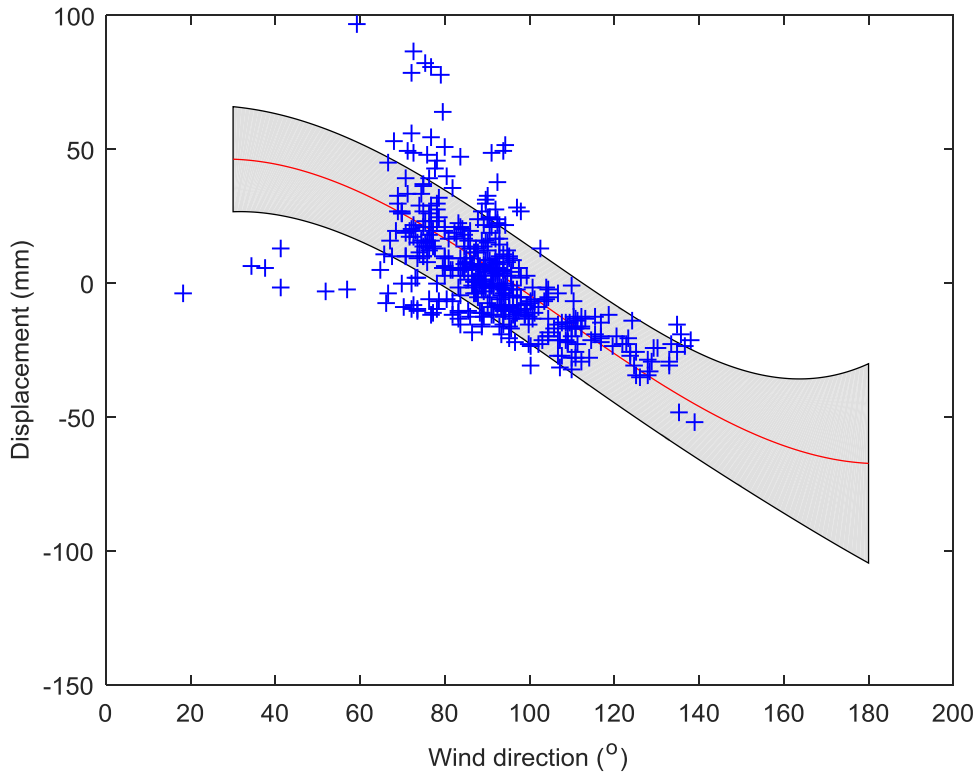

Figure 4.24 Predicted displacement under varying wind direction using P-GPR3

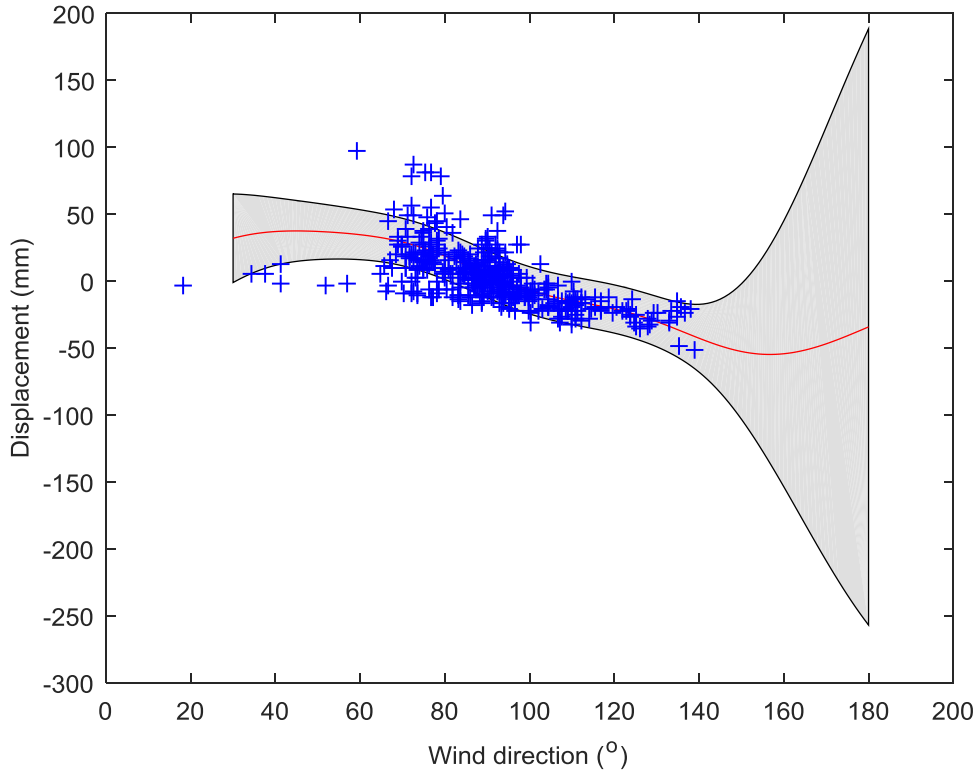

Figure 4.25 Predicted displacement under varying wind direction at using SE-GPR

According to Figure 4.18 to Figure 4.21, it is seen that the estimated mean function shape of the three P-GPR models follow the definition of first, second, and third order polynomial function respectively, as defined through the explicit covariance functions. Except for P-GPR1, which is essentially a linear relationship regression with almost constant confidence interval, both P-GPR2 and P-GPR3 have small uncertainties when variables are close to the observation clusters, and increasing uncertainties when input variables move away from the observation clusters. Similar result can be observed from the prediction result of the SE-GPR model. The uncertainties predicted by SE-GPR increase as the input variables go far away from the observation cluster. For SE-GPR, although it has the best performance in predicting displacement within the

observation cluster, when the wind speed keeps going larger, the predicted displacement starts to decrease. This result is same as the SE-GPR performance in linear regression prediction, due to the essential characteristic defined by its SE covariance function. Therefore SE-GPR is not suitable for prediction of displacement responses under extreme conditions far beyond the observation cluster.

Similar to Figure 4.18 to Figure 4.21, features related to the characterization of GPR models are coincident with the results found in Figure 4.22 to Figure 4.25. As the input wind directions for prediction are almost within the observation ranges, the uncertainties predicted by P-GPR models seem relatively constant for three polynomial order assumptions. However, for SE-GPR, the uncertainties become very large when the wind direction is larger than 150°, where seldom information is provided in this region. In addition to the essential characteristics of different GPR models, a negative correlation between wind direction and displacement response can be observed in all GPR models in Figure 4.22 to Figure 4.25. This finding suggests that with the wind direction increasing (changing from northeast to south), the wind load on the bridge has less influence on the displacement responses, at least within the observation ranges. Since the TMB runs west-east, the smaller wind direction indicates a larger attack angle, and therefore induces a larger lateral displacement. The prediction results consist with the physical interpretations.

After performance comparison of the four GPR models in predicting displacement responses under extreme condition far beyond the observation cluster, it is believed that the P-GPR models perform better than SE-GPR model. Based on the log marginal likelihood and RMSE criteria, P-GPR2 is finally selected as the optimal GPR model.

4.3.6 Displacement prognosis in terms of second order P-GPR

The pre-processed mean displacement responses at three locations including main cable, 1/2 main span, and 1/4 main span, are fed into the outperformed P-GPR2 model for displacement response prediction and prognosis, together with the same wind data during typhoon periods. The optimized model hyperparameters using the training data for sample sets from three locations are listed in Table 4.5. It is seen that for the three sample sets, the P-GPR2 model all performs satisfactorily, with comparable log marginal likelihood and RMSE. According to the optimization results, the P-GPR2 model performs best in prediction using displacement observations from 1/4 main span among the three locations. It has the largest log marginal likelihood and the smallest RMSE. The estimated noise standard deviation σ_n for the model dealing with displacement observations from 1/4 main span is also the smallest.

Table 4.5 Optimization of P-GPR2 model at three locations

	Hyperparameter				Log marginal likelihood	RMSE
	l	σ_0	σ_f	σ_n		
Main cable	7.3021	24.1939	8.9533	9.1004	-1.48×10^3	11.4069
1/2 main span	7.6070	27.5598	9.9924	8.7952	-1.46×10^3	12.4330
1/4 main span	8.7291	28.7645	9.7359	8.1730	-1.43×10^3	10.0300

The wind-induced displacement responses under extreme conditions are of great interest in practical structural design and health condition assessment. According to the design documents, the designed 10-min average wind speed for serviceability limit state is 53.3 m/s for a return period of 120 years. The wind speed ranges from 0 m/s to the designed critical wind speed at 0.1 m/s interval are fed into the P-GPR2 model as predicting wind speed input. The wind direction ranges from 30° to 180° at 1° interval are used as predicting wind direction input. The prediction results including mean function for the three sample sets are plotted in Figure 4.26 to Figure 4.28, together with the original sample measurements. When the wind speed reaches the 120-year return-period design value, the wind direction should also be determined in order to get the maximum mean displacement prediction. Here the wind direction is

considered in two cases: (i) the wind direction is chosen with largest probability at 90°; (ii) the wind direction is chosen at smallest reasonable wind direction at 30°. The second case is chosen because of the negative correlation between wind direction and displacement response observed in Section 4.3.5. Therefore, the largest displacement at 53.3 m/s wind speed is believed to appear when wind direction is at 30°.

The predicted mean displacements at 90° and 30° wind directions for the three locations are listed in Table 4.6 and Table 4.7. It can be seen in Table 4.6, that the predicted mean displacements at 90° wind direction are 596 mm and 621.8 mm for main cable and 1/2 main span respectively, which are very close with similar standard deviation. This may be explained by the fact that the main cable GPS rover station is also located at 1/2 main span. The two locations are very close, thus similar displacement responses are observed. The predicted displacement at 1/4 main span has smallest value, about 424.5 mm, which is coincident with the fact that the 1/4 main span location has smaller lateral displacement than 1/2 main span location. The predicted standard deviation at 1/4 main span is also the smallest.

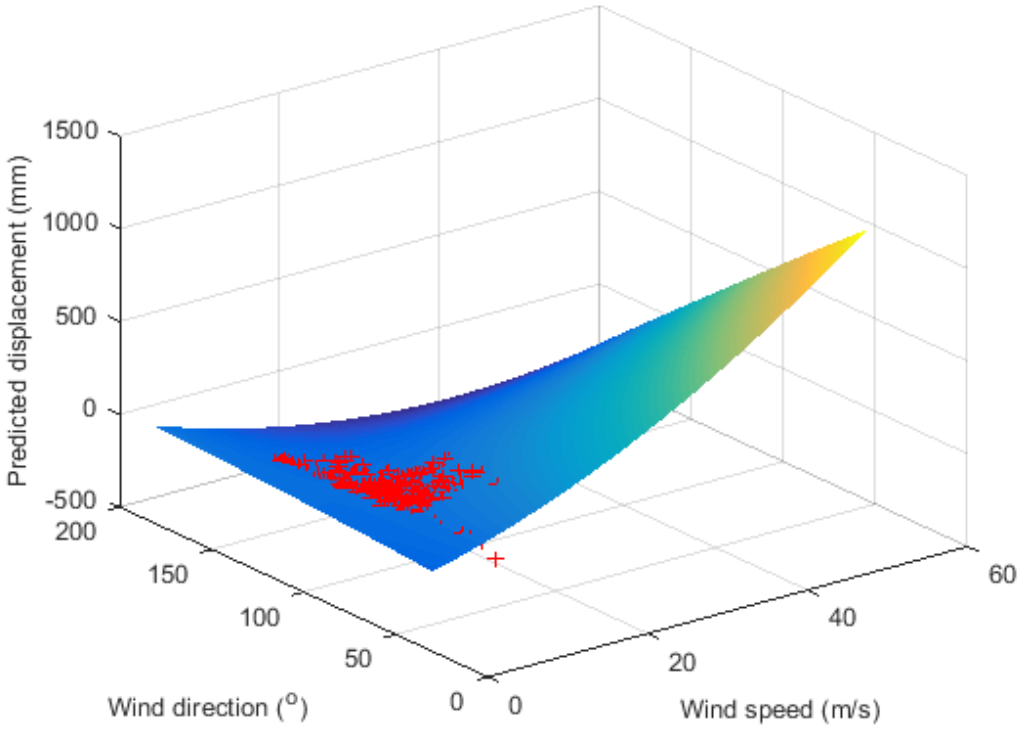

Figure 4.26 Predicted mean displacement at main cable

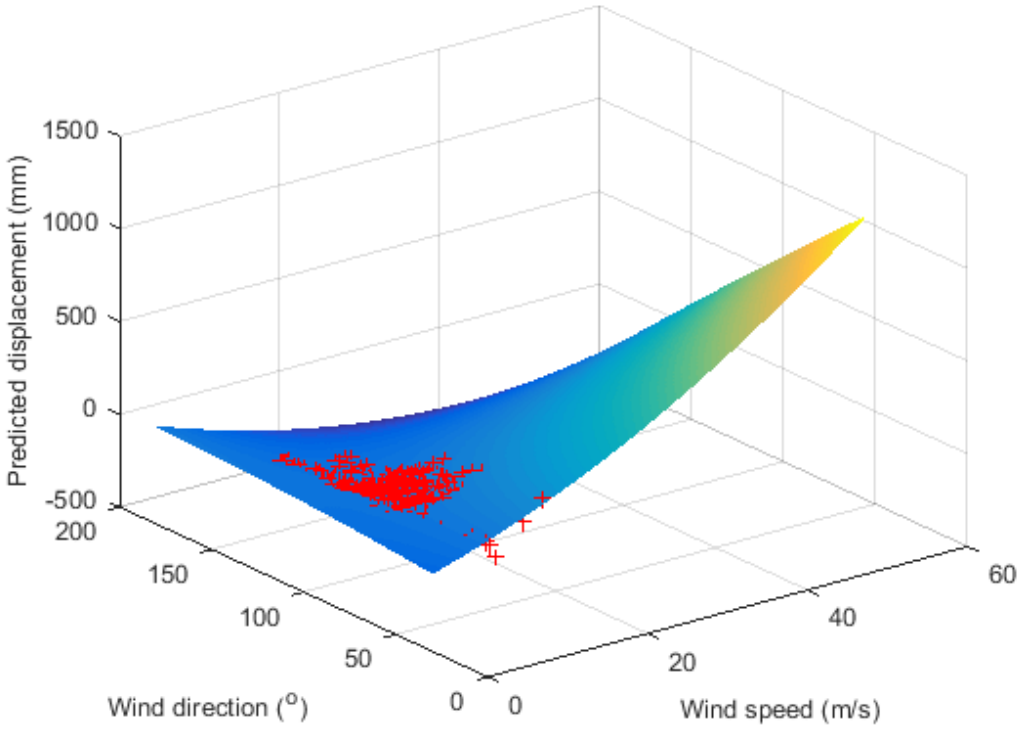

Figure 4.27 Predicted mean displacement at 1/2 main span

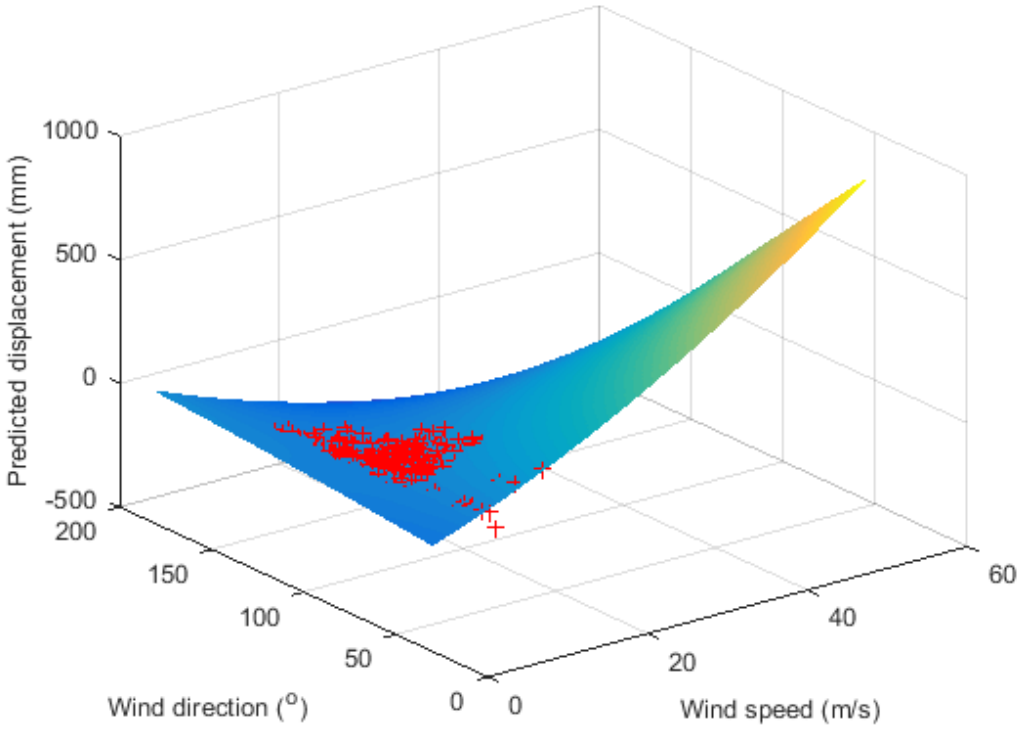

Figure 4.28 Predicted mean displacement at 1/4 main span

Table 4.6 Predicted mean displacement at 90° wind direction (east)

	Predicted mean displacement $\bar{D}$ **(mm)**	**Standard deviation** σ_D
Main cable	596.0	102.72
1/2 main span	621.8	109.645
1/4 main span	424.5	97.73

Table 4.7 Predicted mean displacement at 30° wind direction

	Predicted mean displacement $\bar{D}$ (mm)	**Standard deviation σ_D**
Main cable	1108.3	102.32
1/2 main span	1181.9	110.33
1/4 main span	911.9	97.05

Table 4.8 Predicted total displacement at three locations

	Predicted total displacement $\hat{D}$ (mm)	
	90° wind direction	30° wind direction
Main cable	[446.1, 746.0]	[958.9, 1257.7]
1/2 main span	[450.8, 792.9]	[1009.8, 1354.0]
1/4 main span	[265.2, 583.8]	[753.7, 1070.1]

Making use of Equation (4.4) in Section 4.3.2, the total lateral displacement $\hat{D}$ is predicted based on the estimated mean displacement $\bar{D}$, corresponding standard deviation σ_D, and peak factor m_p. The predicted total displacement responses with fluctuations are listed in Table 4.8. After adding the dynamic displacement component into the total displacement responses, the maximum displacement under extreme condition becomes fluctuated, and the confidence interval are provided based on the dynamic displacement component. According to Table 4.8, the maximum total displacement at 1/2 main span under extreme wind speed of 53.3 m/s and the most

unfavorable wind direction of 30° is 1.35 m. Even under the worst situation, the predicted total displacement is still much smaller than the designed maximum allowable total lateral displacement of 2.9 m. The results suggested that the design is reasonable with appropriate safety reserve.

4.4 Summary

GPR model is formulated to establish the relationship between the lateral displacement and wind data for the TMB. Explicit polynomial covariance function is derived to formulate P-GPR. Generally-used SE-GPR discussed in Chapter 3 is also adopted for comparison. The SE-GPR is flexible and performs well in prediction within the observation cluster but unsatisfactorily when testing data is far away from the observation cluster. Among the three polynomial relationships considered in this study, the P-GPR with second order is selected as the optimal GPR model with the largest log marginal likelihood and smallest RMSE. The outperformed P-GPR2 is further used to predict the lateral displacement under extreme design wind speed at 53.3 m/s. The wind direction for maximum displacement prediction is considered in two cases. Even in the most unfavorable case with wind direction at 30°, the predicted total displacement is still within the designed maximum allowable total lateral displacement. The results suggested that the design is reasonable with appropriate safety reserve.

When the relationship between regression data is not explicitly clear, SE-GPR has excellent prediction performance within the observation cluster, with the smallest

RMSE. However, as the testing data moves far away from the observation cluster, the estimated mean function based on SE covariance function becomes undesirable. This characteristic makes SE-GPR not suitable for estimating targets far outside the observation cluster.

When the testing data moves far away from the observation cluster, although the P-GPR model estimates the mean functions with desirable trends, the estimated uncertainties become increased. With the implementation of SHM, more data under severe conditions will be available, and thus the estimated uncertainties can be reduced.

CHAPTER 5

CONCLUSIONS AND RECOMMENDATIONS

5.1 Conclusions

The development of structural health monitoring (SHM) enables to gain rich information about the in-service performance of bridges. By integrating the monitoring data from an online SHM system, the structural condition of the monitored structure can be assessed and the health status can be evolutionarily traced. The advancement in SHM technology has been evolving from the monitoring-based diagnosis to the monitoring-based prognosis. Conventional analytical methods process the monitoring data with deterministic parameters and coefficients and have difficulty in determining the uncertainties involving measurement noises, modeling errors, structure complexity, and etc. In recent years, the Bayesian modeling approach with Gaussian process (GP) has earned attention because of its characteristic which allows for the probabilistic processing and has high flexibility in modeling different kinds of relationships as well. The covariance functions in GP can determine the distribution of target function which is of great importance and therefore should be carefully chosen in order to fit the real covariance distribution of the data regression relationship. The squared exponential (SE) covariance is commonly chosen in GP because it corresponds to a linear combination of infinite number of basis functions and has the largest flexibility. But when the relationship is known a priori, the explicitly defined

covariance function may perform better than the general-purposed SE one. The research efforts in this thesis have been devoted to exploring the flexibility of GP in modeling different relationships by explicitly adapting the model, for the purpose of structural health condition assessment using the monitoring data. The major contributions are as follows.

1. **Development of a linear GP regression (L-GPR) model based on the explicit definition of model functions using the temperature and expansion joint displacement monitoring data from the Ting Kau Bridge (TKB).**

GP with Bayesian framework provides flexible non-parametric modeling abilities and probabilistic inference predictions based on Mercer kernels, and it becomes popular in civil engineering fields in recent years. However, no investigation has been reported on the influence of covariance function definition on the performance of Gaussian process regression (GPR) model. The contribution of this study lies in the formulation of GPR model with an explicit linear covariance function and comparison between L-GPR and general-purposed GPR model with SE covariance function (SE-GPR) using the SHM data. The GPR models have been formulated to establish the relationship between the temperature and expansion joint displacement using the monitoring data from the TKB. The performance of L-GPR has been examined and the structural health condition of the TKB has been examined using the GPR model. The specific findings and conclusions are as follows:

(i) The covariance function for a linear relationship is derived. With the explicit linear covariance function, the GPR model can get the same theoretical results as the Bayesian linear model. Using the log marginal likelihood maximization method, the hyperparameters exist in the GPR model are successfully optimized.

(ii) As a non-parametric model, GPR model cannot provide parameter values in model formulation and optimization. Instead, GPR provides probability distribution directly over function values. The results provided by GPR model is the estimated mean function and its uncertainties described as covariance function. Although the GPR model cannot provide the estimated parameters of the algorithm structure, it can generate the same theoretical results as Bayesian linear model. The non-parametric feature makes GP more suitable when the physical structure is complex and parametric model is not available.

(iii) The performance of optimized L-GPR and SE-GPR models is compared using the same sample data set. The predicted mean function from L-GPR is linear, which coincide with the explicit definition through its covariance function. Although SE-GPR does not have a linear definition, the estimated mean function tends to be almost linear with very smooth curve at the regions where sample data are observed. But this smooth curve varies larger with larger uncertainties as the prediction goes far away from the observation cluster. This

result is reasonably foreseeable due to the SE covariance functions characteristics. However, when the prediction goes far away from the observation cluster, the L-GPR still performs well as a linear model. When predicting temperature-induced expansion joint displacement using the testing data of temperature within or close to the observation ranges, both L-GPR and SE-GPR perform satisfactorily. However, when the prediction inputs move away from the observation cluster, L-GPR still performs well with stable uncertainties, while SE-GPR performs worse and have mean function inaccurate with large uncertainties. Therefore, the L-GPR performs better and explicit covariance functions should be chosen when the relationship characteristic is known a priori.

(iv) The outperformed L-GPR is used to predict the expansion joint displacements under extreme design temperatures at two expansion joints. The predicted mean displacement range at the expansion joint DSGPW01 under designed working environment is about 291.53 mm, which is close to the designed displacement range of 297 mm. The predicted mean displacement range at the expansion joint DSGAW01 under designed working environment is about 335.64 mm, which is close to the designed displacement range 339 mm. However according to the 95% confidence interval estimation, the displacement range may lie in [255.24, 327.81] for DSGPW01 and [296.48, 374.79] for DSGAW01. If the 95% predicted interval is considered for the

health condition assessment, risks exist that the displacement range may exceed the designed value. Therefore, for the sake of safety, it is recommended to improve the temperature-induced displacement designing for similar bridges.

2. **Development of a generalized linear GPR model based on the explicit definition of model functions using the lateral displacement and wind data from the Tsing Ma Bridge (TMB).**

A simple linear relationship provides drawback on the model because of the limited flexibility inside the model. If the actual relationship between the input and output variables cannot be reasonably approximated by a linear relationship, an inaccurate simple linear model will give poor predictions with large errors. In practical cases, the linear relationships may not be satisfied, and therefore a generalized model is needed. The contribution of this stage of study is the extension of the simple linear GPR model to a generalized linear model, by a projection of variables before the linear combination. The projection is flexible to any functions thus the generality still holds. Using the lateral displacement and wind data from the TMB, a generalized linear GPR model has been formulated to model the polynomial relationship (P-GPR) between the data. Performance comparisons have been made between the explicit P-GPR with different order polynomials and the general-purposed SE-GPR. Finally, the structural health evaluation and prediction has been realized using the optimal generalized linear GPR model. The specific findings and conclusions are as follows:

(i) The extension of simple linear model to generalized linear model is achieved by transforming the input variables $\mathbf{x}$ into some high dimensional space first, using a set of mapping functions $\phi(\mathbf{x})$, and then applying the linear relationship in this mapping space. The covariance function for a generalized linear relationship is derived in terms of $\phi(\mathbf{x})$ without loss of generality. As an application based on generalized model, $\phi(\mathbf{x})$ is defined as $\phi(\mathbf{x}) = \{x_0^{k_0} x_1^{k_1} x_2^{k_2} \mid \text{for all } k_0 + k_1 + k_2 = p\}$ for a polynomial relationship with *p*th order polynomial. Then the GPR models with explicit polynomial covariance function are formulated and optimized using the log marginal likelihood maximization method.

(ii) Four GPR models are formulated including three P-GPR models with first three order polynomials, and one SE-GPR. The SE-GPR model has similar performance as mentioned before, due to its essential characteristics. It performs well in predicting displacement when the input is within or close to the observation cluster. But when the wind speed keeps increasing, the predicted displacement starts to decrease, which is due to the SE covariance function characteristics, but obviously does not conform to reality. The P-GPR models perform well in predicting displacement not only when the inputs are within or close to the observation cluster, but also when the input goes far away from the observation ranges. In addition, the shape of predicted mean functions coincides with the order of polynomials defined through the covariance

functions, indicating that the explicit covariance functions successfully control the trend and distribution of mean function.

(iii) The prediction performance of the GPR models are evaluated using the testing data group. The log marginal likelihood and root mean square error (RMSE) are used as performance indicators. Four considered models have similar log marginal likelihood and RMSE. Among the four models, the SE-GPR performs best in predicting testing data which are located within the observation cluster, with the largest log marginal likelihood and the smallest RMSE. But due to its essential characteristics mentioned above, it is not capable of predicting target displacement under extreme conditions far outside the observation cluster. The P-GPR with second order polynomial (P-GPR2) has competitive log marginal likelihood and RMSE among the other three P-GPR models, and is finally chosen as the optimal GPR model for establishing the relationship between the lateral displacement and wind data for the TMB.

(iv) The outperformed P-GPR2 is used to predict the lateral displacement under extreme design wind speed at 53.3 m/s at three locations of the TMB, including one location on the main cable and two on the main span deck. The wind direction for maximum displacement prediction is considered in two cases: the most probable direction and the most unfavorable direction. The predicted total displacement is compared with the designed allowable value to examine the

structural health condition. Results show that the maximum total displacement at 1/2 main span under extreme wind speed of 53.3 m/s and the most unfavorable wind direction of 30° is 1.35 m. Even under the worst situation, the predicted total displacement is still much smaller than the designed maximum allowable total lateral displacement of 2.9 m. The results suggested that the design is reasonable with appropriate safety reserve.

5.2 Recommendations for further studies

In this MPhil study, the flexibility of GP in modeling different relationships is explored by explicitly modifying the model, for the purpose of structural health condition assessment using the monitoring data. However, the exploration is in the basic level and the developed methodology in structural health evaluation based on GPR still needs more research efforts. More research work is expected to improve the GPR methods for better benefiting the structural health evaluation problems. As GP is still new to SHM fields, some research problems are untouched. The recommendations for future research work are as follows.

1. **Development of generalized linear GPR model with different explicit covariance function definition.**

The application of derived generalized linear GPR model in this study focused on a polynomial relationships. However there exist other regression relationships in

different SHM applications, for example exponential relationship between wind speed and displacement. Within the generalized linear relationship requirement, the proposed generalized linear GPR model is suitable to model any basis function $\phi(\mathbf{x})$ without loss of generality. However, the covariance function should be derived explicitly according to the relationship knowledge. This problem needs to be explored in different regression relationships.

2. Development of nonlinear GPR model.

Except for the generalized linear relationships, SHM problems may also involve nonlinear relationships, or sometimes the exact relationships between measurements may even be unknown. If the nonlinear relationships are known a priori, or determined by assumption, explicit covariance functions can be derived for formulation of explicit GP models.

On the other hand, if the nonlinear model is unknown, traditional parametric methods are not suitable and the general-purposed SE covariance could be adopted, since it corresponds to a linear combination of infinite number of basis functions and is flexible for estimating any form of basis functions. However, the SE covariance function has drawback since it only works well within the observation clusters but has weak capability in predicting target values under extreme conditions outside the observation clusters. Therefore, SE covariance function could be chosen for regression and prediction for the case close to the observation clusters. As for output prediction

under extreme conditions, it is hopeful that this problem will become non-decisive with long-term SHM monitoring and more data obtained under severe conditions available. The more available data from severe conditions may contribute to make the prediction more accurate.

3. Development of GP forecasting model using time-series monitoring data.

In this MPhil study, the regression capability of GP models is mainly focused on mapping the input measurement variables to the target output. However, this capability of GP can be extended to forecasting by utilizing the historical monitoring data as input to forecast the next-step structural response in the time domain. The forecasting problem is also an important field in SHM research. The forecasting of the future states and performance from the measured structural responses contributes to condition prognosis, control of real-world engineering structures, sensor fault diagnosis, signal outlier detection, and reconstruction of incomplete data. The real-time data gradually accumulated from a monitoring system will contribute to the improvement of the forecasting accuracy.

4. Development of source separation model based on GP.

In a generalized linear GPR model, the outputs are treated as a generalized linear combination of inputs, which is similar to source separation problem. It has been proved that the covariance functions in GP model enable to define the characteristics

and trends of mean functions. Therefore, if the prior information of source functions are available, for example the smoothness, stationarity, or periodicity property of the function, the sources can be restrained through appropriate covariance functions. The source separation can be realized by extracting each source with special restraints one by one from the mixed measurement results.

5. Damage detection and localization using GP.

The GP can provide prognosis of the structural condition. When in-service measurements are available, the deviation of monitoring data from predicted results can be evaluated. Subsequently, the abnormality of the monitoring data can be assessed, and thus the structural condition can be evaluated. The noise level estimated in GP process can further provide reliability probability for the assessment. Therefore the reliability assessment can be achieved. Since GP is model-free and has high flexibility in modelling different kinds of relationships, when the location information is provided in model formulation, localization can be achieved. Thus the damage detection and localization can be achieved by means of GP.

REFERENCES

AASHTO (1989), *AASHTO Guide Specifications: Thermal Effects in Concrete Bridge Superstructures*, Washington, D.C.: American Association of State Highway and Transportation Officials.

Adams, R., Cawley, P., Pye, C., & Stone, B. (1978). A vibration technique for non-destructively assessing the integrity of structures. *Journal of Mechanical Engineering Science, 20*(2), 93-100.

Akgül, F., & Frangopol, D. M. (2004). Time-dependent interaction between load rating and reliability of deteriorating bridges. *Engineering Structures, 26*(12), 1751-1765.

Aktan, A., Catbas, F., Grimmelsman, K., & Tsikos, C. (2000). Issues in infrastructure health monitoring for management. *Journal of Engineering Mechanics, 126*(7), 711-724.

Aktan, A. E., Farhey, D. N., Brown, D. L., Dalal, V., Helmicki, A. J., Hunt, V. J., & Shelley, S. J. (1996). Condition assessment for bridge management. *Journal of Infrastructure Systems, 2*(3), 108-117.

Aktan, A. E., Farhey, D. N., Helmicki, A. J., Brown, D. L., Hunt, V. J., Lee, K. L., & Levi, A. (1997). Structural identification for condition assessment: experimental arts. *Journal of Structural Engineering, 123*(12), 1674-1684.

Albrecht, P., & Naeemi, A. H. (1984). Performance of weathering steel in bridges. *NCHRP report* (272).

Anderson, S., Aram, P., Bhattacharya, B., & Kadirkamanathan, V. (2014). Analysis of composite plate dynamics using spatial maps of frequency-domain features described by Gaussian processes. *IFAC Proceedings Volumes, 47*(1), 949-954.

Ang, A. H. S., & Tang, W. H. (1984). *Probability Concepts in Engineering Planning and Design*. Wiley, New York.

Ansari, F. (2009). Fiber optic sensors for structural health monitoring of civil infrastructure systems. *Structural Health Monitoring of Civil Infrastructure Systems,* edited by Karbhari, V.M. and Ansari, F., CRC Press, New York.

ASCE, (2005), *2005 Report Card for America's Infrastructure*. Reston, VA: America Society of Civil Engineers.

Ashkenazi, V., & Roberts, G. (1997). Experimental monitoring of the Humber Bridge using GPS. *Proceedings of the Institution of Civil Engineers-Civil Engineering*, London, UK.

Ayyub, B. M., & Haldar, A. (1984). Practical structural reliability techniques. *Journal of Structural Engineering, 110*(8), 1707-1724.

Ayyub, B. M., & McCuen, R. H. (2011). *Probability, Statistics, and Reliability for Engineers and Scientists*. CRC Press, New York.

Basheer, P., Chidiact, S., & Long, A. (1996). Predictive models for deterioration of concrete structures. *Construction and Building Materials, 10*(1), 27-37.

Bergmeister, K., & Santa, U. (2001). Global monitoring concepts for bridges. *Structural Concrete, 2*(1), 29-39.

Bernardo, J., Berger, J., Dawid, A., & Smith, A. (1998). Regression and classification using Gaussian process priors. *Bayesian Statistics, 6*, 475.

Bishop, C. M. (1995). *Neural Networks for Pattern Recognition*. Oxford University Press.

Brown, C., Karuna, R., Ashkenazi, V., Roberts, G., & Evans, R. (1999). Monitoring of structures using the Global Positioning System. *Proceedings of the Institution of Civil Engineers. Structures and buildings, 134*(1), 97-105.

Brown, J. (1987). *The Performance of Concrete in Practice: a Field Study of Highway Bridges*. TRRL Wokingham, UK.

Brownjohn, J. M. (2007). Structural health monitoring of civil infrastructure. *Philosophical Transactions of the Royal Society of London A: Mathematical, Physical and Engineering Sciences, 365*(1851), 589-622.

Brownjohn, J., & Koo, K.Y. (2010). Structural health monitoring and real-time performance diagnosis of landmark structures in the UK. *Proceedings of the 5th World Conference on Structural Control and Monitoring*, Tokyo (CD-ROM).

Cai, C.S, & Montens, S. (2000), Wind effects on long-span bridges. In *Bridge Engineering Handbook*, edited by Chen, W.F. and Duan, L., Boca Raton: CRC Press.

Capps, M. (1968). *The thermal behavior of the Beachley Viaduct/Wye Bridge*. TRRL Report LR 234, Ministry of Transport, Road Research Laboratory, Crowthorne,

UK, 1968.

Carden, E. P., & Fanning, P. (2004). Vibration based condition monitoring: a review. *Structural Health Monitoring, 3*(4), 355-377.

Catbas, F. (2009). Structural health monitoring: applications and data analysis. *Structural Health Monitoring of Civil Infrastructure Systems*, edited by Karbhari, V.M. and Ansari, F., CRC Press, New York.

Catbas, F. N., & Aktan, A. E. (2002). Condition and damage assessment: issues and some promising indices. *Journal of Structural Engineering, 128*(8), 1026-1036.

Catbas, F. N., Susoy, M., & Frangopol, D. M. (2008). Structural health monitoring and reliability estimation: Long span truss bridge application with environmental monitoring data. *Engineering Structures, 30*(9), 2347-2359.

Cattan, J., & Mohammadi, J. (1997). Analysis of bridge condition rating data using neural networks. *Computer‐Aided Civil and Infrastructure Engineering, 12*(6), 419-429.

Chae, M., Yoo, H., Kim, J., & Cho, M. (2012). Development of a wireless sensor network system for suspension bridge health monitoring. *Automation in Construction, 21*, 237-252.

Chakraborty, S., & DeWolf, J. T. (2006). Development and implementation of a continuous strain monitoring system on a multi-girder composite steel bridge. *Journal of Bridge Engineering, 11*(6), 753-762.

Chan, W. S., Xu, Y. L., Ding, X. L., Xiong, Y. L., & Dai, W. J. (2006). Assessment of

dynamic measurement accuracy of GPS in three directions. *Journal of Surveying Engineering, 132*(3), 108-117.

Chang, L. M., & Lee, Y. J. (2002). Evaluation of performance of bridge deck expansion joints. *Journal of Performance of Constructed Facilities, 16*(1), 3-9.

Chang, P. C., Flatau, A., & Liu, S. (2003). Review paper: health monitoring of civil infrastructure. *Structural Health Monitoring, 2*(3), 257-267.

Chang, S. P., Yee, J., & Lee, J. (2009). Necessity of the bridge health monitoring system to mitigate natural and man-made disasters. *Structure and Infrastructure Engineering, 5*(3), 173-197.

Chen, T., Morris, J., & Martin, E. (2007). Gaussian process regression for multivariate spectroscopic calibration. *Chemometrics and Intelligent Laboratory Systems, 87*(1), 59-71.

Cheng, J., & Xiao, R. C. (2006). A simplified method for lateral response analysis of suspension bridges under wind loads. *Communications in Numerical Methods in Engineering, 22*(8), 861-874.

Cherkassky, V., & Mulier, F. M. (2007). *Learning from Data: Concepts, Theory, and Methods*. John Wiley & Sons.

Cheung, M. S., Tadros, G., Brown, T., Dilger, W., Ghali, A., & Lau, D. (1997). Field monitoring and research on performance of the Confederation Bridge. *Canadian Journal of Civil Engineering, 24*(6), 951-962.

Cho, S., Jo, H., Jang, S., Park, J., Jung, H. J., Yun, C. B., & Seo, J. W. (2010). Structural health monitoring of a cable-stayed bridge using wireless smart sensor technology: data analyses. *Smart Structures and Systems, 6*(5-6), 461-480.

Cornell, C. A. (1967). Bounds on the reliability of structural systems. *Journal of the Structural Division, 93*(1), 171-200.

Cressie, N. (2015). *Statistics for Spatial Data*. John Wiley & Sons.

Cristianini, N., & Scholkopf, B. (2002). Support vector machines and kernel methods: the new generation of learning machines. *Ai Magazine, 23*(3), 31.

Czarnecki, A. A., & Nowak, A. S. (2008). Time-variant reliability profiles for steel girder bridges. *Structural Safety, 30*(1), 49-64.

Deng, Y., Ding, Y., & Li, A. (2010). Structural condition assessment of long-span suspension bridges using long-term monitoring data. *Proceedings of the Fifth International IABMAS Conference*, 11-15 July 2010, Philadelphia, USA.

Deng, Y., Li, A., & Ding, Y. (2009). Research and application of correlation between beam end displacement and temperature of long-span suspension bridge. *Journal of Highway and Transportation Research and Development, 5*, 012.

Denton, S. (2002). Data estimates for different maintenance options for reinforced concrete cross-heads. *Personal communication for Highways Agency,* UK.

Desjardins, S., Londono, N., Lau, D., & Khoo, H. (2006). Real-time data processing, analysis and visualization for structural monitoring of the confederation bridge. *Advances in Structural Engineering, 9*(1), 141-157.

Diana, G., & Cheli, F. (1989). Dynamic interaction of railway systems with large bridges. *Vehicle System Dynamics, 18*(1-3), 71-106.

Doebling, S. W., Farrar, C. R., Prime, M. B., & Shevitz, D. W. (1996). *Damage identification and health monitoring of structural and mechanical systems from changes in their vibration characteristics: a literature review.* Los Alamos National Laboratory report LA-13070-MS.

Ebeling, C. E. (2004). *An Introduction to Reliability and Maintainability Engineering*: Tata McGraw-Hill Education.

Elbadry, M. M., & Ghali, A. (1983). Temperature variations in concrete bridges. *Journal of Structural Engineering, 109*(10), 2355-2374.

Ellingwood, B. (1980). *Development of a Probability Based Load Criterion for American National Standard A58: Building Code Requirements for Minimum Design Loads in Buildings and Other Structures* (Vol. 13). US Department of Commerce, National Bureau of Standards.

Ellingwood, B., MacGregor, J. G., Galambos, T. V., & Cornell, C. A. (1982). Probability based load criteria: load factors and load combinations. *Journal of the Structural Division, 108*(5), 978-997.

Enright, M. P., & Frangopol, D. M. (1998). Service-life prediction of deteriorating concrete bridges. *Journal of Structural Engineering, 124*(3), 309-317.

Erdogan, Y. S., Gul, M., Catbas, F. N., & Bakir, P. G. (2014). Investigation of uncertainty changes in model outputs for finite-element model updating using

structural health monitoring data. *Journal of Structural Engineering*, *140*(11), 04014078.

Estes, A. C., & Frangopol, D. M. (1999). Repair optimization of highway bridges using system reliability approach. *Journal of Structural Engineering*, *125*(7), 766-775.

Farrar, C. R., Baker, W., Bell, T., Cone, K., Darling, T., Duffey, T., & Migliori, A. (1994). *Dynamic characterization and damage detection in the I-40 bridge over the Rio Grande*. Los Alamos National Laboratory report LA-12767-MS.

Feng M.R. (2008). Construction of bridges and roads to bring benefit to people's livelihood. *Journal of Highway and Transportation Research and Development*, *12*, 1–5.

FHWA (2001), *Bridge Scour and Stream Instability Countermeasure Experience, Selection, and Design Guidance*. Second Edition, Federal Highway Administration, FHWA-NHI-01-003.

FHWA. (2014). National Bridge Inventory. Retrieved October 18, 2014, from https://www.fhwa.dot.gov/bridge/nbi/ascii.cfm.

Frangopol, D. M., Strauss, A., & Kim, S. (2008). Bridge reliability assessment based on monitoring. *Journal of Bridge Engineering*, *13*(3), 258-270.

Fricker, T. E., Oakley, J. E., Sims, N. D., & Worden, K. (2011). Probabilistic uncertainty analysis of an FRF of a structure using a Gaussian process emulator. *Mechanical Systems and Signal Processing*, *25*(8), 2962-2975.

Friswell, M. I. (2007). Damage identification using inverse methods. *Philosophical Transactions of the Royal Society of London A: Mathematical, Physical and Engineering Sciences, 365*(1851), 393-410.

Friswell, M., & Penny, J. (1997). Is damage location using vibration measurements practical? *Proceeding of Euromech 365 international workshop*, Damas.

Frýba, L. (1996). *Dynamics of Railway Bridges*. Thomas Telford Publishing.

Fujino, Y., Murata, M., Okano, S., & Takeguchi, M. (2000). Monitoring system of the Akashi Kaikyo Bridge and displacement measurement using GPS. *Proceeding of the SPIE's 5th Annual International Symposium on Non-destructive Evaluation and Health Monitoring of Aging Infrastructure*, 6 March 2000, Newport Beach, Canada.

Goebel, K., Saha, B., & Saxena, A. (2008). A comparison of three data-driven techniques for prognostics. *Proceeding of the 62nd meeting of the society for machinery failure prevention technology,* 6-8 May 2008, Virginia Beach, USA.

Green, D., & Unruh, W. G. (2006). The failure of the Tacoma Bridge: A physical model. *American Journal of Physics, 74*(8), 706-716.

Gu, M., Xu, Y., Chen, L., & Xiang, H. (1999). Fatigue life estimation of steel girder of Yangpu cable-stayed bridge due to buffeting. *Journal of Wind Engineering and Industrial Aerodynamics, 80*(3), 383-400.

Gul, M., & Catbas, F. N. (2010). Damage assessment with ambient vibration data using a novel time series analysis methodology. *Journal of Structural Engineering,*

137(12), 1518-1526.

Guo, J., Xu, L., Dai, L., McDonald, M., Wu, J., & Li, Y. (2005). Application of the real-time kinematic global positioning system in bridge safety monitoring. *Journal of Bridge Engineering*, *10*(2), 163-168.

Guo, T., Liu, J., Zhang, Y., & Pan, S. (2014). Displacement monitoring and analysis of expansion joints of long-span steel bridges with viscous dampers. *Journal of Bridge Engineering*, *20*(9), 04014099.

Hasofer, A. M., & Lind, N. C. (1973). *An Exact and Invariant First-order Reliability Format*. University of Waterloo, Solid Mechanics Division.

Hasofer, A. M., & Lind, N. C. (1974). Exact and invariant second-moment code format. *Journal of the Engineering Mechanics Division*, *100*(1), 111-121.

Hensman, J., Mills, R., Pierce, S., Worden, K., & Eaton, M. (2010). Locating acoustic emission sources in complex structures using Gaussian processes. *Mechanical Systems and Signal Processing*, *24*(1), 211-223.

Herbrich, R., Lawrence, N. D., & Seeger, M. (2003). Fast sparse Gaussian process methods: The informative vector machine. *Advances in Neural Information Processing Systems*. MIT Press.

Hohenbichler, M., & Rackwitz, R. (1988). Improvement of second-order reliability estimates by importance sampling. *Journal of Engineering Mechanics*, *114*(12), 2195-2199.

Holmes, J. D. (2015). *Wind Loading of Structures*. CRC press.

Hosser, D., Klinzmann, C., & Schnetgöke, R. (2008). A framework for reliability-based system assessment based on structural health monitoring. *Structure and Infrastructure Engineering, 4*(4), 271-285.

Jahanshahi, M. R., & Masri, S. F. (2012). Adaptive vision-based crack detection using 3D scene reconstruction for condition assessment of structures. *Automation in Construction, 22*, 567-576.

Kareem, A. (2008). Numerical simulation of wind effects: a probabilistic perspective. *Journal of Wind Engineering and Industrial Aerodynamics, 96*(10), 1472-1497.

Kawamura, K., Miyamoto, A., Frangopol, D. M., & Kimura, R. (2003). Performance evaluation of concrete slabs of existing bridges using neural networks. *Engineering Structures, 25*(12), 1455-1477.

Keerthi, S., & Chu, W. (2006). A matching pursuit approach to sparse Gaussian process regression. *Advances in Neural Information Processing Systems, 18*, MIT Press, Cambridge, Massachusetts, 643-650.

Khodaparast, H. H., Mottershead, J. E., & Badcock, K. J. (2011). Interval model updating with irreducible uncertainty using the Kriging predictor. *Mechanical Systems and Signal Processing*, *25*(4), 1204-1226.

Ko, J.M., & Ni, Y.Q. (2005). Technology developments in structural health monitoring of large-scale bridges. *Engineering Structures, 27*(12), 1715-1725.

Koshiba, A., Abe, M., Sunaga, T., & Ishii, H. (2001). Bridge inspection in steel road bridge based on real measurement. *Current and Future Trends in Bridge*

Design Construction and Maintenance, 2, Thomas Telford, London, 268-273.

Laflamme, S., Kollosche, M., Connor, J., & Kofod, G. (2012). Soft capacitive sensor for structural health monitoring of large–scale systems. *Structural Control and Health Monitoring*, *19*(1), 70-81.

Lark, R. J., & Flaig, K. D. (2005). The use of reliability analysis to aid bridge management. *Structural Engineer, 83*(5), 27-31.

Leemis, L. M. (1995). *Reliability: Probabilistic Models and Statistical Methods*. Prentice-Hall, Inc.

Li, D., Maes, M. A., & Dilger, W. H. (2008). Evaluation of temperature data of Confederation Bridge: thermal loading and movement at expansion joint. *Proceedings of the 2008 Structure Congress*, Alberta, Canada.

Li, Q., Xu, Y. L., Wu, D., & Chen, Z. (2010). Computer-aided nonlinear vehicle-bridge interaction analysis. *Journal of Vibration and Control, 16*(12), 1791-1816.

Li, Y. (2004). *Effect of Spatial Variability on Maintenance and Repair Decisions for Concrete Structures*. TU Delft, Delft University of Technology.

Li, Z., Chan, T. H., & Ko, J. M. (2002). Evaluation of typhoon induced fatigue damage for Tsing Ma Bridge. *Engineering Structures, 24*(8), 1035-1047.

Liang, M. T., Wu, J. H., & Liang, C. H. (2001). Multiple layer fuzzy evaluation for existing reinforced concrete bridges. *Journal of Infrastructure Systems, 7*(4), 144-159.

Lima, J. M., & de Brito, J. (2009). Inspection survey of 150 expansion joints in road

bridges. *Engineering Structures, 31*(5), 1077-1084.

Lin, C. C., Wang, C. E., Wu, H. W., & Wang, J. F. (2005). On-line building damage assessment based on earthquake records. *Smart Materials and Structures, 14*(3), S137.

Liu, Y., Mohanty, S., & Chattopadhyay, A. (2010). Condition based structural health monitoring and prognosis of composite structures under uniaxial and biaxial loading. *Journal of Nondestructive Evaluation, 29*(3), 181-188.

Lombardo, F. T., Main, J. A., & Simiu, E. (2009). Automated extraction and classification of thunderstorm and non-thunderstorm wind data for extreme-value analysis. *Journal of Wind Engineering and Industrial Aerodynamics, 97*(3), 120-131.

Long, X., Li, L., & Hu, L. (2010). Time domain analysis of buffeting responses of Sidu river suspension bridge. *Engineering Mechanics, 27*(1), 113-117.

MacKay, D. J. (1997). Gaussian processes-a replacement for supervised neural networks? *Tutorial at the Tenth Annual Conference on Neural Information Processing Systems.*

MacKay, D. J. (1998). Introduction to Gaussian processes. *NATO ASI Series F Computer and Systems Sciences, 168,* 133-166.

Madsen, H. O., Krenk, S., & Lind, N. C. (2006). *Methods of Structural Safety*. Courier Corporation.

Maeck, J., Peeters, B., & De Roeck, G. (2001). Damage identification on the Z24

Bridge using vibration monitoring. *Smart Materials and Structures, 10*(3), 512.

Manevitz, L. M., & Yousef, M. (2001). One-class SVMs for document classification. *Journal of Machine Learning Research, 2*(Dec), 139-154.

Manson, G., Worden, K., & Allman, D. (2002). Experimental validation of a damage severity method. *Proceeding of the 1st European Workshop on Structural Health Monitoring*, Paris, France.

Manson, G., Worden, K., & Allman, D. (2003a). Experimental validation of a structural health monitoring methodology: Part II. Novelty detection on a Gnat aircraft. *Journal of Sound and Vibration, 259*(2), 345-363.

Manson, G., Worden, K., & Allman, D. (2003b). Experimental validation of a structural health monitoring methodology: Part III. Damage location on an aircraft wing. *Journal of Sound and Vibration, 259*(2), 365-385.

Mathiessen, C. (2000). Bridging the Oresund: Potential regional dynamics. *Journal of Transport Geography, 8*, 175-195.

Melchers, R. (1999). *Structural Reliability Analysis and Prediction* (2nd ed.). Chichester: John Wiley.

Melkumyan, A., & Ramos, F. (2009). A sparse covariance function for exact Gaussian process inference in large datasets. *Proceedings of the Twenty-First International Joint Conference on Artificial Intelligence*, Pasadena, USA.

Micic, T., Chryssanthopoulos, M., & Baker, M. (1995). Reliability analysis for highway bridge deck assessment. *Structural Safety, 17*(3), 135-150.

Miyata, T., Yamada, H., Katsuchi, H., & Kitagawa, M. (2002). Full-scale measurement of Akashi–Kaikyo Bridge during typhoon. *Journal of Wind Engineering and Industrial Aerodynamics, 90*(12), 1517-1527.

Mohamad, H., Soga, K., Bennett, P. J., Mair, R. J., & Lim, C. S. (2011). Monitoring twin tunnel interaction using distributed optical fiber strain measurements. *Journal of Geotechnical and Geoenvironmental Engineering, 138*(8), 957-967.

Mohanty, S., Chattopadhyay, A., Peralta, P., & Das, S. (2011). Bayesian statistic based multivariate Gaussian process approach for offline/online fatigue crack growth prediction. *Experimental Mechanics, 51*(6), 833-843.

Mohanty, S., Das, S., Chattopadhyay, A., & Peralta, P. (2009). Gaussian process time series model for life prognosis of metallic structures. *Journal of Intelligent Material Systems and Structures, 20*(8), 887-896.

Mufti, A. A. (2002). Structural health monitoring of innovative Canadian civil engineering structures. *Structural Health Monitoring, 1*(1), 89-103.

Nairac, A., Corbett-Clark, T. A., Ripley, R., Townsend, N. W., & Tarassenko, L. (1997). Choosing an appropriate model for novelty detection. *Proceedings of the 5th IEEE International Conference on Artificial Neural Networks*, 227–232.

Nakamura, S. I. (2000). GPS measurement of wind-induced suspension bridge girder displacements. *Journal of Structural Engineering, 126*(12), 1413-1419.

Neal, R. M. (1997). Monte Carlo implementation of Gaussian process models for Bayesian regression and classification. *arXiv preprint physics/9701026*.

Neal, R. M. (2012). *Bayesian Learning for Neural Networks* (Vol. 118). Springer Science & Business Media.

Ni, Y.Q., Hua, X.G., Wong, K.Y., & Ko, J.M. (2007). Assessment of bridge expansion joints using long-term displacement and temperature measurement. *Journal of performance of constructed facilities, 21*(2), 143-151.

Ni, Y.Q., Ko, J.M., Zhou, H.F., & Hua, X.G. (2004). Challenges in developing structural health monitoring system for a long-span cable-stayed bridge. *Proceeding of the US-Korea Joint Seminar/Workshop on Smart Structures Technologies*, Seoul, Korea, 373-386

Ni, Y.Q., Wong, K.Y., & Xia, Y. (2011). Health checks through landmark bridges to sky-high structures. *Advances in Structural Engineering, 14*(1), 103-119.

Ni, Y.Q., Xia, H.W., Wong, K.Y., & Ko, J.M. (2011). In-service condition assessment of bridge deck using long-term monitoring data of strain response. *Journal of Bridge Engineering, 17*(6), 876-885.

Ni, Y. Q., and Xia, Y. X. (2016). Strain-based condition assessment of a suspension bridge instrumented with structural health monitoring system. *International Journal of Structural Stability and Dynamics, 16*(04), 1640027.

Nowak, A. S., & Collins, K. R. (2012). *Reliability of Structures*. CRC Press.

Nowak, A. S., & Czarnecki, A. (2005). System reliability models for girder bridges. *Transportation Research Record: Journal of the Transportation Research Board* (11s), 79-85.

Nowak, A. S., & Eamon, C. D. (2008). Reliability analysis of plank decks. *Journal of Bridge Engineering, 13*(5), 540-546.

Nowak, A. S., & Lind, N. C. (1979). Practical bridge code calibration. *ASHRAE Journal, 105*(12).

Ou, J., & Li, H. (2010). Structural health monitoring in mainland China: review and future trends. *Structural Health Monitoring, 9*(3), 219-231.

Park, J. W., Lee, J. J., Jung, H. J., & Myung, H. (2010). Vision-based displacement measurement method for high-rise building structures using partitioning approach. *NDT & E International, 43*(7), 642-647.

Peeters, B., & De Roeck, G. (2001). One-year monitoring of the Z 24-Bridge: environmental effects versus damage events. *Earthquake Engineering & Structural Dynamics, 30*(2), 149-171.

Peil, U. (2005). Assessment of bridges via monitoring. *Structure and Infrastructure Engineering, 1*(2), 101-117.

Pines, D., & Aktan, A. E. (2002). Status of structural health monitoring of long‐span bridges in the United States. *Progress in Structural Engineering and Materials, 4*(4), 372-380.

Ponnuswamy, S. (2008). *Bridge Engineering*. Tata McGraw-Hill Education.

Pontis (2001), *User's Manual, Release 4.0.* Cambridge Systematics, Inc.: Cambridge, MA.

Priestley, M. N. (1978). Design of concrete bridges for temperature gradients. *ACI*

Journal, 75(5), 209–217.

Quiñonero-Candela, J., & Rasmussen, C. E. (2005). A unifying view of sparse approximate Gaussian process regression. *Journal of Machine Learning Research, 6*(Dec), 1939-1959.

Rackwitz, R., & Flessler, B. (1978). Structural reliability under combined random load sequences. *Computers & Structures, 9*(5), 489-494.

Rafiq, M. I. (2005). *Health monitoring in proactive reliability management of deteriorating concrete bridges.* Ph.D. thesis, University of Surrey.

Rasmussen, C. E. (1997). *Evaluation of Gaussian processes and other methods for non-linear regression.* Ph.D. thesis, University of Toronto.

Rasmussen, C. E., & Williams, C. K. I. (2006). *Gaussian Processes for Machine Learning*. MIT Press.

Ratay, R. T. (2005). *Structural Condition Assessment*. John Wiley & Sons, Inc. Hoboken, NJ.

Ravindra, M. K., & Galambos, T. V. (1978). Load and resistance factor design for steel. *Journal of the Structural Division, 104*(9), 1337-1353.

Riding, K. A., Poole, J. L., Schindler, A. K., Juenger, M. C., & Folliard, K. J. (2007). Temperature boundary condition models for concrete bridge members. *ACI Materials Journal, 104*(4), 379.

Roeder, C. (1998). Fatigue and dynamic load measurements on modular expansion joints. *Construction and Building Materials, 12*(2), 143-150.

Rohmer, J., & Foerster, E. (2011). Global sensitivity analysis of large-scale numerical landslide models based on Gaussian-Process meta-modeling. *Computers & Geosciences, 37*(7), 917-927.

Rytter, A. (1993). *Vibrational based inspection of civil engineering structures.* Dept. of Building Technology and Structural Engineering, Aalborg University.

Santoni, G. B., Yu, L., Xu, B., & Giurgiutiu, V. (2007). Lamb wave-mode tuning of piezoelectric wafer active sensors for structural health monitoring. *Journal of Vibration and Acoustics, 129*(6), 752-762.

Sasmal, S., & Ramanjaneyulu, K. (2008). Condition evaluation of existing reinforced concrete bridges using fuzzy based analytic hierarchy approach. *Expert Systems with Applications, 35*(3), 1430-1443.

Schölkopf, B., & Smola, A. J. (2002). *Learning with Kernels: Support Vector Machines, Regularization, Optimization, and Beyond*. MIT Press.

Schroeder, J. L., Smith, D. A., & Peterson, R. E. (1998). Variation of turbulence intensities and integral scales during the passage of a hurricane. *Journal of Wind Engineering and Industrial Aerodynamics, 77*, 65-72.

Seeger, M. (2004). Gaussian processes for machine learning. *International Journal of Neural Systems, 14*(02), 69-106.

Seeger, M., Williams, C., & Lawrence, N. (2003). Fast forward selection to speed up sparse Gaussian process regression. *Proceeding of the Ninth International Workshop on Artificial Intelligence and Statistics*, Key West, USA.

Silverman, B. W. (1986). *Density Estimation for Statistics and Data Analysis* (Vol. 26). CRC Press.

Snelson, E., & Ghahramani, Z. (2006). Sparse Gaussian processes using pseudo-inputs. *Advances in Neural Information Processing Systems, 18*, 1257.

Snelson, E., & Ghahramani, Z. (2007). Local and global sparse Gaussian process approximations. *Proceedings of the Eleventh International Workshop on Artificial Intelligence and Statistics*, 21-24 March 2007, San Juan, Puerto Rico. Omnipress.

Sohn, H., Farrar, C. R., Hemez, F. M., Shunk, D. D., Stinemates, D. W., Nadler, B. R., & Czarnecki, J. J. (2003). A review of structural health monitoring literature: 1996–2001. *Los Alamos National Laboratory*.

Sohn, H., & Oh, C.K. (2009). Statistical pattern recognition, *Encyclopedia of Structural Health Monitoring*, Boller C., Chang F. K., Fujino Y. (eds.), John Wiley and Sons, Chichester, UK, Chapter 30.

Srivastava, A. N., & Das, S. (2009). Detection and prognostics on low-dimensional systems. *IEEE Transactions on Systems, Man, and Cybernetics, Part C (Applications and Reviews), 39*(1), 44-54.

Sundararajan, C. R. (2012). *Probabilistic Structural Mechanics Handbook: Theory and Industrial Applications*. Springer Science & Business Media.

Tabsh, S. W., & Nowak, A. S. (1991). Reliability of highway girder bridges. *Journal of Structural Engineering, 117*(8), 2372-2388.

Thoft-Christensen, P., & Baker, M. J. (2012). *Structural Reliability Theory and its Applications*. Springer Science & Business Media.

Thoft-Christensen, P., Jensen, F., Middleton, C., & Blackmore, A. (1996). Assessment of the reliability of concrete slab bridges. *Reliability and Optimization of Structural Systems*, edited by Frangopol, D. M., Corotis, R. B., and Rackwitz, R., Pergamon, Tarrytown, New York, 321–328.

Thoft-Christensen, P., & Murotsu, Y. (2012). *Application of Structural Systems Reliability Theory*. Springer Science & Business Media.

Thompson, P. D., Small, E. P., Johnson, M., & Marshall, A. R. (1998). The Pontis bridge management system. *Structural Engineering International, 8*(4), 303-308.

Torres-Arredondo, M., & Fritzen, C. P. (2012). Impact monitoring in smart structures based on Gaussian processes. *Proceedings of the 4th international symposium on NDT in aerospace*, 13-15November 2012, Augsburg, Germany.

Vanhatalo, J., & Vehtari, A. (2012). Modeling local and global phenomena with sparse Gaussian processes. *arXiv preprint arXiv:1206.3290*.

Vapnik, V. N. (1998). *Statistical Learning Theory* (Vol. 1). Wiley New York.

Vapnik, V. N. (2013). *The Nature of Statistical Learning Theory*. Springer Science & Business Media.

Villalba, S., & Casas, J. R. (2013). Application of optical fiber distributed sensing to health monitoring of concrete structures. *Mechanical Systems and Signal*

Processing, *39*(1), 441-451.

Virlogeux, M. (1992). Wind design and analysis for the Normandy Bridge. *Proceedings of the First International Symposium on Aerodynamics of Large Bridges*, 19-21 February 1992, Copenhagen, Denmark.

Wan, H. P., & Ni, Y. Q. (2017). Bayesian modeling approach for forecast of structural stress response using structural health monitoring data. *Journal of Structural Engineering*, in review.

Wan, H. P., & Ren, W. X. (2014). Parameter selection in finite-element-model updating by global sensitivity analysis using Gaussian process metamodel. *Journal of Structural Engineering, 141*(6), 04014164.

Wan, H. P., & Ren, W. X. (2015). A residual-based Gaussian process model framework for finite element model updating. *Computers & Structures, 156*, 149-159.

Wan, H. P., Ren, W. X., & Todd, M. D. (2017a). An efficient metamodeling approach for uncertainty quantification of complex systems with arbitrary parameter probability distributions. *International Journal for Numerical Methods in Engineering*, *109*(5), 739-760.

Wan, H. P., Todd, M. D., and Ren, W. X. (2017b). "Statistical framework for sensitivity analysis of structural dynamic characteristics. DOI: 10.1061/ (ASCE) EM.1943-7889.0001314.

Wang, G. X., & Ding, Y. L. (2014). Mathematical modeling for lateral displacement induced by wind velocity using monitoring data obtained from main girder of

Sutong cable-stayed bridge. *Mathematical Problems in Engineering*.

Wang, H., Li, A. Q., Jiao, C. K., & Li, X. P. (2010). Characteristics of strong winds at the Runyang Suspension Bridge based on field tests from 2005 to 2008. *Journal of Zhejiang University-Science A, 11*(7), 465-476.

Wang, H., Li, A., Niu, J., Zong, Z., & Li, J. (2013). Long-term monitoring of wind characteristics at Sutong Bridge site. *Journal of Wind Engineering and Industrial Aerodynamics, 115*, 39-47.

Wang, C. (1994), *Temperature effects in hardening concrete*. Ph.D. thesis, University of Calgary.

Wisniewski, D., Casas, J. R., Henriques, A. A., & Cruz, P. J. (2009). Probability-based assessment of existing concrete bridges—stochastic resistance models and applications. *Structural Engineering International, 19*(2), 203-210.

Wong, K. Y. (2004). Instrumentation and health monitoring of cable‐supported bridges. *Structural Control and Health Monitoring, 11*(2), 91-124.

Wong, K.Y. (2007). Design of a structural health monitoring system for long-span bridges. *Structure and Infrastructure Engineering, 3*(2), 169-185.

Wong, K. Y., Man, K. L., & Chan, W. Y. (2001). Application of global positioning system to structural health monitoring of cable-supported bridges. *Health Monitoring and Management of Civil Infrastructure Systems*, *4337*, 390-401.

Wong, K. Y., & Ni, Y. Q. (2009). Structural health monitoring of cable-supported bridges in Hong Kong. *Structural Health Monitoring of Civil Infrastructure*

Systems, edited by Karbhari, V.M., and Ansari, F., Woodhead Publishing, Cambridge, UK, 371-411.

Worden, K., & Dulieu-Barton, J. M. (2004). An overview of intelligent fault detection in systems and structures. *Structural Health Monitoring, 3*(1), 85-98.

Worden, K., & Manson, G. (2007). The application of machine learning to structural health monitoring. *Philosophical Transactions of the Royal Society of London A: Mathematical, Physical and Engineering Sciences, 365*(1851), 515-537.

Worden, K., Manson, G., & Allman, D. (2003). Experimental validation of a structural health monitoring methodology: Part I. Novelty detection on a laboratory structure. *Journal of Sound and Vibration, 259*(2), 323-343.

Worden, K., Manson, G., & Fieller, N. R. (2000). Damage detection using outlier analysis. *Journal of Sound and Vibration, 229*(3), 647-667.

Worden, K., & Staszewski, W. (2000). Impact location and quantification on a composite panel using neural networks and a genetic algorithm. *Strain, 36*(2), 61-68.

Wu, Q., Law, R., & Xu, X. (2012). A sparse Gaussian process regression model for tourism demand forecasting in Hong Kong. *Expert Systems with Applications, 39*(5), 4769-4774.

Wu, Z., & Fujino, Y. (2005). Structural health monitoring and intelligent infrastructure. *Smart Materials and Structures, 14*(3), 153-167.

Wu, Z. S., Xu, B., & Harada, T. (2003). Review on structural health monitoring for

infrastructure. *Journal of Applied Mechanics, 6*, 1043-1054.

Xia, H., Ni, Y., Wong, K., & Ko, J. (2012). Reliability-based condition assessment of in-service bridges using mixture distribution models. *Computers & Structures, 106*, 204-213.

Xia, H., Xu, Y., & Chan, T. H. (2000). Dynamic interaction of long suspension bridges with running trains. *Journal of Sound and Vibration*, *237*(2), 263-280.

Xia, Y., Hao, H., Zanardo, G., & Deeks, A. (2006). Long term vibration monitoring of an RC slab: temperature and humidity effect. *Engineering Structures*, *28*(3), 441-452.

Xu, F., Chen, A., & Zhang, Z. (2013). Aerostatic wind effects on the Sutong Bridge. *Proceedings of the 3rd International Conference on Intelligent System Design and Engineering Application*, 247–256.

Xu, Y., & Chan, W. (2009). Wind and structural monitoring of long span cable-supported bridges with GPS. *Proceedings of the 7th Asia-Pacific Conference on Wind Engineering*, 8-12 November 2009, Taipei, Taiwan.

Xu, Y., & Chen, J. (2004). Characterizing nonstationary wind speed using empirical mode decomposition. *Journal of Structural Engineering, 130*(6), 912-920.

Xu, Y., Li, Q., Wu, D., & Chen, Z. (2010). Stress and acceleration analysis of coupled vehicle and long-span bridge systems using the mode superposition method. *Engineering Structures, 32*(5), 1356-1368.

Xu, Y., Liu, T., & Zhang, W. (2009). Buffeting-induced fatigue damage assessment of

a long suspension bridge. *International Journal of Fatigue, 31*(3), 575-586.

Xu, Y., & Zhan, S. (2001). Field measurements of Di Wang tower during typhoon York. *Journal of Wind Engineering and Industrial Aerodynamics, 89*(1), 73-93.

Xu, Y. L., & Xia, Y. (2011). *Structural Health Monitoring of Long-Span Suspension Bridges*. CRC Press.

Yanev, B. (2003). Structural health monitoring as a bridge management tool. *Structural Health Monitoring and Intelligent Infrastructure*, edited by Wu, Z.S., and Abe, M., Balkema, 87-95.

Yang, Y. B., Yau, J. D., & Hsu, L. C. (1997). Vibration of simple beams due to trains moving at high speeds. *Engineering Structures, 19*(11), 936-944.

Yu, M., Liao, H., Li, M., Ma, C., & Liu, M. (2013). Field measurement and wind tunnel test of buffeting response of long-span bridge under skew wind. *Journal of Experiments in Fluid Mechanics, 27*(3), 51-55.

Yun, C. B., Lee, J. J., & Koo, K. Y. (2011). Smart structure technologies for civil infrastructures in Korea: recent research and applications. *Structure and Infrastructure Engineering, 7*(9), 673-688.

Zheng, R., & Ellingwood, B. R. (1998). Role of non-destructive evaluation in time-dependent reliability analysis. *Structural Safety, 20*(4), 325-339.

Zhang, R., & Mahadevan, S. (2000). Model uncertainty and Bayesian updating in reliability-based inspection. *Structural Safety, 22*(2), 145-160.

Zhou, H.F., Dou, H.Y., Qin, L.Z., Chen, Y., Ni, Y.Q., & Ko, J.M. (2014). A review of

full-scale structural testing of wind turbine blades. *Renewable and Sustainable Energy Reviews, 33*, 177-187.

Zhu, B., & Frangopol, D. M. (2013). Incorporation of structural health monitoring data on load effects in the reliability and redundancy assessment of ship cross-sections using Bayesian updating. *Structural Health Monitoring*, *12*(4), 377-392.

Zuk, W. (1965). Thermal behavior of composite bridges-insulated and uninsulated. *Highway Research Record* (76).